Title
Technology Readiness and Development of the Reheat Air-Brayton Combined Cycle Power Conversion System using Molten Salt

Author
Gallagher, Shane

Publication Date
2021

Peer reviewed|Thesis/dissertation

Technology Readiness and Development of the Reheat Air-Brayton Combined Cycle Power Conversion System using Molten Salt

by

Shane Eric Gallagher

A dissertation submitted in partial satisfaction of the

requirements for the degree of

Doctor of Philosophy

in

Engineering - Nuclear Engineering

in the

Graduate Division

of the

University of California, Berkeley

Committee in charge:

Professor Per F. Peterson, Chair
Professor Van P. Carey
Assistant Professor Raluca O. Scarlat

Spring 2021

Technology Readiness and Development of the Reheat Air-Brayton Combined Cycle Power Conversion System using Molten Salt

Abstract

Technology Readiness and Development of the Reheat Air-Brayton Combined Cycle Power Conversion System using Molten Salt

by

Shane Eric Gallagher

Doctor of Philosophy in Engineering - Nuclear Engineering

University of California, Berkeley

Professor Per F. Peterson, Chair

Electricity markets are being significantly influenced by the rapid adoption of renewable energy sources. Traditional baseload energy sources such as coal and nuclear are not currently designed to be profitable in this new energy market environment. Moreover, integration of these energy sources, while popular for reducing dependence on carbon-based energy sources, have led to technical challenges in maintaining grid stability. As the penetration of renewables increases, these challenges will also be exacerbated.

This dissertation presents a novel power conversion system, the Reheat Air-Brayton Combined Cycle (RACC), capable of mitigating these issues. The RACC can be coupled to any heat source capable of producing high temperature molten salt, such as a molten salt nuclear reactor or concentrated solar power. It provides superior operational flexibility, which improves grid stability and allows traditionally inflexible energy sources to take advantage of electricity market price fluctuations.

This dissertation is split into five sections. The first section details the economic motivation for the RACC and gives a brief introduction into the various components of the RACC including a novel salt to air heat exchanger, a modified gas turbine, a thermal energy storage system, and advanced heat recovery steam generator control.

The second section introduces the technology readiness of each of these major components of the RACC. This section also introduces novel work performed in this dissertation to increase the technology readiness level of the salt to air heat exchanger and the system control for the RACC.

The third section describes the Vessel and Accelerated Creep Experiment (VACE), an experiment designed to validate the design of the Coiled Tube Air Heater (CTAH), the novel salt to air heat exchanger design for the RACC. This section discusses the motivation, design, methodology, and results of VACE.

Sections four and five discuss the efforts to develop and demonstrate the controls and operation of the RACC. The fourth section presents a dynamic model of the RACC that was

developed for the demonstration of RACC transient operation. The choice of modeling software is discussed. The model is described in detail, and results for various operating scenarios are presented and compared to previous modeling efforts. The fifth section discusses the implementation of the dynamic model described in the fourth section into a power plant operator room simulator known as the Advanced Reactor Controls and Operation (ARCO) facility. Future work made possible through this facility is presented.

Acknowledgements

My time as a graduate student has been one of the most transformative periods of my life. On a national scale, these years were marked by two contentious presidential elections, record-breaking wildfires, civil unrest, and a devastating global pandemic. On a personal scale, these years were marked by my increased personal commitment to family and church service. I became a foster parent to two beautiful children and branch president to the Oakland Mandarin branch of The Church of Jesus Christ of Latter-day Saints. Without question, this has been one of the most challenging and rewarding times of my life.

As I reflect on all the people in my life that have encouraged, pushed, pulled, and carried me to this point, I am overwhelmed with humility and gratitude. Of all the people I want to acknowledge, one person stands above the rest, my wife Alisha Gallagher. She has been there through every celebration and every disappointment. Her support is unparalleled and has meant everything to me.

While at Berkeley I was blessed with incredible mentors. First and foremost, Dr. Per Peterson. Working with him as my advisor was a highlight of my graduate education. Next, Harry Andreadas who seemed to always be looking out for me, helping me find my research topic, training me on the tools to do that research, and checking in on me long after his time at Berkeley was over. Also, our safety coordinator Alan Bolind who not only kept me from electrocuting myself, but also made time for me any time I had a technical question or needed guidance. Also, I would be remiss if I did not mention the US Department of Energy Clean Energy Research Center for Water and Energy Technologies (CERC WET) program and all the scholars and professionals I met through this program. The incredible experiences I had while traveling to China to collaborate with local scholars were unforgettable and formative to my education.

While at Berkeley I was also lucky to cross paths with brilliant graduate and undergraduate students and wonderful friends. Thank you to Chris Poresky, Andrew Greenop, James Kendrick, Dane DeWit, Ishak Johnson, Omar Alzabi, Theo Ong, Li Min, Clara Alivisatos, Brian He, Geoff Leondhart, Audrey Tenzeldam, and Clement Messeri.

Next, I want to recognize a few people who had a dramatic and direct effect on helping me to this point. Dr. Matthew Memmott not only got me started in my nuclear career, but was also an example of tenacious optimism. Bijan Davari and Audrey Angelos, fellow Apros users, helped me break through many mental roadblocks from countless hours of debugging. Juha Kuronen from Fortum spent many early mornings and late nights providing me with invaluable Apros training from Finland. I am especially grateful for my therapist Dr. David Riland. Most of my milestones over the past few years would not have happened without his counsel.

Family has been incredibly important to me through this process. I am grateful for my parents, Dennis and Glenna Gallagher, and for the values they instilled in me. I am grateful for my father-in-law, Matthew Montague, who has been a father to me since my dad passed away in 2014; and my mother-in-law, Andrea Montague, who has been my unofficial guidance counselor

since I was a freshman in college. I am also grateful for my church family in the Oakland 7th Chinese Branch and the many prayers that they offered on my behalf. And finally my sister, Melissa Harris, one of my favorite people. Other than my wife, nobody knows me better, and she always knows exactly what I need to hear.

Finally I want to recognize my Heavenly Father and my Savior Jesus Christ. While serving a mission for the church in Taiwan, I adopted the mantra of one of the local church leaders, “有信心有辦法”, which means, “With faith, there is a way.” The decision to have faith in and follow Jesus Christ has led to every good thing in my life.

Table of Contents

List of Figures

List of Tables

Acronyms and Abbreviations

ARCO	Advanced Reactor Control and Operation
ASME	American Society of Mechanical Engineers
B&PV	Boiler and pressure vessel
CAISO	California Independent System Operator
CC	Combined Cycle
CERC WET	Clean Energy Research Center for Water and Energy Technologies
CIET	Compact Integral Effects Test
CSP	Concentrated Solar Power
CTAH	Coiled Tube Air Heater
DAQ	Data acquisition
DOD	Department of Defense
DOE	Department of Energy
EHS	Emergency Health and Safety
FIRES	Firebrick resistance-heated energy storage
GAO	Government Accountability Office
GT	Gas Turbine
HP	High-pressure
HRSG	Heat Recovery Steam Generator
IET	Integral Effects Test
LP	Low-pressure
NG	Natural Gas
O&M	Operation and Maintenance
OPC UA	Open Platform Communications Unified Architecture
PB-FHR	Pebble bed Fluoride-salt-cooled High-temperature Reactor
PID	Proportional-Integral-Derivative
PR	Pressure ratio
RACC	Reheat Air-Brayton Combined Cycle
SCL	Simantics Constraint Language
SMR	Small modular reactor
ST	Steam turbine
TH	Thermal Hydraulic
THEEM	Transverse Heat Exchange Effectiveness Model
TRL	Technology Readiness Level
VACE	Vessel and Accelerated Creep Experiment

1 Introduction

The subject of this dissertation is the development and evaluation of the technology readiness of a novel power conversion system, the Reheat Air-Brayton Combined Cycle (RACC). The RACC is capable of being coupled to various heat sources to provide both base load and load following power. The open Air-Brayton cycle provides potential technical and economic benefits when compared to traditional Rankine steam cycles while still allowing the feasibility to use a Rankine bottoming cycle or other combined process heat application.

Many components of the RACC are readily available commercially and there is extensive experience in operating these components, however assembling these components for this use is a novel innovation for nuclear and solar thermal power. Moreover, the RACC utilizes components that are not currently commercially available such as the Coiled Tube Air Heater (CTAH). This dissertation will discuss the development of these components and the control of this system to discern the viability of this technology.

1.1 Dissertation Structure

This dissertation begins with an introduction to the market and technological motivations for developing a low carbon flexible baseload energy source. A brief technology overview of the RACC is then given with a summary of how it is able to meet these market and technology demands.

Chapter two will then introduce the reader to the technology readiness of each major aspect of the RACC. This chapter also introduces the specific areas of development that will be focused on for the novel work of this dissertation.

Chapter three describes the motivation, design, methodology, and results for an experiment conducted in order to further the technology readiness of the CTAH.

Chapter four discusses the dynamic modeling of the RACC for the intent of demonstrating the transient operation of the system. An overview of the chosen software is given. The model is described in detail, and results for various operating scenarios are presented. Results are compared to previous modeling efforts.

Chapter five discusses the implementation of the dynamic model described in chapter four into the control system of advanced reactor integral effects tests (IET) and its role in enabling IETs to operate with realistic dynamic heat loads matching the scaled loads that RACC would create. The use of this dynamic model for testing in the Compact Integral Effects Test (CIET) facility is reviewed, for a scaled reactor design referred to as the Mark 2 Pebble Bed Fluoride Salt Cooled Reactor (Mk-2 PB-FHR).

Finally, in chapter six a concluding discussion of the results and impact of this research is given. Suggestions for future work are also explored.

1.2 Motivation

There are many ways to evaluate the value of an energy source such as: Capacity, Dispatch ability, Flexibility, Reliability, Environmental impact, Price, etc. Throughout the history of power production and among different parts of the world, emphasis on different key indicators can vary. Over the past few decades, the environmental impact caused by human activity has become increasingly important. This has led to rapid integration of variable renewables such as wind and solar energy. While variable renewables provide low carbon electricity, they lack the reliability and flexibility of dispatchable energy sources. The effect of this intermittent behavior on the grid has been known for a while. In 2013 the California Independent System Operator (CAISO) presented predictions on how renewables would affect the grid and presented what is known as 'the duck curve' shown in Figure 1-1 [1]. Due to the rapid growth of solar, the duck curve has actually under-predicted the effects on the grid as shown in Figure 1-2 [2].

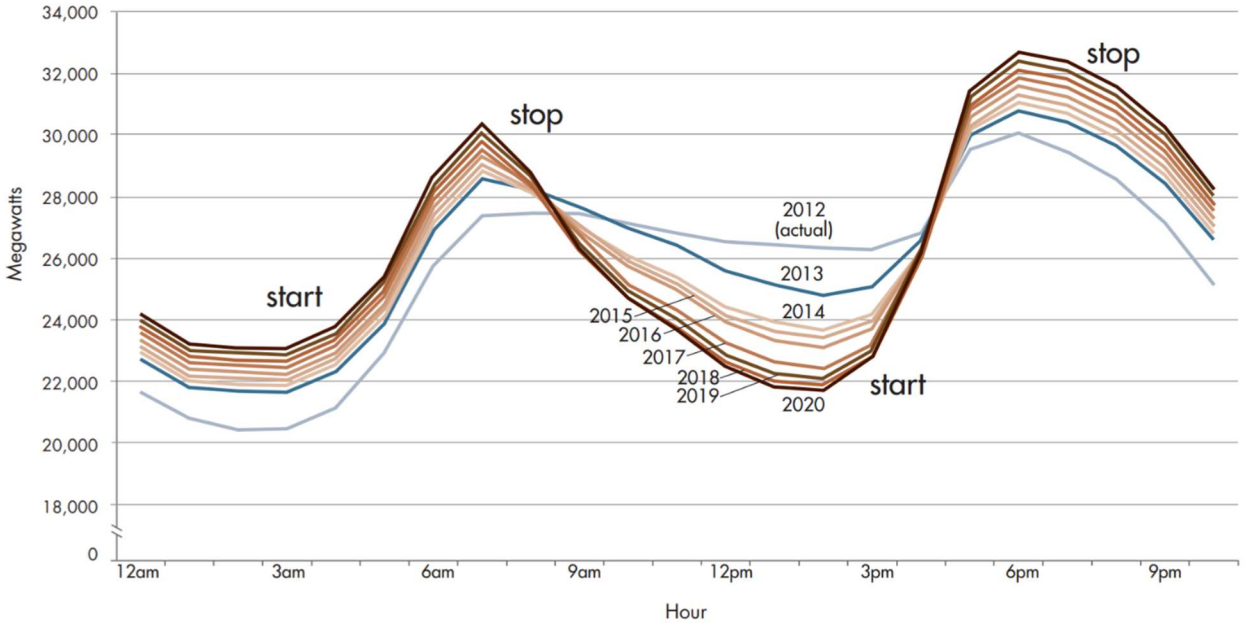

Figure 1-1: CAISO Duck Curve[1]

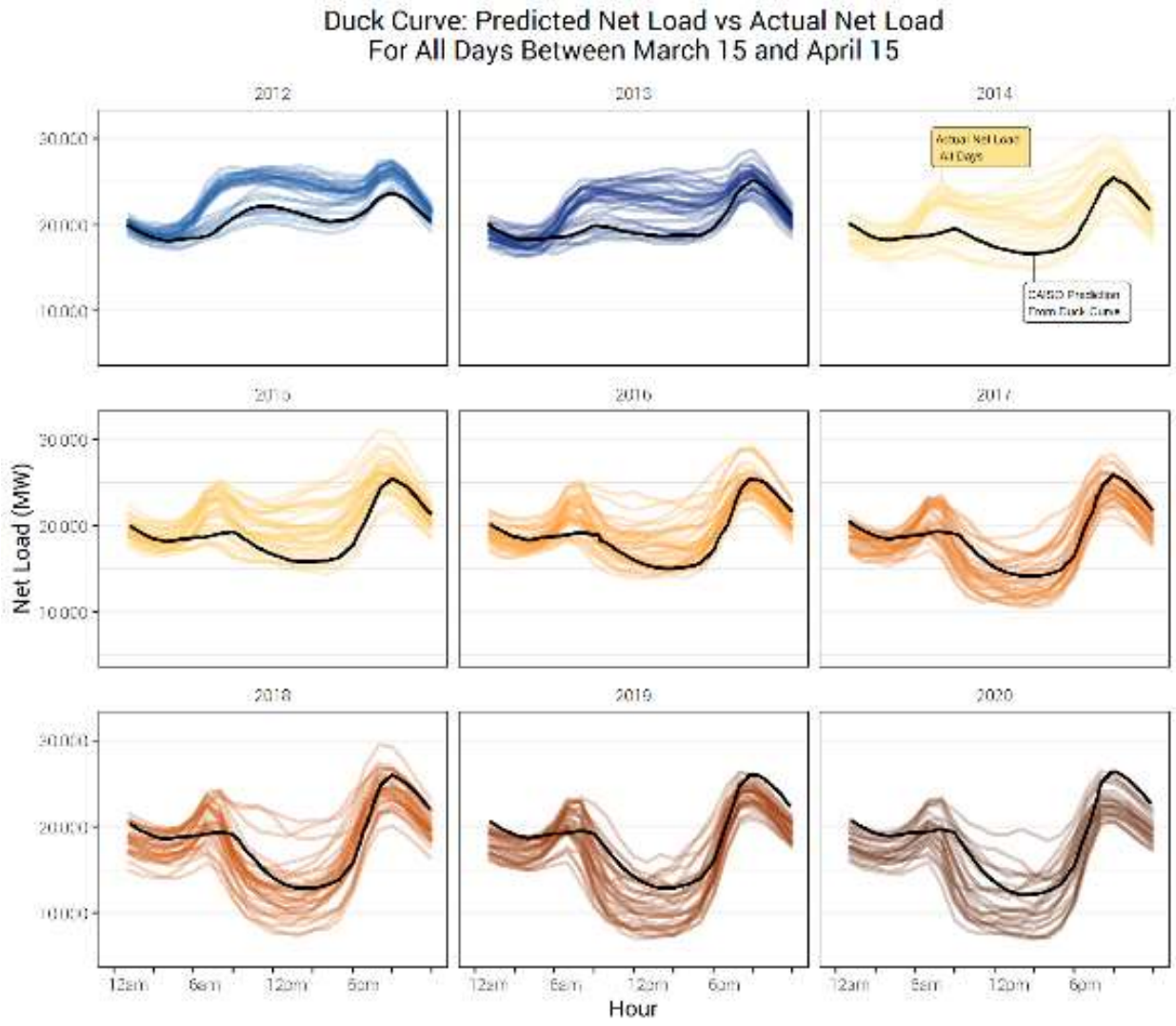

Figure 1-2: Duck Curve Predicted vs. Actual[2]

CAISO predicted that real-time net demand would have increasingly short, steep ramps where generation resources would have to be brought on or shutdown rapidly with risk of over-supply during the day as well as decreased frequency response. These conditions result in greater difficulty maintaining grid reliability[1].

Steep ramp rates introduce a technical problem because electricity must be consumed at the same time it is generated. If other energy sources are not able to complement the generation profile of variable renewables, these increasingly steep demand curves introduce the risk of over or under production of electricity, causing blackouts and brownouts. Currently wind and solar make up approximately a quarter of the California energy generation mix, and as that percentage increases, the challenge increases.

The technical challenge of increasingly steep ramp rates also has significant impact on electricity markets. In 2012 electricity prices could have $35/MWh fluctuations and now the

average is $65/MWh. Figure 1-3 shows a similar graph to the duck curve illustrating these large price fluctuations. There is also a growing number of days with negative electricity prices as shown in

Figure 1-4. It has been predicted that as early as 2035, California could see over 2,000 hours of electricity prices at or below $0/MWh, see Figure 1-6[3].

Figure 1-3: Price of electricity has had increasingly large swings[4]

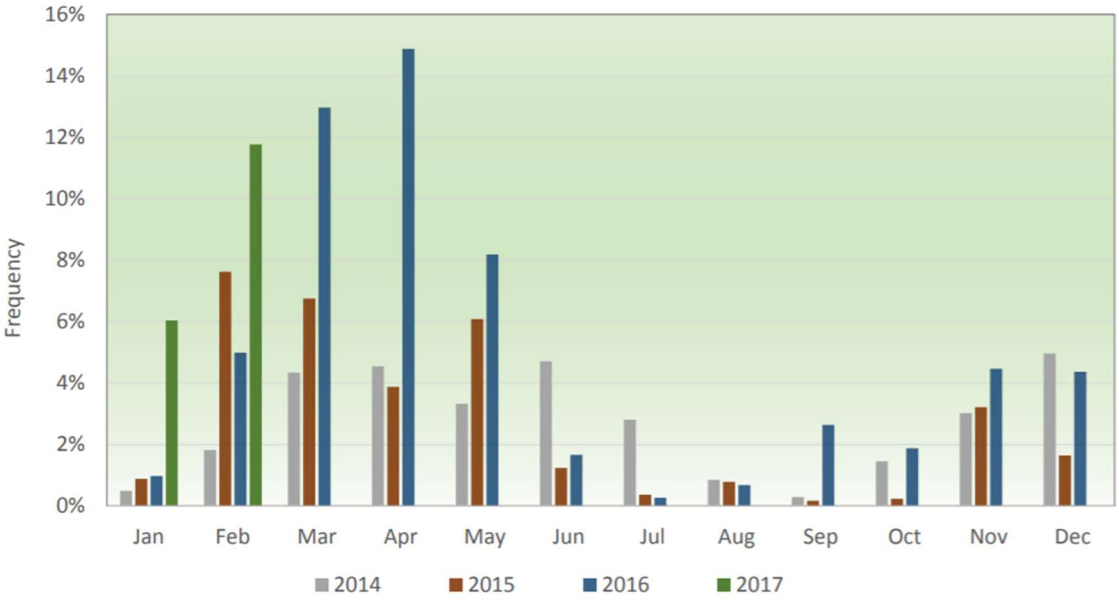

Figure 1-4: Frequency of Negative Pricing is increasing every year[5]

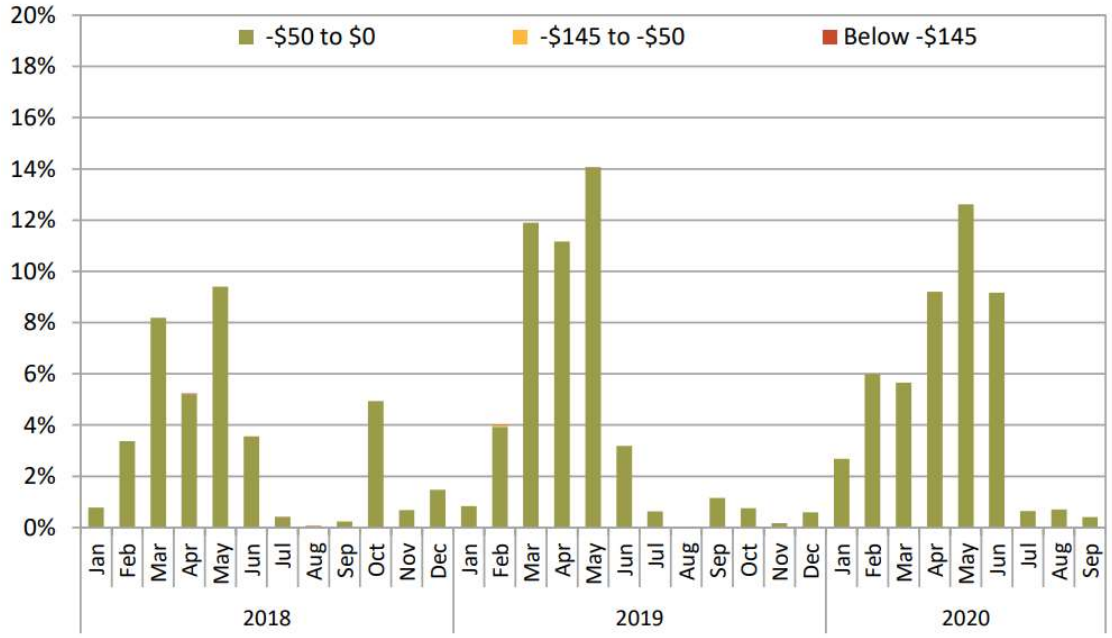

Figure 1-5: Frequency of negative prices by month[6]

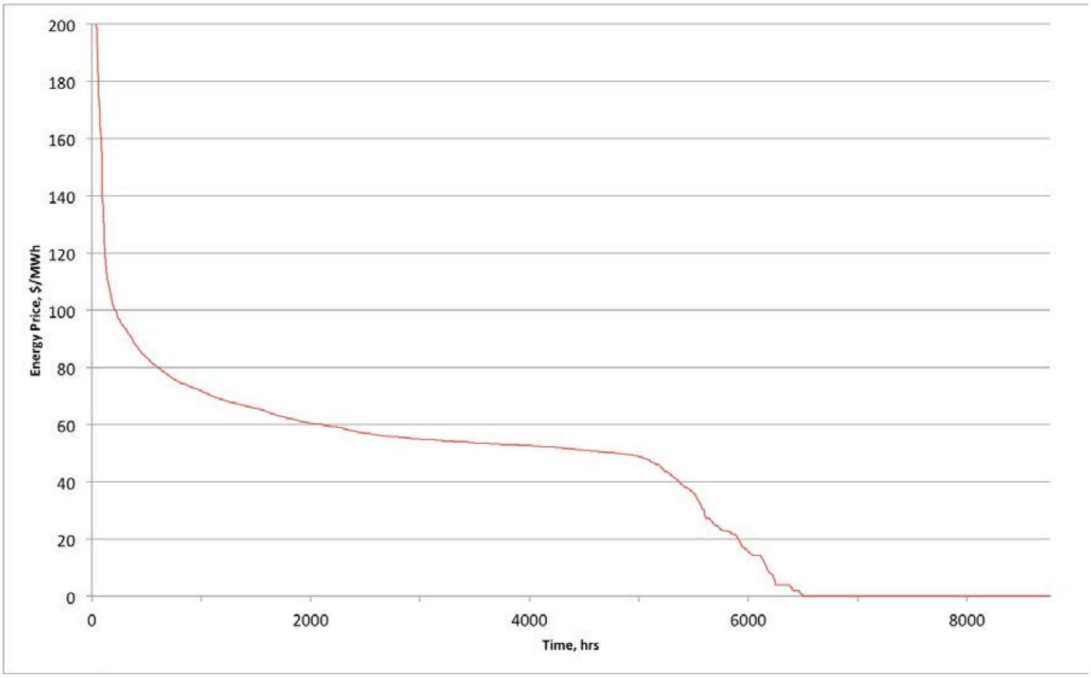

Figure 1-6: Cost duration curve for electricity prices over all hours of the year 2035 sorted from highest to lowest.[3]

To understand how this can happen it is important to understand how the electricity market in California operates. Utilities make bids for how much electricity they will produce at a given price. The utility with the lowest bid is the first to be allowed to sell electricity to the grid followed by the next lowest bid. This continues until the amount of generation meets the demand

for a given time. The bid of the last generator to sell electricity sets the price of electricity and is the price that all the generators allowed to produce electricity will receive. The utilities with bids higher than that price do not get to sell electricity to the grid[7]. If the electricity market were a true free market, with no utilities able to exercise market power, utilities would always bid their marginal cost of production, since if they bid less, they would be spending more than they would earn, and if they bid more, they risk losing the opportunity to produce electricity at a profit.

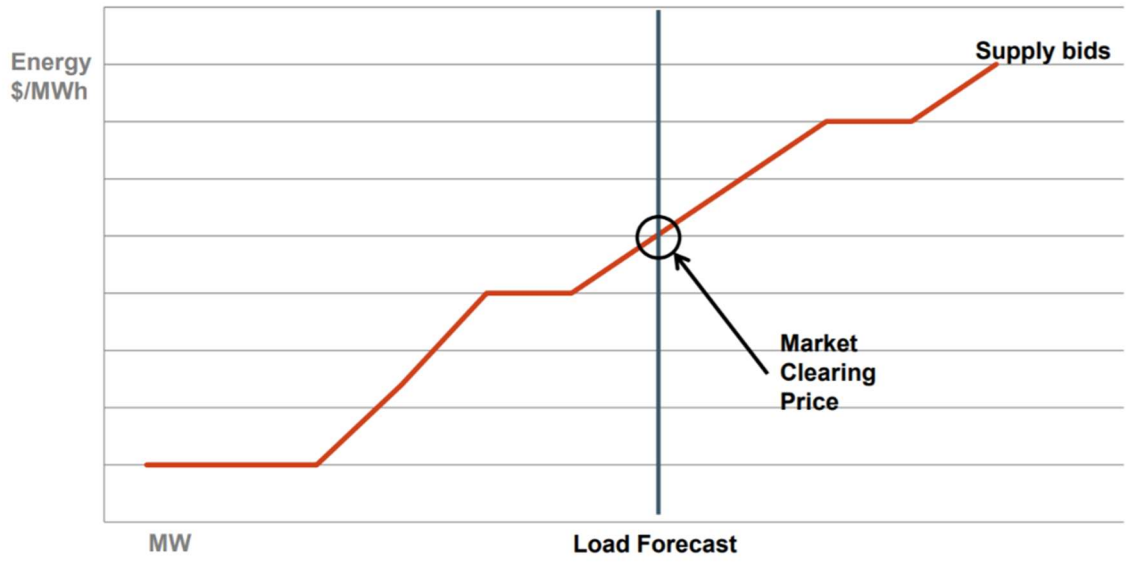

Figure 1-7: Market Clearing Price is where the Supply bids equal the Load Forecast[7].

Unfortunately, steep ramp rates cause some significant market failures for electricity markets. While counterintuitive, there are situations in which a utility would bid below their marginal cost of production. Occasionally utilities will even make negative price bids or in other words, pay the grid operator to produce electricity. For instance, wind and solar energy have essentially no marginal cost since the energy source is free. Wind and solar also receive government subsidies. This means that wind and solar utilities could bid at a negative price up to the amount of the subsidy and still make a profit off the electricity they produce[8][9]. Also, some generators do not have the flexibility to shut down, even if prices are below their marginal cost of production. For instance, when a nuclear power plant shuts down, it can take up to two days to restart. Therefore, some utilities will bid well below their marginal cost, even negative prices just so they can produce later when prices are higher[9].

Currently, the technology best equipped to complement the intermittency of renewables is the gas turbine. Gas turbines are capable of extremely fast ramp rates compared to nuclear and coal power plants. For this reason, as well as the low price of natural gas, gas turbines are representing an increasing percentage of the US energy mix[10].

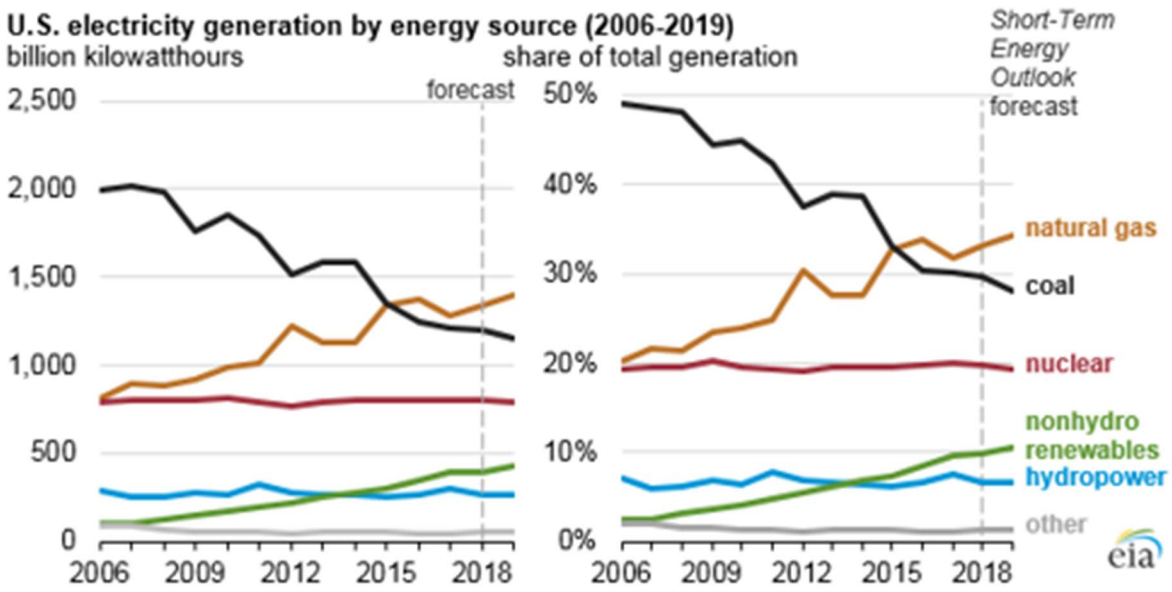

Figure 1-8: The use of Natural Gas in Electricity Generation has been steadily increasing[11].

While it is true that natural gas produces less CO_2 than coal, in order to completely eliminate our dependence on fossil fuels, it is imperative to develop power cycle technology capable of using zero carbon energy sources while mimicking the reliability and flexibility of gas turbines.

Table 1-1: While Natural Gas represented a larger share of U.S. electricity generation in 2019, it produced significantly less CO2 emissions[12]

Source	Million metric tons	Share of sector total
Coal	973	60%
Natural gas	619	38%
Petroleum	16	1%
Other[2]	11	<1%
Total	1,619	

1.3 Technology Overview

The Reheat Air Brayton Combined Cycle uses a modified gas turbine to replace natural gas with some other heat source. It does this by utilizing a novel heat exchanger called the Coiled Tube Air Heater (CTAH) to use high temperature molten salt to heat air rather than burn natural gas. A thermal energy storage system is used to increase the flexibility of the system and like typical combined cycles a heat recovery steam generator is used as the bottoming cycle to increase overall efficiency. The RACC is able to operate in two regimes: a 'baseload' regime where only heat from the molten salt is used to heat the air; and 'peaking' regime where supplemental heat from the thermal energy storage system or co-firing of natural gas or syngas is used to boost energy production. A brief description of each component is given here, a detailed discussion of the current state of the art of the RACC will be given in chapter two.

1.3.1 Working Fluid

Molten salt could be used to heat many different working fluids. For instance, it could be used to run a traditional Steam Rankine cycle by heating water. There are also many closed Brayton cycle concepts that use helium, argon, or supercritical CO_2. Each of these working fluids have their own strengths and weaknesses. While worthwhile to explore these other working fluids, air was chosen to preserve the option to have natural gas co-firing to increase ramp rates. Other working fluids would lack oxygen for combustion, eliminating the option for co-firing. Moreover, open air Brayton cycles are commonly used in industry, and multiple gas turbine vendors manufacture gas turbines similar to the one designed for the RACC. This makes it a more economical development path compared to the less commonly used closed Brayton cycle. Ambient air flows through the various components of the RACC in the following manner[13]:

i. Air intake occurs through a filter bank, and the air is compressed to a pressure ratio of 18.5. For a nominal 15°C, 1.01 bar ambient condition the air exits the compressor at a temperature of 418°C.
ii. After the compressor outlet, the air passes through a HP CTAH and is heated up to a turbine inlet temperature of 670°C.
iii. The air is then expanded to approximately the same temperature as the compressor outlet temperature, 418°C. This criterion determines the expansion ratio of the first expansion stage at nominal design conditions.
iv. The air is then reheated back up to 670°C by passing through a second, LP CTAH. It is important to design this LP external heating system to have minimum pressure drop in order to achieve acceptable circulating power loss and cycle efficiency.
v. After the LP CTAH, the air can be sent directly to the LP expansion, or it can be sent through the FIRES TES to provide power peaking. A third option is for a fuel such as natural gas to be injected and burned to increase the turbine inlet temperature and the power output.
vi. The heated air is then expanded down to nearly atmospheric pressure and 395-700°C, depending on the peak power level, by passing through the set of LP turbine blades, before entering the HRSG. The HRSG must be designed to accommodate a relatively wide range of air inlet temperatures due to the large change that occurs between low-carbon base-load operation and peak power operation with natural gas injection.

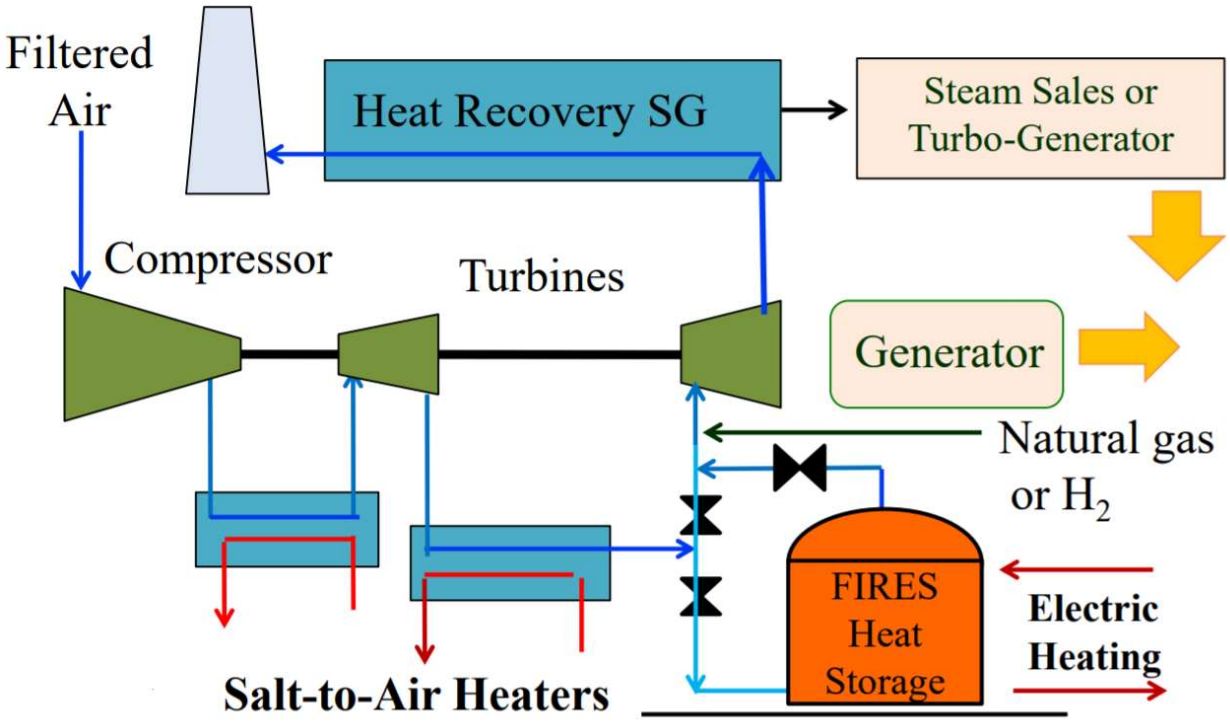

Figure 1-9: RACC Overview[14]

1.3.2 Heat Source and Heat Transfer Fluid

The RACC uses molten salt as the primary loop heat transfer fluid, with air as the working fluid for the topping cycle and water for the bottoming cycle. Molten salt has become an increasing popular heat transfer fluid. The melting point of salts can range from 250°C to 1000°C, depending on the specific salt composition. Molten salts have a large and stable liquid temperature range, high heat capacity, and high thermal energy storage density. It isn't practical to use water at these temperatures due to the high pressures needed to maintain liquid phase, and heat transfer oils degrade at high temperatures[15].

The RACC can be coupled with any heat source that is capable of providing high temperature molten salt. The most common power sources looking at utilizing molten salt as a heat transfer are nuclear power and concentrated solar thermal power. The design basis used in this dissertation is the Mark 1 Pebble Bed Fluoride Salt Cooled High Temperature Reactor (Mk1 PB-FHR), however much of the work of this dissertation on RACC power conversion is agnostic to the heat source, only assuming that the RACC heat source is providing high temperature molten salt. As an example, this RACC power conversion system can also be used for the "Mk2 PB-FHR", a generic scaled FHR design developed at UC Berkeley that allows the Compact Integral Effects Test (CIET) facility to study a range of scaled PB-FHR designs, as well as concentrating solar. Chapters four and five will also discuss how these techniques can be used for other heat sources besides FHRs.

The Mk1 PB-FHR is a small modular reactor that uses nuclear fission to produce 236MWth of heat. Unlike traditional nuclear power plants which use fuel rods, the Mk1 uses fuel

encapsulated within graphite pebbles. The fuel pebbles remain in the annular core and the molten salt flows over the bed of pebbles. Nuclear fission heats the molten fluoride salt from 600°C to 700°C. The fluoride salt is a mixture of enriched lithium fluoride and beryllium fluoride called flibe ($^{7}Li_2BeF_4$). Since the RACC can use many different molten salts and heat sources, further description of the Mk1 PB-FHR will not be given here. More information on this topic can be found in the Technical Design Report [16].

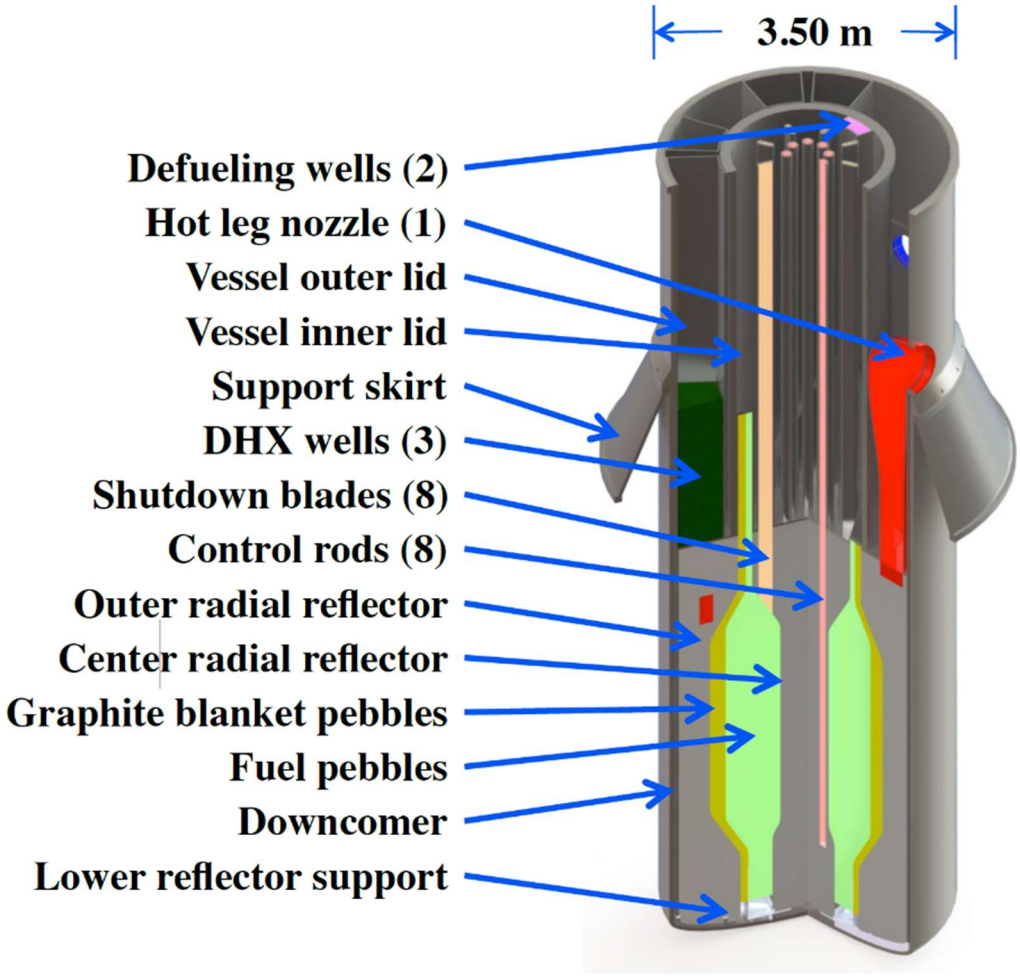

Figure 1-10: The Mk1 PB-FHR reactor vessel[16]

1.3.3 Coiled Tube Air Heater (CTAH)

The CTAH uses an annular tube bundle formed by coiled tubes, with air flow radially outward over the tubes. A key difference between CTAHs and most power plant steam generators is that CTAHs have a higher pressure on the shell side than on the tube side, so the tubes operate in compression rather than tension.

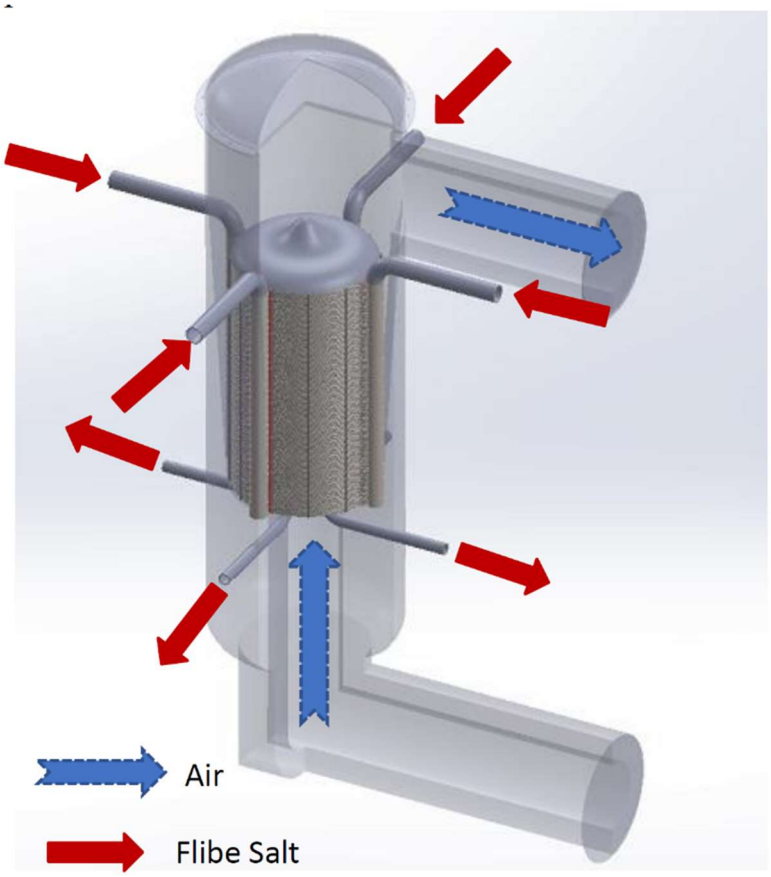

Figure 1-11: CAD Model of Mk1 PB-FHR CTAH[17]

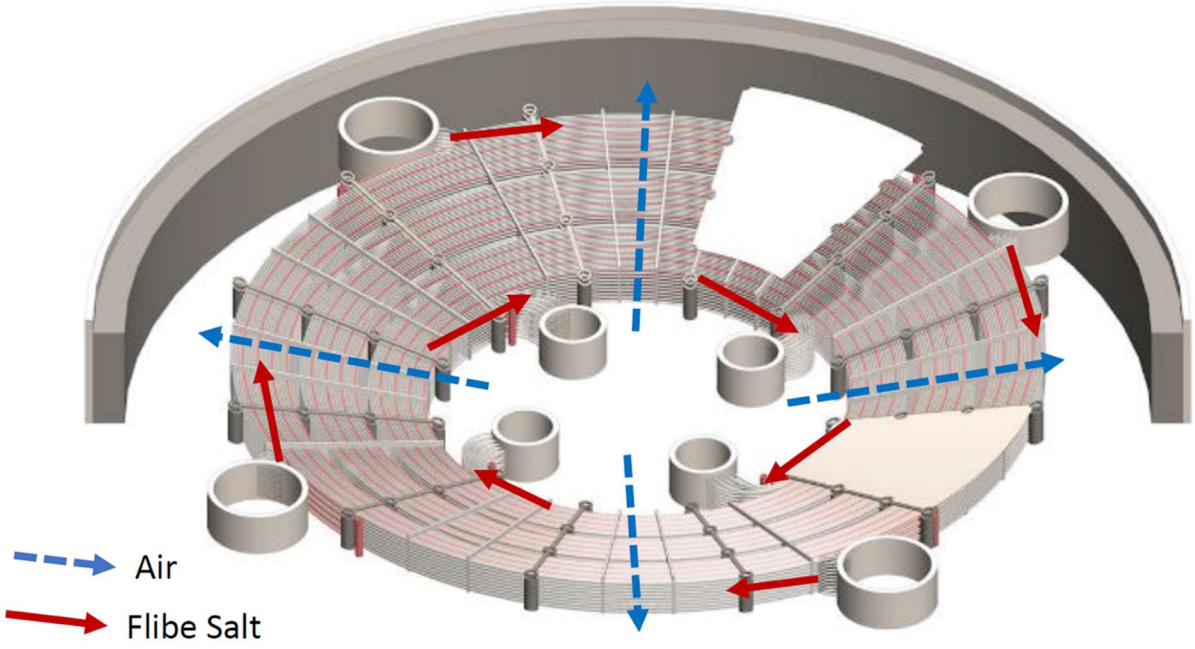

Figure 1-12: Cross section of CTAH[17]

High-pressure air from the power conversion system compressor enters the bottom of each vessel at a nominal temperature of 420°C, depending upon operating conditions, flows into the center of the coiled tube bundle, flows radially outward in cross flow across the coiled tubes, and then exits upward from the vessel having been heated to the gas outlet temperature (nominally 670°C). During GT operation, the maximum salt pressure in the CTAHs is under 3.0 bar, which is lower than the pressure of the air in the HP (18.8 bar) and LP (5.0 bar) CTAHs[16].

1.3.4 Modified Gas Turbine

The baseline RACC power conversion system uses a modified GE 7FB GT. The GE 7FB was selected because it operates at 3600 rpm and thus generates 60-Hz electricity appropriate for the U.S. power grid, and it is the largest rail-shippable GT manufactured by GE.

The modifications needed to accommodate nuclear heat for the GE 7FB include an extended shaft to accommodate reheat, a redesigned GT casing, addition of a 4th row of turbine blades, removal of the can-annular combustors and replacement by fuel nozzle injectors in an external silo-type combustor within the air ducts. Additionally, options under consideration include removal of air cooling of the first expansion stage and lower strength metals due to the low temperatures they encounter[18].

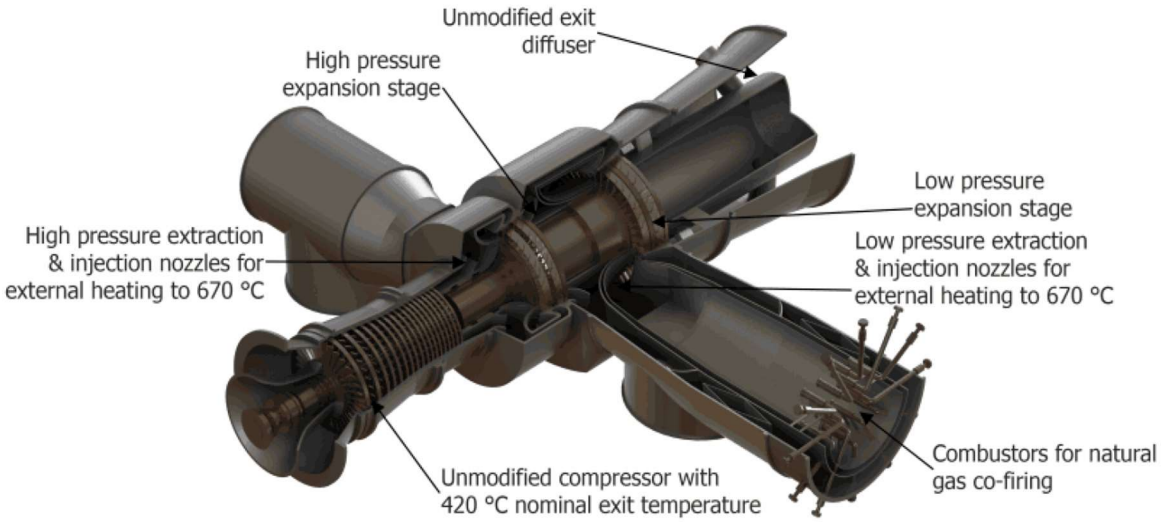

Figure 1-13: Modified Gas Turbine to introduce external air heating and reheating with co-firing[18]

1.3.5 Thermal Energy Storage System

Many different thermal energy storage systems are being developed. The “firebrick resistance-heated energy storage” (FIRES) energy storage system being developed at MIT was chosen for the RACC. FIRES is able to reach peak temperatures of 1600 °C which means it is capable of providing the high temperature air necessary for peak power production. Also, since it is resistively heated, it is able to rapidly switch from discharging to charging operation[19].

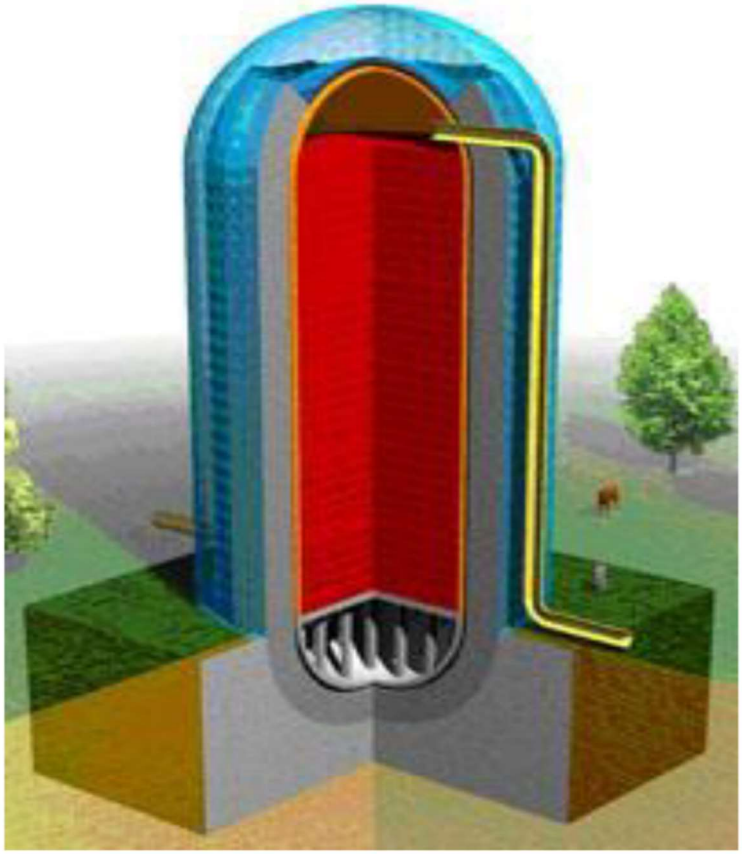

Figure 1-14: FIRES Schematic[14]

1.3.6 Heat Recovery Steam Generator

Heat recovery steam generators (HRSGs) are commonly used in NGCC power plants. The GT of a NGCC plant is typically run at a constant temperature, varying airflow, and fuel input to control the power output. Therefore, a typical HRSG will receive air from the GT exhaust at a constant temperature. HRSGs also have large thermal masses, making them respond much slower than the GT. Besides during start up and shut down, HRSGs are operated with very little control[20]. The RACC GT does not operate at constant temperature and rather operates at a constant air flow while varying the temperature entering the low-pressure turbine. This means that the GT exhaust temperature, and the temperature of the air entering the HRSG will fluctuate between 400°C and 700°C. While the hardware of the RACC HRSG will remain the same as traditional NGCC plants, the RACC HRSG will require more sophisticated controls logic in order to optimize performance and extend the lifetime of the equipment.

2 Technology Readiness of the RACC and Remaining Key Gaps

2.1 Technology Readiness Level

Technology Readiness Levels (TRLs) are a measurement system rating the maturity of a technology from least mature (TRL 1) to most mature (TRL 9)[21]. TRLs have been utilized for decades now to evaluate the progress of new technologies and to determine future research and development plans and goals. A formal process for determining the TRL of a technology was originally developed by NASA. Technology readiness reviews were suggested as early as 1969 as NASA was making plans for the post-Apollo era. However, it was in 1989 that NASA introduced the concept of readiness levels. In 1991, NASA introduced a nine-level TRL scale that has become the model for TRL usage and was later adapted for many other institutions. For instance, in 1999 the US Department of Defense (DOD) began developing a modified version of the NASA TRL scale to minimize risk in response to criticism from the US Government Accountability Office (GAO), due to previous programs suffering delays and cost increases. The DoD in 2003 published the DoD Technology Readiness Assessment Deskbook. Now they use this scale to focus efforts on technologies with TRLs of 7 or more to reduce risk. This has influenced NASA and DOD suppliers to also adopt the TRL scale[22].

The US Department of Energy (DoE) in 2011 introduced a tailored version of the NASA and DOD technology readiness assessment model. This version was used to determine the TRL of the various components of the RACC. The description of each TRL is given in Table 2-1 [23]. In this chapter the current level of development of the different components of the RACC will be discussed and a TRL assigned.

Table 2-1: DOE Technology Readiness Levels adapted from the NASA and DOD versions[23]

Relative Level of Technology Development	Technology Readiness Level	TRL Definition	Description
System Operations	**TRL 9**	Actual system operated over the full range of expected mission conditions.	The technology is in its final form and operated under the full range of operating mission conditions. Examples include using the actual system with the full range of wastes in hot operations.
System Commissioning	**TRL 8**	Actual system completed and qualified through test and demonstration.	The technology has been proven to work in its final form and under expected conditions. In almost all cases, this TRL represents the end of true system development. Examples include developmental testing and evaluation of the system with actual waste in hot commissioning. Supporting information includes operational procedures that are virtually complete. An Operational Readiness Review (ORR) has been successfully completed prior to the start of hot testing.
	TRL 7	Full-scale, similar (prototypical) system demonstrated in relevant environment	This represents a major step up from TRL 6, requiring demonstration of an actual system prototype in a relevant environment. Examples include testing full-scale prototype in the field with a range of simulants in cold commissioning. Supporting information includes results from the full-scale testing and analysis of the differences between the test environment, and analysis of what the experimental results mean for the eventual operating system/environment. Final design is virtually complete.
Technology Demonstration	**TRL 6**	Engineering/ pilot-scale, similar (prototypical) system validation in relevant environment	Engineering-scale models or prototypes are tested in a relevant environment. This represents a major step up in a technology's demonstrated readiness. Examples include testing an engineering scale prototypical system with a range of simulants. Supporting information includes results from the engineering scale testing and analysis of the differences between the engineering scale, prototypical system/environment, and analysis of what the experimental results mean for the eventual operating system/environment. TRL 6 begins true engineering development of the technology as an operational system. The major difference between TRL 5 and 6 is the step up from laboratory scale to engineering scale and the determination of scaling factors that will enable design of the operating system. The prototype should be capable of performing all the functions that will be required of the operational system. The operating environment for the testing should closely represent the actual operating environment.
Technology Development	**TRL 5**	Laboratory scale, similar system validation in relevant environment	The basic technological components are integrated so that the system configuration is similar to (matches) the final application in almost all respects. Examples include testing a high-fidelity, laboratory scale system in a simulated environment with a range of simulants and actual waste. Supporting information includes results from the laboratory scale testing, analysis of the differences between the laboratory and eventual operating system/environment, and analysis of what the experimental results mean for the eventual operating system/environment. The major difference between TRL 4 and 5 is the increase in the fidelity of the system and environment to the actual application. The system tested is almost prototypical.

Relative Level of Technology Development	Technology Readiness Level	TRL Definition	Description
Technology Development	**TRL 4**	Component and/or system validation in laboratory environment	The basic technological components are integrated to establish that the pieces will work together. This is relatively "low fidelity" compared with the eventual system. Examples include integration of ad hoc hardware in a laboratory and testing with a range of simulants and small-scale tests on actual waste. Supporting information includes the results of the integrated experiments and estimates of how the experimental components and experimental test results differ from the expected system performance goals. TRL 4-6 represent the bridge from scientific research to engineering. TRL 4 is the first step in determining whether the individual components will work together as a system. The laboratory system will probably be a mix of on hand equipment and a few special purpose components that may require special handling, calibration, or alignment to get them to function.
Research to Prove Feasibility	**TRL 3**	Analytical and experimental critical function and/or characteristic proof of concept	Active research and development (R&D) is initiated. This includes analytical studies and laboratory-scale studies to physically validate the analytical predictions of separate elements of the technology. Examples include components that are not yet integrated or representative tested with simulants. Supporting information includes results of laboratory tests performed to measure parameters of interest and comparison to analytical predictions for critical subsystems. At TRL 3 the work has moved beyond the paper phase to experimental work that verifies that the concept works as expected on simulants. Components of the technology are validated, but there is no attempt to integrate the components into a complete system. Modeling and simulation may be used to complement physical experiments.
Basic Technology Research	**TRL 2**	Technology concept and/or application formulated	Once basic principles are observed, practical applications can be invented. Applications are speculative, and there may be no proof or detailed analysis to support the assumptions. Examples are still limited to analytic studies. Supporting information includes publications or other references that outline the application being considered and that provide analysis to support the concept. The step up from TRL 1 to TRL 2 moves the ideas from pure to applied research. Most of the work is analytical or paper studies with the emphasis on understanding the science better. Experimental work is designed to corroborate the basic scientific observations made during TRL 1 work.
	TRL 1	Basic principles observed and reported	This is the lowest level of technology readiness. Scientific research begins to be translated into applied R&D. Examples might include paper studies of a technology's basic properties or experimental work that consists mainly of observations of the physical world. Supporting information includes published research or other references that identify the principles that underlie the technology.

2.2 RACC

As mentioned in Chapter one, advances in GT technology in the last 75 years has led to interest in coupling nuclear power and concentrating solar power (CSP) to air Brayton combined cycles[24]. The RACC, currently under investigation at the University of California, Berkeley, is an open-air Brayton cycle, based on a modified commercial combustion turbine, with the ability to provide flexible capacity to the grid. It supplements its baseload power production, generated by external heating of molten salt from nuclear, concentrating solar power, or other heat source. The RACC can also boost power output via co-firing or thermal energy storage heat extraction. Utilizing multiple stages of heating and optional peak power production gives the RACC superior cycle efficiencies, low carbon emissions, and high flexibility[13].

The main components of the RACC were briefly introduced in Chapter one and include the Coiled Tube Air Heater (CTAH) heat exchanger, a modified gas turbine, a firebrick resistance-heated energy storage (FIRES) thermal energy storage system, and a Heat Recovery Steam Generator (HRSG) capable of operating at multiple operation regimes. The RACC is shown schematically in Chapter one and is copied here as Figure 2-1 for the reader's convenience and Table 2-2: Key RACC design parameters shows the key RACC design parameters. The remainder of this chapter will discuss the current state of the art of these components and key gaps remaining in the RACC.

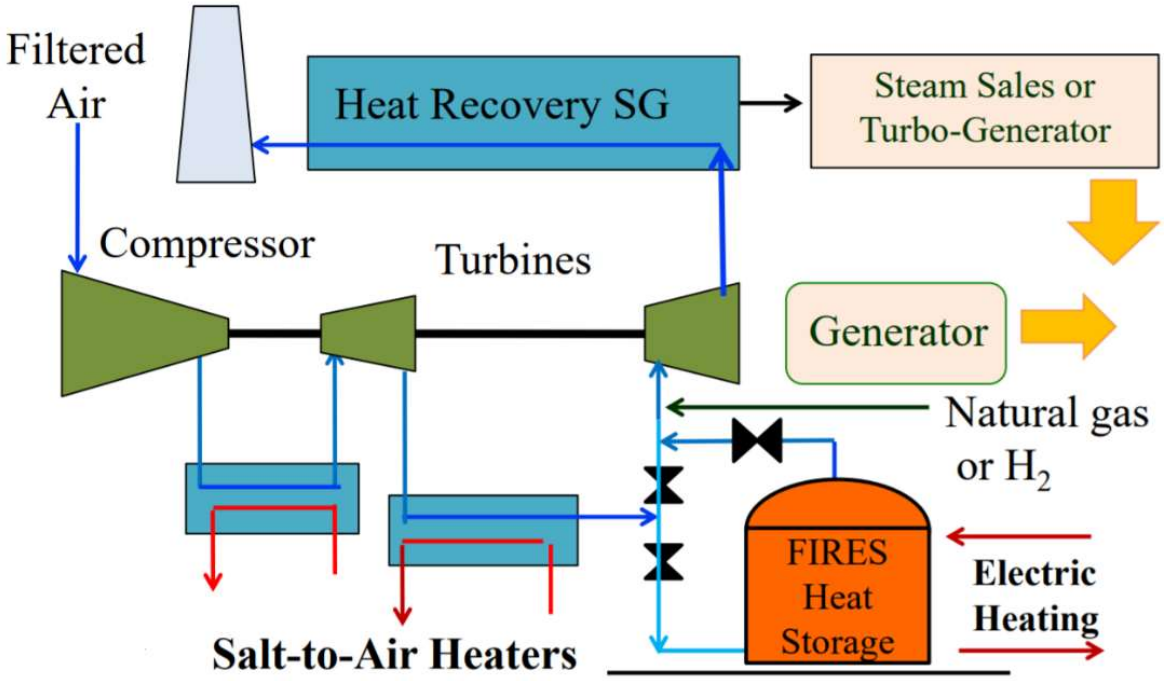

Figure 2-1: Schematic for an RACC power conversion system with a single stage of reheat[14]

Table 2-2: Key RACC design parameters

Nominal ambient temperature	15 °C
Elevation	Sea level
Compression ratio	18.52
Compressor outlet pressure	1,858,000 Pa
Compressor outlet temperature	418.7 °C
Compressor outlet mass flow (total flow is 440.4 kg/s; balance used for turbine blade cooling)	418.5 kg/sec
CTAH outlet temperature	670 °C
Base-load net electrical power output	100 MWe
Base-load thermal efficiency	42.5%
Co-firing turbine inlet temperature	1065 °C
Co-firing net electrical power output	241.8 MWe
Co-firing efficiency (gas-to-peak-power) [a]	66.4%

a. Co-firing efficiency is defined as the additional net power output over baseload divided by the additional heat input of the fossil fuel/natural gas. It is a measure of conversion efficiency of natural gas to electricity calculated on a lower heating value basis.

2.2.1 CTAH

The most thorough description of the development of the CTAH is presented in the doctoral dissertation of Dr. Andrew Greenop. His work as well as the work of others in the UC Berkeley Nuclear Engineering Thermal Hydraulics Lab will be summarized here.

Development of the CTAH began using the Mk1 PB-FHR as a design basis. The Mk1 design required all components to be compact enough to be rail shippable (3.5m vessel diameter), while maintaining a sufficient effectiveness. Generally, a compact heat exchanger has small flow passages which tend to give a high heat transfer coefficient. Conversely, these small flow passages often lead to high friction pressure loss for one or both fluids in the heat exchanger, so minimizing friction loss was priority in the design. In order to reduce friction loss, especially for low-density fluids, such as gases, heat exchangers are designed to have low mass velocities. Since this results in lower heat transfer rate per unit of surface area, the designs require a large amount of surface area to offset the low mass velocities. Therefore, having a compact heat exchanger means that the design has an overall small volume with a large heat transfer surface area, especially for the gas [17].

Traditional heat exchanger designs such as U tube Shell and Tube Heat Exchangers are not able to meet these constraints because these designs have a low heat transfer surface area density (~100-300 m^2/m^3) compared to compact heat exchanger designs (>700 m^2/m^3)[25]. And the design generally has low effectiveness within the given volume constraints. Effectiveness is defined as the ratio of the actual heat transfer to the maximum possible heat transfer. Also newer heat exchanger designs such as Printed Circuit Heat Exchangers, while compact and effective, do not perform well when exposed to thermal transients that are anticipated in the operation of the RACC[17].

A third option is a design first proposed in 1970, the “radial-flow heat exchanger”[26]. This design is a type of shell-and-tube heat exchanger where one fluid flows outward radially over the tubes, and the other fluid flows inside the coiled tubes as shown in Figure 2-1. This design provides the advantages of being both compact and highly effective, while being able to tolerate the potential thermal transients of the RACC and is therefore the heat exchanger of choice for the RACC[17].

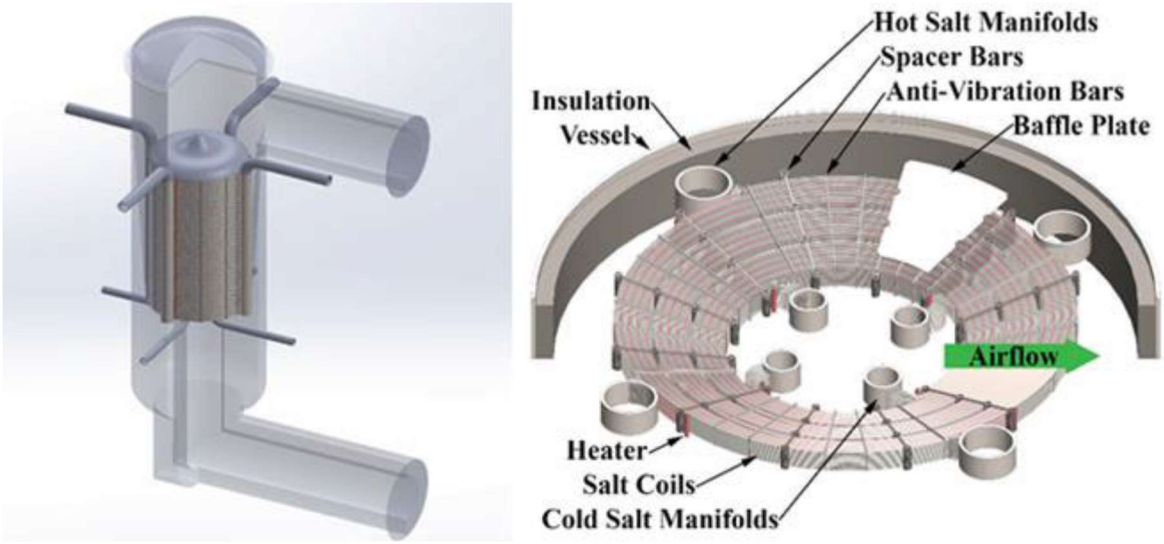

Figure 2-2: Isometric view of a reference CTAH assembly and sub-bundle 3D model with major components labeled[16]

A simulation tool known as the Transverse Heat Exchange Effectiveness Model (THEEM) has been developed which utilizes 0-D, 2-D, and 3-D modified finite volume models to optimize the design of the CTAH as well as predict the performance of a given CTAH design. Inputs to THEEM include system geometry, fluid properties, and mean inlet conditions. An algorithm is used to generate the size of the mesh to accurately model flow over a bank of tubes using empirical correlations. The 2-D model is a finite volume steady state analysis on a 2-D section of one sub-bundle of the CTAH. It calculates total heat transfer, heat transfer distribution, and temperature and pressure distribution of fluids in both the tubes and shell of the CTAH. The 3-D model calculates the flow rate into each 2-D vertical sub bundle before performing the 2-D analysis on each 2-D sub bundle. The 3-D model treats each 2-D cross section as a heat exchanger in parallel with the other 2-D cross sections. The 0-D model uses estimated outlet temperatures to provide a rough calculation for system geometry. The curvature of the tubes in CTAH causes secondary flow to enhance heat transfer, therefore a modified Reynolds number is used to account for this curvature. The heat transfer correlations used in THEEM were chosen such that THEEM can be used in both laminar and turbulent flow regimes. For a more detailed description of THEEM please refer to the Doctoral dissertation of Dr. Andrew Greenop[17].

Various lab scale experiments have been used to validate THEEM. The most recent and most sophisticated lab scale experiment to validate THEEM was the Coiled-tube Air-heater Separate Effects Test (CASET) facility. CASET was designed to match as closely as possible the prototypical Mk1 PB-FHR CTAH design. Key differences include not sloping the tubes to reduce cost, using an acrylic vessel to allow visible inspection and to lower the weight, and using

water in place of molten salt. The vessel has 21 penetrations along the perimeter of the top of the vessel to allow for flow, temperature, and pressure measurements at various points around the tube bundle. CASET tube bundle dimensions are shown in Table 2-3.

The complete CASET setup is shown in Figure 2-3. Nominal experimental Parameters are shown in Table 2-4[17]. THEEM was able to predict temperature change of both air and water with an error of only 1-4%. Unfortunately, THEEM didn't predict pressure drop accurately (up to 60% error). Possible reasons for the large deviation could be from flow maldistribution across the bundle, air entrapped in the tubes, or incorrect friction factor correlations[17].

Table 2-3: CASET Tube Bundle Design Geometry[17]

Tube Outer Diameter	0.635 cm (0.25 in)
Tube Wall Thickness	0.0508 cm (.02 in)
Longitudinal Pitch-to-Diameter Ratio (SL)	1.256
Transverse Pitch-to-Diameter Ratio (ST)	1.50
Number of Liquid Manifolds	2
Number of Loops	3
Number of Tubes per Layer per Manifold	2
Number of Tube Layers per Sub-bundle	10
Number of Sub-bundles	1
Number of Tie Rod Gaps	1
Width of Tie Rod Gaps	3.80 cm
Number of Tube Holders	8
Annulus Inner Radius	25 cm
Tube Slope	0

Figure 2-3: CASET Complete Experimental Setup[17]

Table 2-4: Nominal Values for CASET Experiment[17]

Air Flowrate	0.649 kg/s
Air Inlet Pressure	1.01 bar
Air Inlet Temperature	25.0°C
Air Outlet Temperature	51.0°C
Water Flowrate	0.100 kg/s
Water Inlet Temperature	70.0°C
Water Outlet Temperature	20.0°C
CTGH Heat Transfer	16.6 kW

A preliminary design for demonstration of air heating under prototypical conditions at a small scale was proposed in 2017 by the UC Berkeley Nuclear Engineering Thermal Hydraulics Lab. A 370 kW air loop with a CTAH test bundle was designed using THERMOFLEX®, a fully flexible program for heat balance modeling and engineering with a graphical user interface[27]. A thermodynamic schematic of the proposed 370 kW test loop is shown in Figure 2-4. Depicted are the primary heating loops containing flinak, a ternary eutectic alkaline metal fluoride salt mixture, coupled to a test CTAH test bundle. Additionally, air isolation valves on either side of the CTAH are shown, as well as an air bypass line, which together control start-up and

shutdown. The test loop operating parameters and properties are shown in Table 2-5. The test bundle geometry is shown in Table 2-6. A CAD model of the design is shown in Figure 2-5.

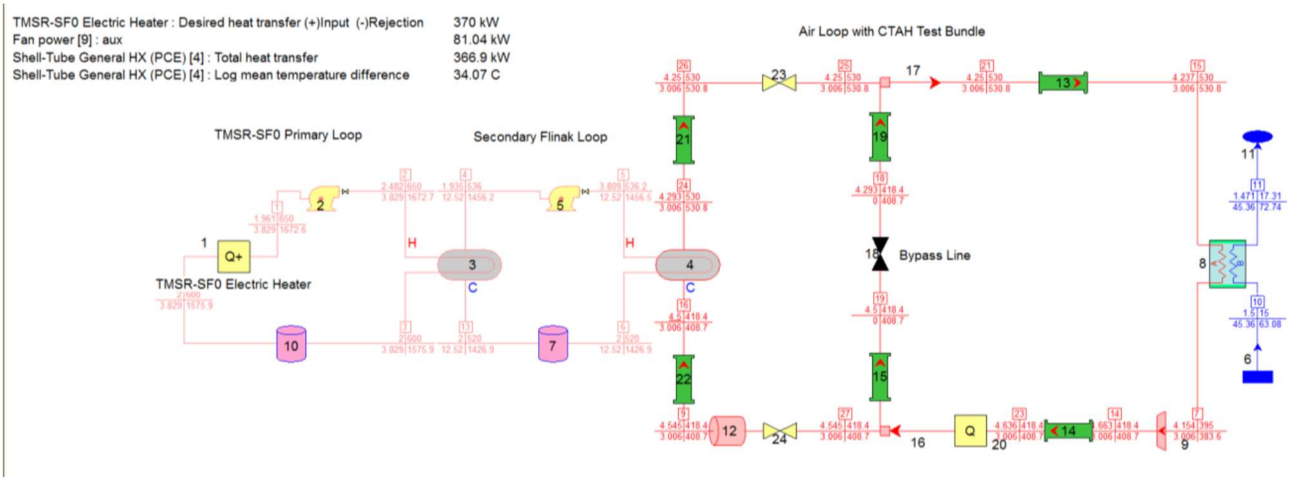

Figure 2-4: Proposed 370 kW CTAH test bundle loop thermodynamic schematic[28]

Table 2-5: Test loop flow operating parameters and properties[28]

Air Mass Flowrate	3 kg/s
Air Inlet Temperature	420°C
Air Inlet Pressure	4.5 bar
Air Density	2.263 kg/m³
Air Viscosity	3.40E-05 Pa·s
Air Velocity	42.2 m/s
Air Duct Diameter	0.2 m
Air Duct Cross Sectional Area	0.031415927 m²
Reynolds number	5.61E+05

Table 2-6: Test Bundle Geometry[28]

Number of Salt Manifolds	1
Number of Loops	3
Tube Outside Diameter	0.00635 m
Tube Wall Thickness	0.00051 m
Transverse Pitch-to-Diameter Ratio	1.4
Longitudinal Pitch-to-Diameter Ratio	1.25
Number of Tube Layers	80
Number of Tubes per Tube Layer per Manifold	5
Bundle Inside Diameter	0.700 m
Bundle Outer Diameter	1.252 m
Bundle Height	0.363 m
Total Number of Tubes	400
Average Tube Length	9.200 m
Total Tube Surface Area	73.41 m^2

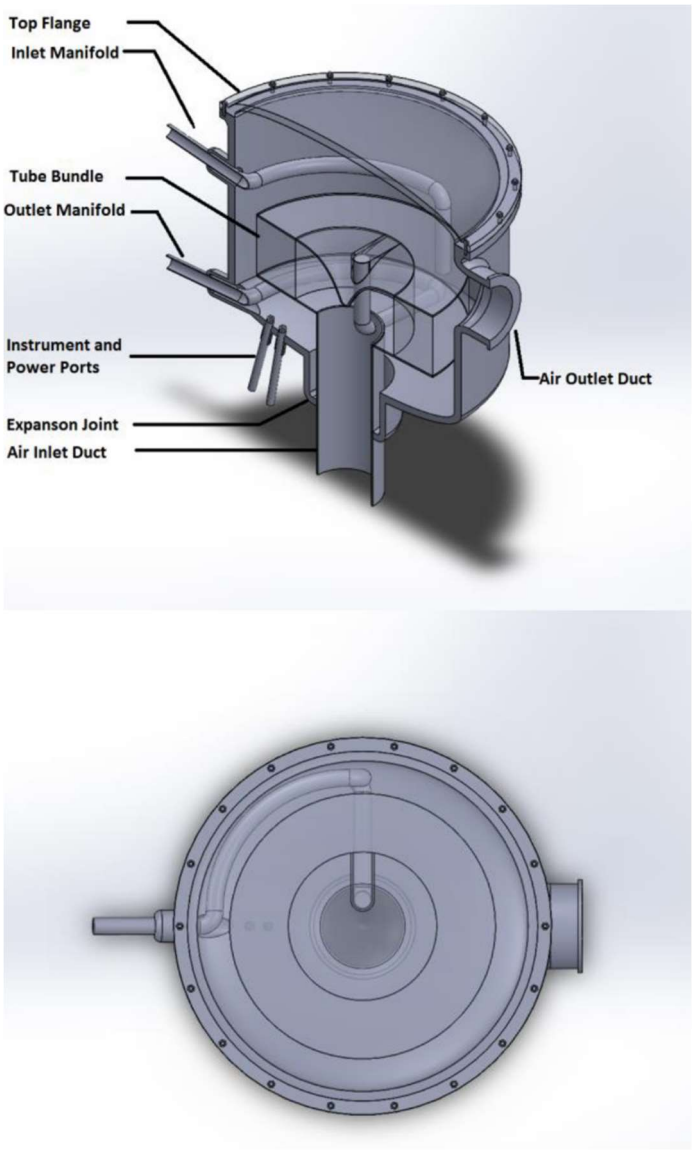

Figure 2-5: CTAH test bundle isometric and top views[28]

This small-scale experiment will be crucial to addressing remaining key gaps. Working with high temperature molten salt introduces complexity to startup, shutdown, and other transients due to the risk of salt freezing in the tubes.

The CTAH operates at 600 – 700 °C with pressure on the shell side up to 20 bar and near atmospheric pressure on the tube side. Typically, this would require advanced materials to be creep resistant and sufficiently strong. However, the CTAH, while relatively compact compared to other heat exchanger designs, still represents one of the largest components of a commercial power plant, therefore there is a large economic incentive to choose a less expensive material to construct the CTAH. One method which has been used in the chemical industry in catalytic cracking units is internal insulation[29]. An example of internal insulation is shown in Figure 2-6. Internal insulation would keep the shell of the CTAH at sufficiently low temperatures to use carbon steel which would otherwise be too weak.

Figure 2-6: Internal insulation in carbon steel pipe[30]

Creep deformation of the tubes due to the high temperature and pressure is also a potential concern. Boiler and pressure codes limit creep deformation to 1% before equipment must be replaced [31]. However, since the CTAH tubes are loaded in compression, rather than tension, it is possible that the tubes could handle far more creep deformation before experiencing failure. Relaxing the constraint of creep deformation would significantly extend the lifetime of the heat exchanger and allow the use of less expensive materials [16].

Validating the use of internal insulation, and the greater allowable creep deformation are two of the remaining key gaps to commercialization of the CTAH for use in the RACC. Work is currently ongoing at UC Berkeley in this area and will be discussed in chapter three of this dissertation.

The CTAH is currently at a TRL of 4. Research and development has clearly gone beyond the paper phase to experimental work. Individual components of the CTAH are being experimentally validated and the first steps have been taken to determine whether the individual components will work together as a system. The 370-kW molten-salt test bundle would take the CTAH to a TRL 5 or higher.

2.2.2 Modified Gas Turbine

The most thorough description of the development of the RACC modified gas turbine is presented in the Doctoral dissertation of Dr. Charalampos Andreades. His work, as well as the work of others within the UC Berkeley Nuclear Engineering Thermal Hydraulics Lab will be presented here.

The initial design of the RACC uses a baseline of a GE 7FB gas turbine. However, due to the need to accommodate reheat, a certain amount of modification is necessary. Fully developing a gas turbine is an expensive endeavor for gas turbine manufacturers. This means that this aspect of the RACC has the lowest TRL. However, The National Academies Press has identified unconventional thermodynamic cycles, and specifically reheat as one of the research areas of high-priority opportunities for substantially accelerated improvements to performance over the next decade[24].

To accommodate the air heaters, inlet/outlet diffusers, similar in concept to those used in large GTs with external combustors can be used. The combustors for the RACC can be either of the "straight-flow" or silo variety, rather than reverse flow, to reduce pressure drops. Flame out is of reduced concern because the air temperature under base-load operation exceeds the auto-ignition temperature[13].

It was determined that the turbine can be modified in one of two ways. One option is to leave the existing number of blade rows and extend the shaft between them in the desired configuration. A second option is to add or remove blade rows to better optimize the pressure ratio of each expansion stage. An additional bearing can be added for flexural support, yielding a three-bearing machine. Overall, a substantially modified turbine casing will be needed. For the RACC baseline design, a single row of blades cannot provide sufficient pressure drop for the RACC expansion stage, so each stage needs at least two rows, for a total of at least four rows of blades [13]. In chapter one, a schematic of the modified GT design was shown and is repeated here as Figure 2-7.

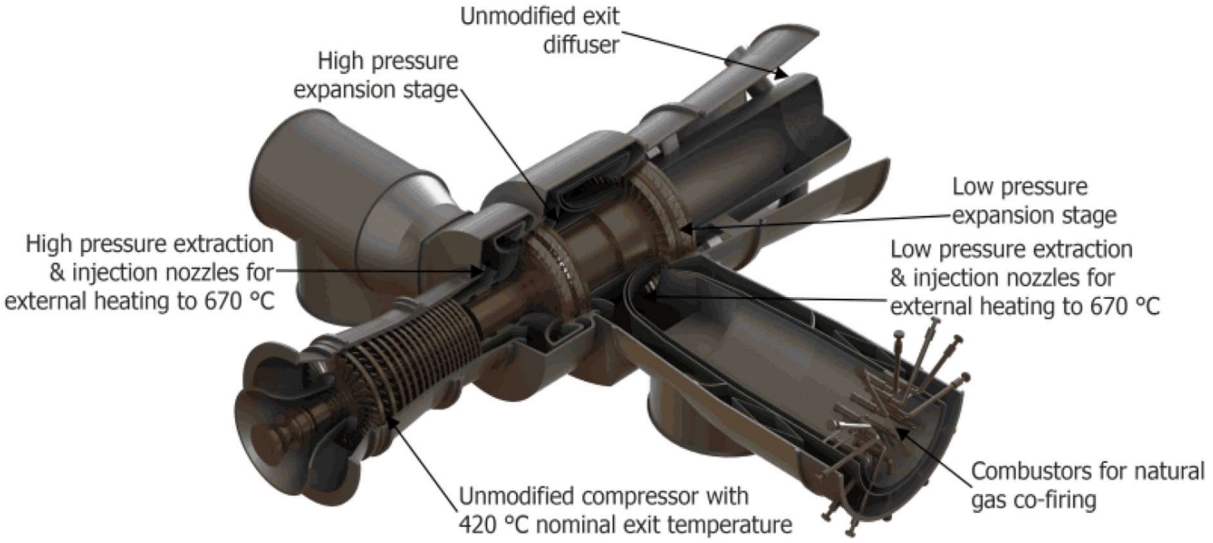

Figure 2-7: Modified Gas Turbine to introduce external air heating and reheating with co-firing[13]

During baseload operation the inlet temperature of both the HP and LP turbine is 670 °C. This is ideal since it is higher than the auto-ignition temperature of natural gas which is 537 °C[32]. Natural Gas can be injected before the final expansion stage increasing the turbine inlet temperature for peak power production. The two constraints limiting the maximum peak power output is the maximum turbine inlet temperature to the final expansion stage and the maximum air temperature entering the HRSG[13]. Typical NGCC HRSG inlet temperatures are around 650 °C and do not exceed 700 °C without significant modifications to the HRSG [33]. This corresponds to a turbine inlet temperature of 1070 °C for the second expansion turbine. This is below temperature limits for modern GTs (1600+ °C)[20].

It is important to note here that this represents a significant change from conventional control of GTs. Gas turbines are typically controlled by varying mass flow rate and keeping the turbine inlet temperature constant since GT efficiency is determined by inlet temperature, not

mass flow rate. The RACC keeps a constant flow rate and varies temperature. The RACC can afford to do this because the marginal cost of fuel in CSP or nuclear is zero or very low compared to the operational costs. The losses from reduced efficiency are made up for with the value of flexible operation. When using natural gas co-firing, which increases the marginal cost, the turbine inlet temperature is maximized, maximizing efficiency.

Another anticipated benefit of this modified GT is the potential for longer lifetime. Due to the increased flexibility from the thermal energy storage system and multiple operating regimes, the number of 'cold starts' and 'warm starts' are reduced. This is significant because each warm start shortens the lifetime by 30 hours and each cold start can shorten the lifetime by 600 hours[20]. The lower temperature baseload operation should also increase equipment lifetime.

Further development of the modified gas turbine is a key gap for the commercialization of the RACC. Currently, all research has been limited to analytical studies, therefore the TRL for the modified GT is TRL 2. The TRL could rapidly increase with the participation of industrial partners, however it is unlikely to rise beyond TRL without industrial participation.

2.2.3 FIRES

Firebrick Resistance-Heated Energy Storage is a thermal energy storage system being developed in the MIT Nuclear Science and Engineering department. Their work will be summarized here.

Grid scale energy storage has become a popular idea to address the intermittency of renewables in recent history. Many different energy storage technologies have been proposed including batteries, pumped hydro, compressed gas, thermal energy storage (molten salt, geothermal, metal, concrete, etc. heat storage media), and many others. The RACC utilizes a resistively heated firebrick chimney due to the low cost, ability to reach high temperatures, and it is relatively easy to incorporate it into the air fluid path. The RACC FIRES closely resembles regenerative heat exchangers called regenerators. Existing industrial examples include hot blast stoves or 'Cowper' stoves shown in Figure 2-8 with an example of brickwork in Figure 2-9 [34]. Cowper stoves are a mature technology that experience temperatures up to 1600 °C with high heat rates (300MW) and lifespans of 20-30 years[35].

The major advantage of the FIRES approach is that it provides an inexpensive way to store electrical energy with significant efficiency, because the electrical energy is converted to heat at a very high temperature and thus the heat can be recovered at high temperature, enabling efficient conversion back to electricity (approximately 90% efficiency is predicted in this dissertation)[36].

Figure 2-8: Hot blast stove[34]

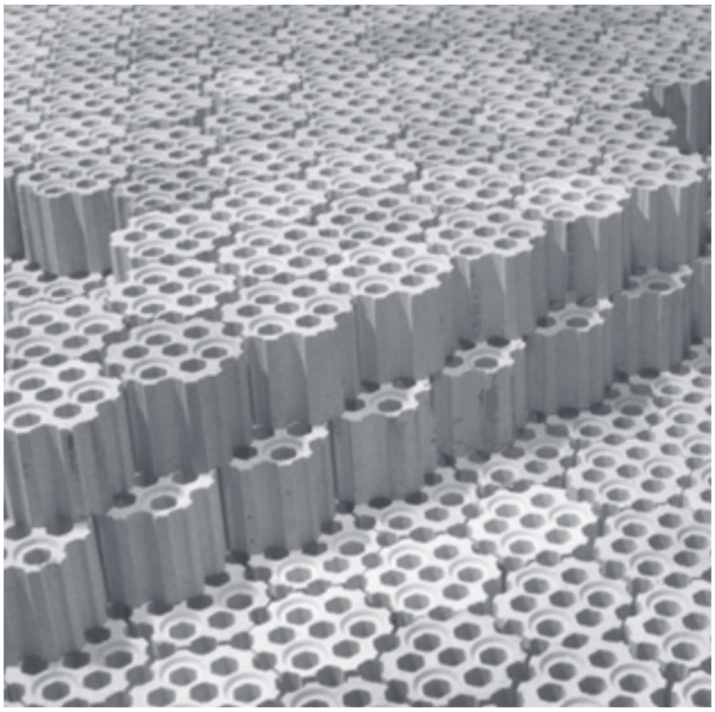

Figure 2-9: Packing of hexagonal bricks, a typical storage inventory of hot blast stoves[34]

Modeling and simulation of the FIRES TES coupled to the RACC has been performed to predict the performance, as well as optimize the size of the system for a Mk1 PB-FHR power plant. Results showed that for 1500MWh of heat storage capacity, FIRES would require just over 3 hours to charge to peak temperatures and would provide over 5 hours of increased turbine inlet temperature and therefore increased power. Results are shown in Figure 2-10 for silicon carbide firebrick and two different heater types (SiC and $MoSi_2$) capable of reaching different maximum temperatures and height to diameter ratios (HDR) of 3 and 5. Results were also promising that FIRES could store heat for a week or more with moderate losses, and if operated with daily cycling, the losses would be very low [35].

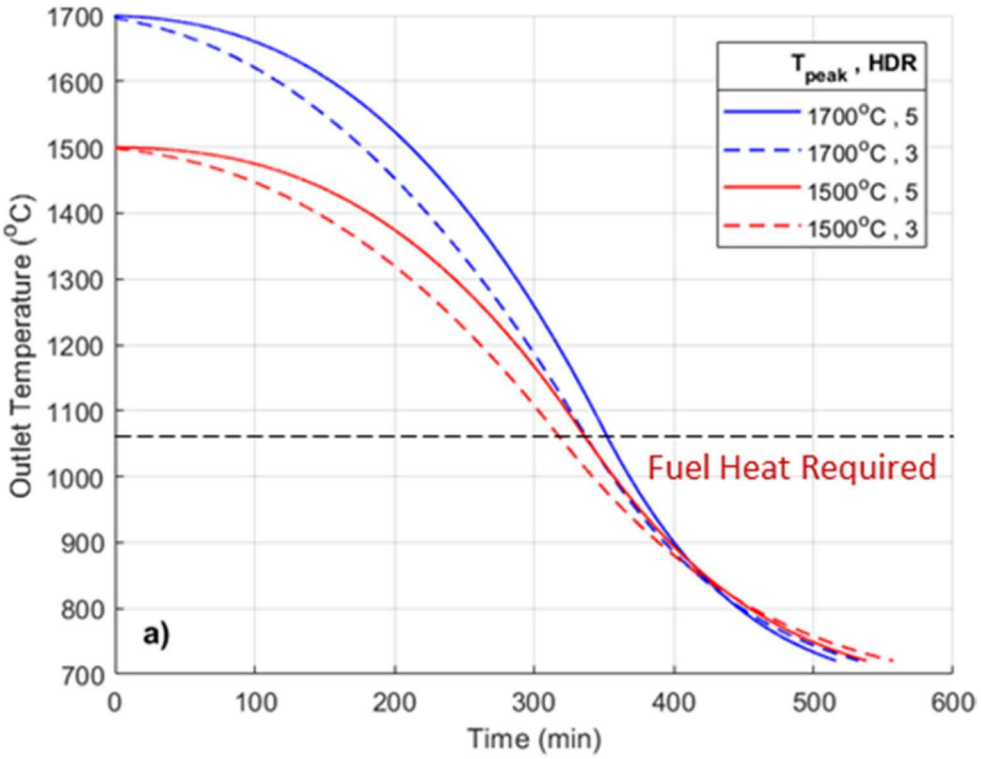

Figure 2-10: Discharge results for FIRES design under Mk1 PB-FHR Power Plant RACC[35]

Due to the significant similarities to components already utilized in industry, it is more difficult to assign a TRL. It could be argued that this component of the RACC has a higher TRL compared to the other components, but since repurposing a cowper stove as a FIRES TES has yet to be tested, FIRES has been assigned a TRL of 5. This places it in the middle of the 'bridge between scientific research and engineering' where the system is 'almost prototypical'.

2.2.4 HRSG and System Controls

Using THERMOFLEX®, a triple pressure reheat HRSG was designed for the Mk1 PB-FHR power plant RACC. The HRSG was sized for the maximum operating conditions during cofired operation. However, in order to maintain sufficient flow rates in base-load operation a control valve is necessary on the ST to set a "low-flow set point pressure." Table 2-7 shows the pressures for base-load and cofired operation for the triple pressure reheat HRSG ST[18].

Table 2-7: Steam cycle pressure selection[18]

	Baseload	**Cofired**	
High-pressure	6.0	20.8	MPa
Intermediate pressure	1.5	3.0	MPa
Low pressure	0.25	0.5	MPa

Conventional HRSGs operate with very little active control outside of startup and shutdown. However, one of the key features of the RACC is its ability to load follow and operate in baseload and peaking modes. Therefore, it is necessary that the HRSG cycle between high-pressure and low-pressure operation, with fluctuating air inlet temperature. Currently, only steady state analysis of the RACC has been performed to see how the RACC will perform in baseload and peaking modes.

Much research has been done to develop dynamic simulation for power plants [37]–[42]. Dynamic simulation provides insight into optimization of the design and operation of a system. It also allows for the development of "Digital Twins" to be used for training and health prognosis and diagnosis of systems.

Dynamic simulation is needed for the RACC and the HRSG in particular to fully quantify the value of the RACC. There remain multiple scenarios that need to be characterized before the RACC will be ready for commercialization. These scenarios include start-up, shutdown, and ramping between baseload and peaking modes. Characterizing these scenarios is necessary for extending the life of equipment by avoiding excessive thermal cycling and undesirable phenomena such as salt freeze in the CTAH. Fully understanding the dynamic behavior of the RACC will also provide greater insight into the increased revenue of an RACC compared to a traditional NGCC. Moreover, in order to maximize profitability of the RACC, an optimized balance between baseload, energy storage, and peak power must be reached. This requires sophisticated price forecasting and thorough understanding of RACC dynamics to fully utilize the flexibility of the RACC.

Heat recovery steam generators are a mature technology that are commonly used in industry. However, the system control of the RACC, and the HRSG in particular, represent a novel challenge. While dynamic simulation of power plants is common in academia and industry, dynamic simulation of the RACC has not been performed prior to the work in this dissertation. The TRL of HRSG is 9 since it is a fully developed technology, while the dynamic control of the RACC including the HRSG is a TRL 3 since work is still ongoing to prove the feasibility of RACC dynamic operation.

2.3 Conclusion and Dissertation Focus

The TRL of the RACC components are listed below in Table 2-8 .

Table 2-8: RACC individual component TRL

	TRL
CTAH	4
Modified GT	2
FIRES	5
HRSG	9
System Control	3
RACC average TRL	4.6

The University of California, Berkeley Nuclear Engineering department, Thermal Hydraulics Lab is uniquely qualified to aid in the development of the RACC. Our lab has experience with multiple modeling software commonly used in the power industry. We also have experience building and operating IETs as well as designing and performing experiments at prototypical conditions of the RACC. The goal of the lab is to "transform the future of nuclear energy by enabling innovation through understanding best practices of other technologies such as biotech, commercial aviation, and commercial space launch." The lab is focused on rapid prototyping iterations to drive innovation and driving down costs. This allows for nimble changes in the design process while gaining experiential knowledge.

The first area of focus for this dissertation is the development of the CTAH. A key factor in driving down the cost and therefore ensuring the economic viability of the CTAH is the ability to use more affordable materials while still maintaining a sufficiently long operation lifetime. Therefore, this dissertation will describe the design of an autoclave using the materials that could potentially be used for the construction of the CTAH. Experiments were performed in this autoclave on samples which emulate the interior components of the CTAH. By operating the autoclave at elevated temperature and pressure, we can accelerate the damage to the samples to predict performance at prototypical conditions. The goal of this work is to participate in bringing the technology readiness level of the CTAH from a 4 to a 5 by performing lab scale experiments which are near prototypical conditions.

The second area of focus is the RACC system operation and control. As previously stated, optimized control of the RACC is key to performance optimization. Therefore, it is necessary to understand the dynamic performance of the RACC in order to develop optimal control schemes. A dynamic model of the RACC was created to evaluate the performance of the RACC. This dynamic model was also implemented into a hardware-in-loop simulator, the Advanced Reactor Controls and Operations (ARCO) facility. This will bring the TRL of the RACC system control from a 3 to a 4.

3 CTAH-VACE

In order to determine the lifetime reliability of the CTAH design, an experimental facility needed to be developed to simulate the prototypical thermal-creep conditions of the desired power conversion cycle of interest. Initially, plans had been made to also use this autoclave to test other working fluids as well as air. The most extreme of which was supercritical CO_2 which would operate at 500°C and 20MPa, and therefore the facility was initially designed with these parameters in mind[43]. Unfortunately, after the experimental facility was procured and assembled, it was discovered that it was incapable of reaching the desired temperature and pressure simultaneously due to heat losses. Fortunately, the facility was able to be back fitted in order to simulate prototypical RACC conditions.

For the RACC, the prototypical conditions are 700°C and 2 MPa. However, it was decided that the operating conditions of the facility could be elevated to 900 °C+ accelerating the effects of thermal creep on the tube-to-manifold joint samples for study. Consequently, the pressure vessel needed to be able to withstand pressures of up to 2+ MPa at temperatures in excess of 900°C. While significantly hotter, the order of magnitude reduction in pressure allowed us to safely use the experimental facility to perform thermal creep testing and obtain initial results.

This chapter will detail the design of the experimental facility, including the back fits implemented for testing RACC conditions. This chapter will also discuss the manufacturing of the samples tested. A description of the experiment methodology as well as the initial results and recommendations for future work will also be presented.

3.1 Design of Experiment

3.1.1 Vessel Design

High temperature and high-pressure vessels are commonly used in various research and industrial processes. For instance, Hot Isostatic Pressing (HIP) units which are used for reducing porosity in metals and increasing density of ceramics can reach temperatures over 1300 °C and pressures ranging from 50 MPa to 100 MPa. Alternatively, many labs use autoclaves for sterilization. Typical autoclaves do not exceed 200 °C and 1 MPa. Both of these commercial systems lay outside of the prototypical conditions required to test CTAH tubesheet joints for thermal creep. The design, control, materials, and operation duration also differ significantly from those of a prototypical CTAH as well, further limiting the potential learning from testing.

It was determined that an experimental facility needed to be designed in order to investigate the feasibility of the CTAH design. This experimental facility was named the CTAH Vessel and Accelerated Creep Experiment (CTAH-VACE, hereafter referred to as just VACE). Designing VACE also allowed us to investigate the feasibility of using lower-cost materials in plant structural facilities, so the VACE vessel was designed with low-carbon steel as the target material, using internal insulation. Additionally, all structural facilities at an actual power plant would need to adhere to ASME Boiler and Pressure Vessel standards, so the vessel was designed according to the stipulations of the ASME Code. Designing VACE according to the Code regulations served another purpose of providing the Thermal Hydraulics research group with familiarity in designing ASME-certified pressure vessels. The lessons learned during the design

of VACE could prove very enlightening for future attempts at producing ASME-code compliant, internally insulated vessels for experiments and CTAH heat exchangers.

As previously mentioned, inspiration from the oil and gas industry was taken to design a low-cost high temperature pressure vessel. Fluidized catalytic cracking units (FCCUs) operate at 700+ °C and up to 5MPa, which is comparable to CTAH operating conditions. FCCUs are constructed with low-cost low carbon steel because they use internal insulation that allows the pressure boundary to operate at reduced temperature. Therefore low-carbon steel was chosen for the VACE autoclave material in order to evaluate the feasibility of using lower cost materials in actual plant facilities[29]. Additionally, to reduce costs, stock pipe materials were selected for the autoclave body in order to reduce complexity during fabrication. The main components consisted of a seamless pipe section, a pipe cap, a raised-face weld neck (RFWN) flange, and a corresponding blind flange. These components would then be welded or bolted together to create a pressure vessel. After the design was completed, it was sent to a vendor for review and ASME certification.

The initial design of the autoclave began with sizing the heater necessary to reach testing conditions for supercritical CO_2. In this case, temperatures would only reach 700 °C, however the pressure would reach 20 MPa. Preliminary calculations determined that the heater required to heat the samples to 700 °C would heat the shell of the autoclave to 110 °C. This then served for the constraint for sizing the dimensions of the vessel. For the initial design, 8" Nominal Pipe Size (NPS) – Schedule 120 stock pipe was chosen because it provided sufficient clearance at its inner diameter to fit the samples, heater, and insulation. It also provided a safety margin based on its rated pressures. Eight-inch Schedule-120 piping has an outer diameter of 8.625 inches, inner diameter of 7.187 inches, and a wall thickness of 0.719 inches. A schematic of the VACE vessel design is shown in Figure 3-1 and a picture of the installed vessel in Figure 3-2 .

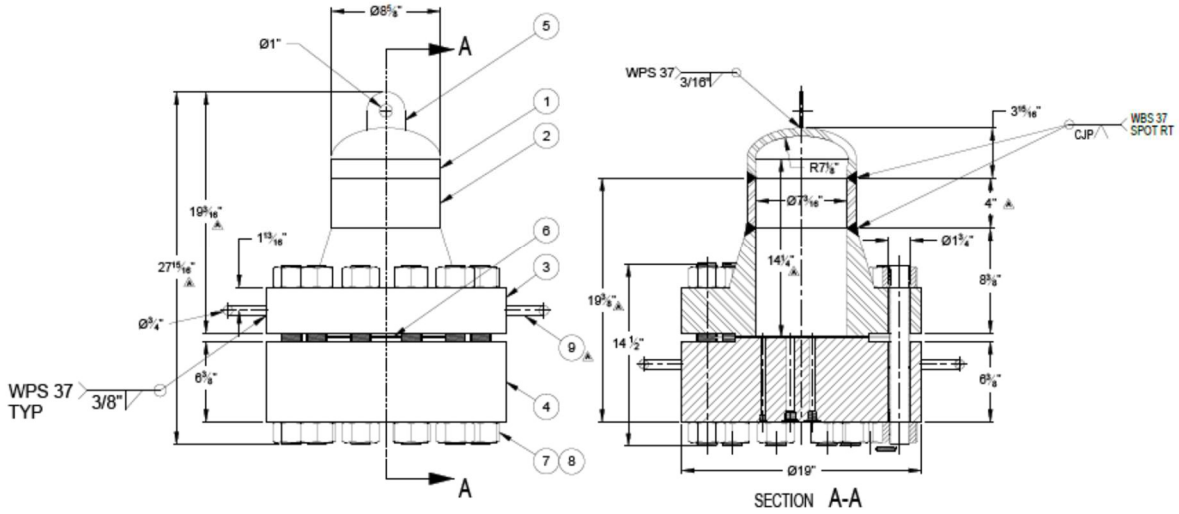

Figure 3-1: VACE Vessel Design Drawing provided by Johansing Iron Works[43]

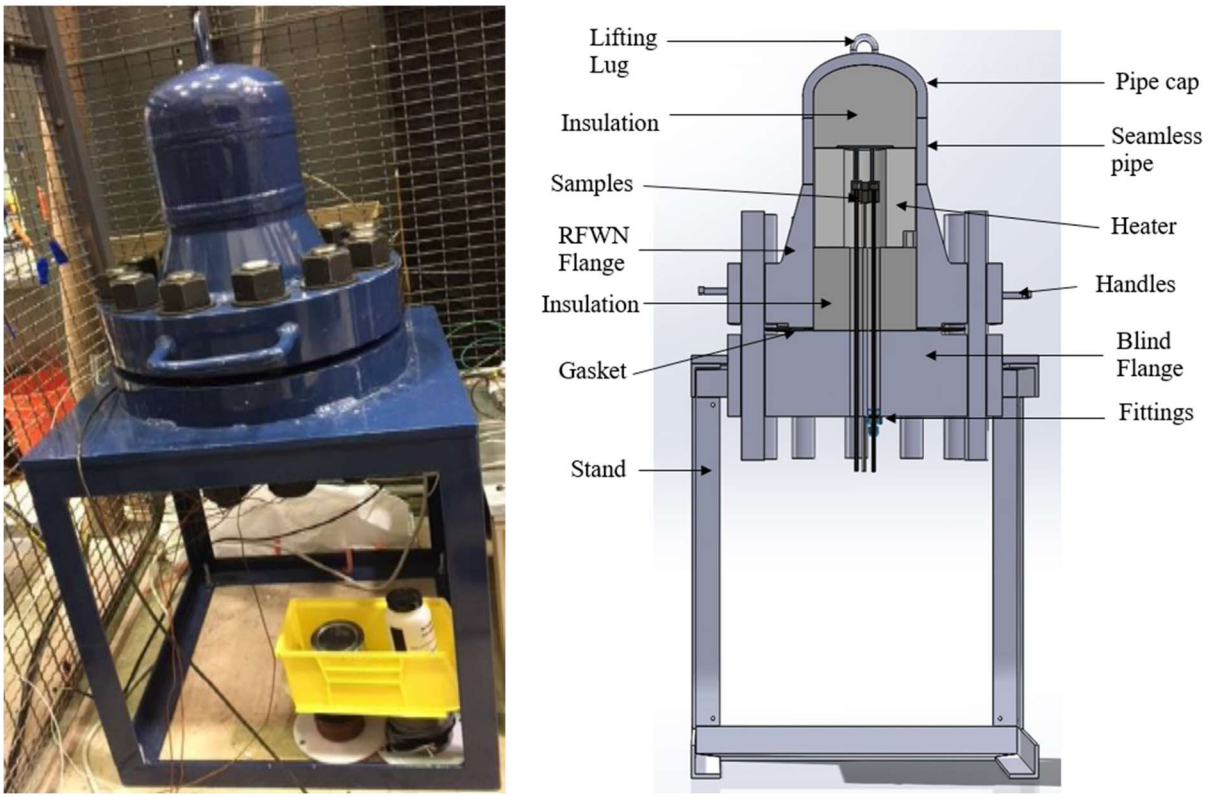

Figure 3-2: VACE Vessel assembly and labeled schematic

Thermocouples were placed through the interior of the vessel as indicated in Figure 3-3. The vessel was to be pressurized by filling the vessel with CO_2 at room temperature to a pressure below the final intended pressure and then heating the CO_2 to raise the pressure to the desired value.

Unfortunately, it was discovered during shakedown testing of VACE that the heater calculations didn't fully account for convective heat transfer caused by natural circulation, and the ceramic fiber insulation chosen did not perform well to suppress natural circulation when operating with high-pressure gas. This prevented the autoclave from reaching the necessary operating temperature and pressure simultaneously, while keeping the wall temperature within safety limits (either temperature or pressure could be reached independently, but not together). This is illustrated in Figure 3-4. It shows the temperature center of the vessel and on the outside of the internal insulation or the inner shell wall of the vessel. Low initial pressures allowed us to exceed the necessary temperatures, while maintaining a safe vessel wall temperature. However, increasing the density of the gas within the vessel reduced the steady state temperature near the center to below the desired experiment parameters and raised the wall temperature to the maximum allowable temperature. This was confirmed with thermal imaging, shown in Figure 3-5.

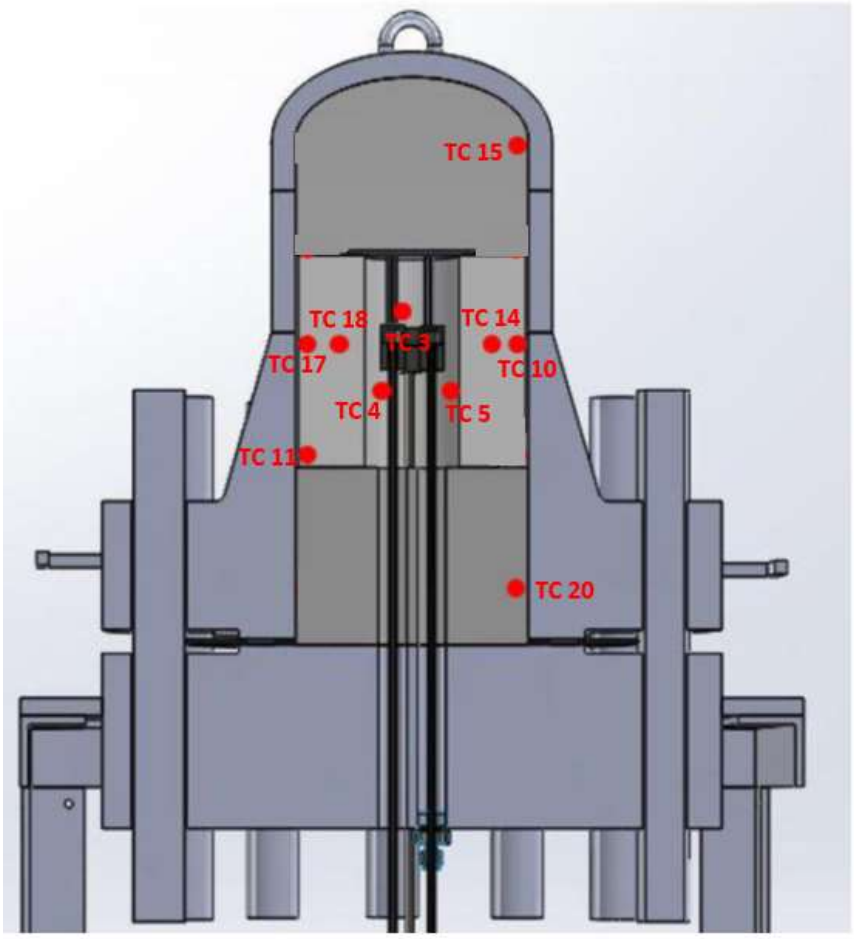

Figure 3-3: Thermocouple placement within VACE Vessel

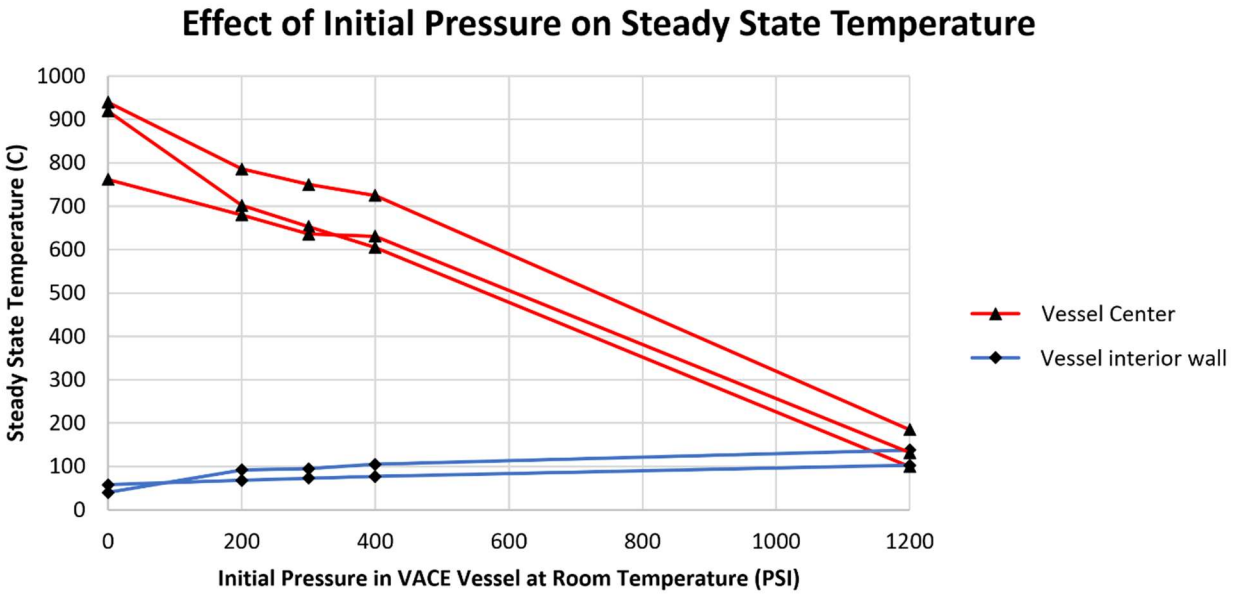

Figure 3-4: Effect of Initial Pressure on Steady State Temperature

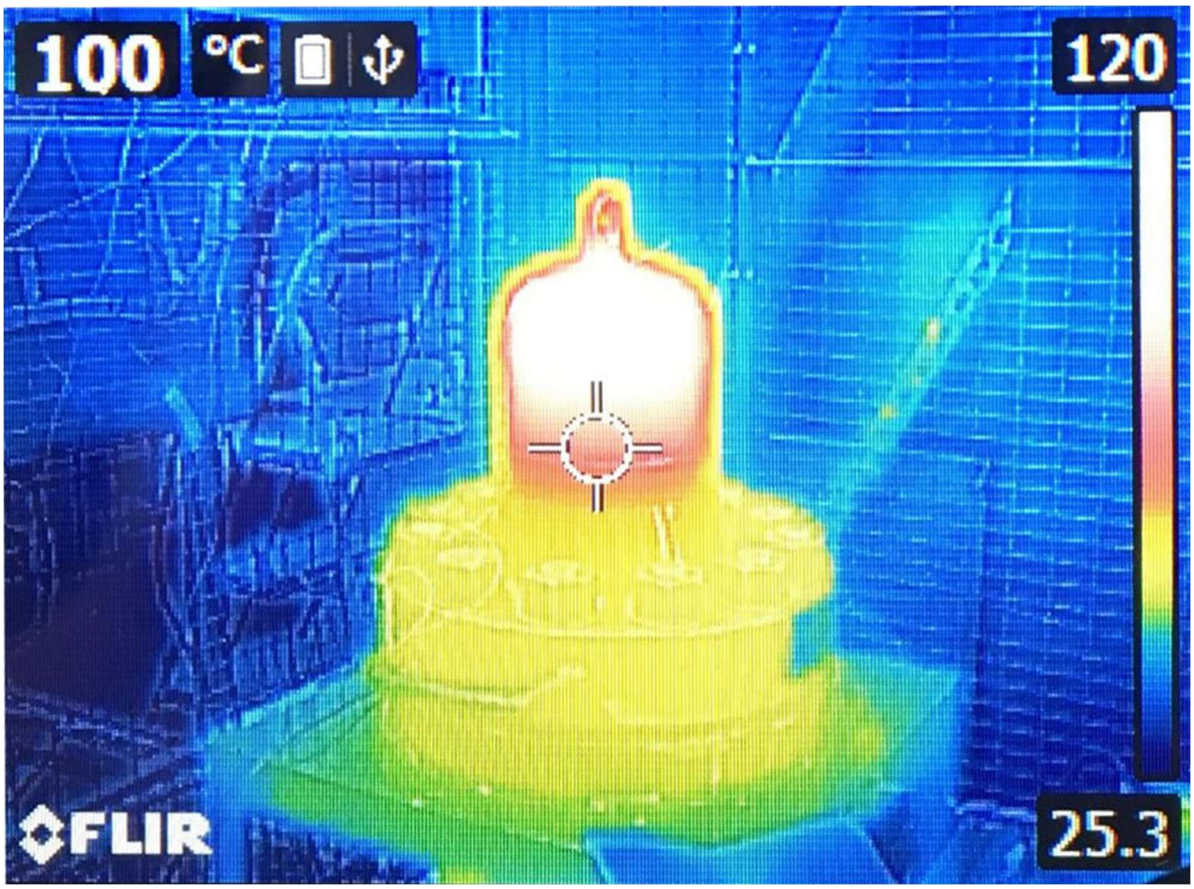

Figure 3-5: Thermal imaging of VACE Vessel during Shakedown testing

Since this was discovered after the vessel had been constructed, a new heater was designed, and new insulation chosen with the constraint that the vessel dimensions and temperature limits were fixed. The goals of the new heater and insulation design were to:

1. Limit convection heat transfer
2. Maximize the power output of the heater to the samples
3. Identify and install insulation with good performance at high-pressure

3.1.2 Heater and Insulation Redesign

To suppress convective heat transfer, an alumina tube, capped on one end, was chosen to be the structure that an updated heater element design would be built on. Alumina has a relatively low thermal conductivity, low thermal expansion, and low permeability, making it an ideal choice to hold the heater. The dimensions of the tube were chosen such that it would have the minimum surface area required to provide enough volume for the heater and samples, thus maximizing the power density of the heater. The first constraint for power output was the voltage and current ratings of our power source. Typical US power outlets provide 120V with a max current of 15A. The second constraint was the length of heater element wire that would fit inside the alumina tube. We then chose the thickest gauge nichrome wire that would fit within these constraints. The nichrome wire was coiled around six alumina lattice bars and then attached to the inner wall of the alumina tube with high temperature ceramic adhesive. The alumina lattices

were machined using waterjet cutting. The design specifications of the heater are shown in Table 3-1. The finished heater is shown in Figure 3-6.

Table 3-1: VACE Heater Specifications

Heater Element Material	Kanthal A-1	
Heater Element Length	≈8.25	Feet
Heater Element Gage	18	
Heater Element Resistance	0.54	Ω/ft
Alumina Tube Outer Diameter	3.5	Inches
Alumina Tube Inner Diameter	3.25	Inches
Alumina Tube Wall Thickness	0.25	Inches
Alumina Tube Height	6.0	Inches
Heater Power	≈1650	Watts

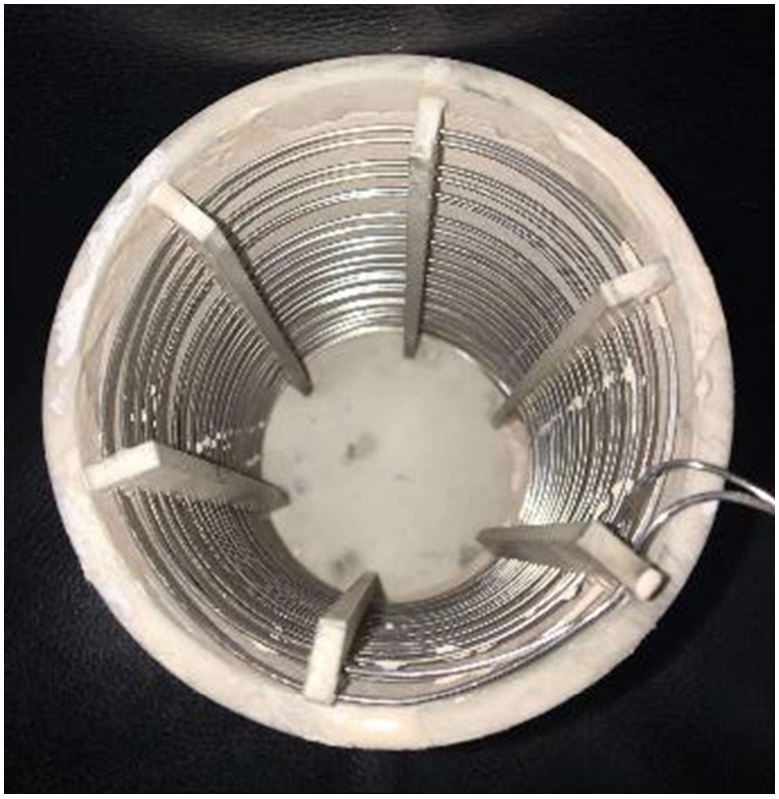

Figure 3-6: VACE Heater

Firebrick was chosen as the internal insulation. It is a common refractory material used in FCCUs. While not the most thermally resistive insulation, it performs well at high-pressure, and has more structural integratory compared to other refractory materials. The firebrick was machined using water jet cutting. Figure 3-7 shows the heater, alumina tube, and insulation installed in the VACE vessel prior to closing the vessel.

Figure 3-7: Firebrick insulation surrounding alumina tube

3.1.3 Gas Supply

A gas control system was developed to supply and discharge gas from the autoclave. This system was designed based on recommendations made by the Office of Environment, Health and Safety (EHS) at U.C. Berkeley. As with the vessel itself, the system needed to withstand the desired operating pressures of 2 MPa and 900°C with adequate safety margin. The design characteristics influenced by the EHS recommendations included the following characteristics:

- Instrumentation and control system would be used to automatically monitor heat and pressure
- Gas cylinders used for supply will be installed in support stands bolted to the building structure and safely stored
- Piping and electrical utilities will be protected from accidental impact and designed to minimize snag potential/trip hazards
- Fail-safe control logic will be installed and verified to shut off gas supply and electrical power, and vent the pressure vessel to the atmosphere if operational parameters shift outside safe control set points

To supply gas to the vessel, the gas cylinders would be directly discharged into the pressure vessel until a desired internal pressure was obtained at the gas equilibrium temperature. This desired pressure would be calculated to achieve a target pressure at elevated temperatures after the autoclave achieved steady-state heating.

Gas is supplied by a 6000psi (41.4 MPa) Argon gas cylinder. During operation the gas cylinder remains open with the regulator set to 300 psi (2.07 MPa). Downstream of the regulator is a solenoid valve followed by a needle valve which is used to more finely control line pressure downstream of the pressure regulators. A manual bleed valve is installed downstream of the needle valve to be used during start up procedures. Prior to beginning experiments, the bleed valve discharge line will be opened and used to evacuate the vessel and the supply lines of unwanted air using a roughing vacuum pump.

Downstream of the needle valve and bleed valve is another solenoid valve used to further isolate the vessel from the supply system. Downstream of this valve is the vessel. There is another line leaving the vessel to another solenoid valve that vents to atmosphere in the event of overheating or over pressurizing the vessel. There is also a pressure relief valve in the event that the solenoid valve fails to open. The autoclave experiment is designed to operate for weeks at a time; thus, solenoid valves were chosen so they could be controlled remotely via digital connection.

3.1.4 Data Acquisition and Control

The final iteration of VACE used five thermocouples to monitor temperature, one on the samples, one in between the alumina tube and firebrick insulation, two between the firebrick insulation and vessel wall, and one on the exterior of the vessel. VACE also has one pressure transducer and one mechanical pressure gauge.

Control of the components used National Instruments' LabVIEW System Design software and data acquisition hardware. Wireless Data Acquisition and Control modules were chosen to allow the operator to operate the experiment from a safe distance. Components that are controlled by LabVIEW are the solenoid valves and the autoclave heater. Measurements from the thermocouples and pressure transducers were compared against programmed safety limits and operator determined set points. Signals were then sent to a microcontroller with high current relays to open or close the valves and to turn the heater on or off. The 'exit' solenoid valve was normally open, meaning during an experiment, if the pressure inside the autoclave exceeds the desired set point or safety limit, or if power was lost to the valve or microcontroller the valve would open. The two upstream valves were both normally closed, so in the case of loss of power, the Argon supply would be isolated. The relay for the heater was also configured such that if power was lost to the microcontroller, the heater would turn off.

These passive safety features were important from the standpoint of UC Berkeley EHS because they ensure that the test facility would revert to a safe, depressurized, non-heated operating point in case electricity cuts off. Apart from the solenoids, all other valves within the test assembly were manually operated.

3.2 Sample Manufacturing and Modeling

The most vulnerable location to experience failure due to creep deformation in the CTAH is the tube-to-tubesheet Joint. Therefore, samples were designed to mimic this joint, as shown in Figure 3-8. Samples were designed according to ASME TEMA standards[31]. Sample dimensions are shown in Table 3-2.

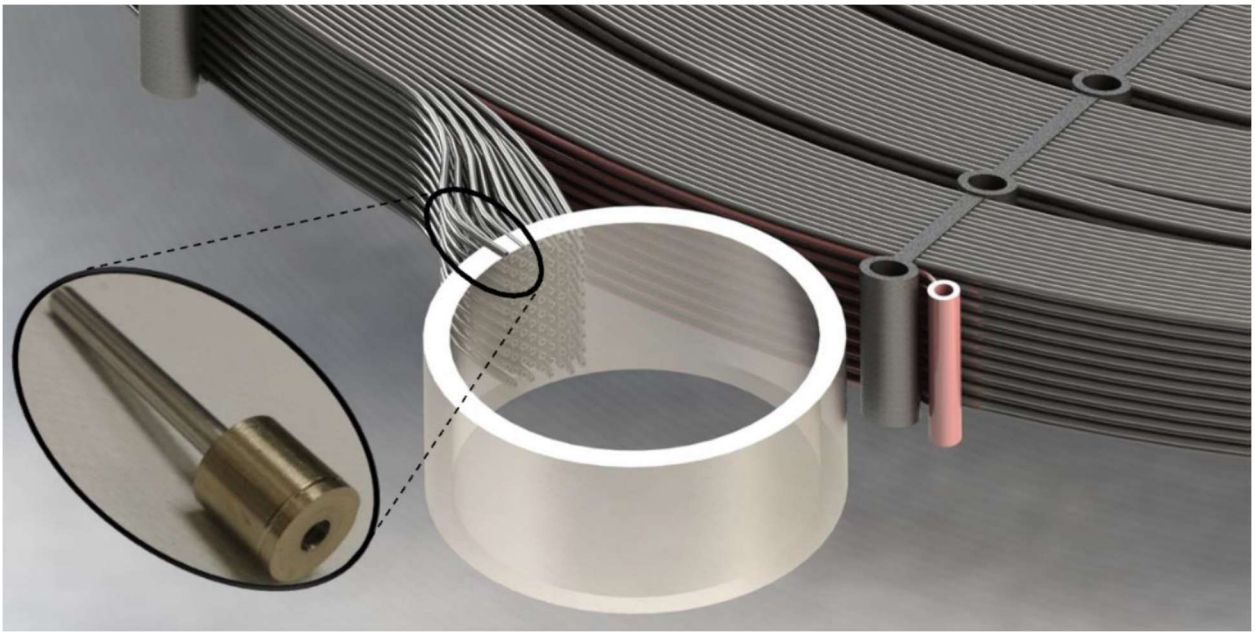

Figure 3-8: CTAH tube-to-tubesheet joint graphic with highlighted joint test sample.

Table 3-2: VACE Sample Dimensions

Tube Outer Diameter	0.253	Inches
Tube Thickness	0.051	Inches
Collar Outer Diameter	0.75	Inches
Collar Hole Diameter	0.259	Inches
Tube and Hole Clearance	0.006	Inches
Collar Length	0.75	Inches
Cap Outer Diameter	0.75	Inches
Cap Inner Diameter	0.5	Inches
Cap Length	0.5	Inches
Expanded Tube Inner Diameter	0.169	Inches
Sample length	20.0	Inches

ASME TEMA standards as well as industrial best practices were followed during the manufacturing of the Samples[31]. Sample tubes were welded to the sample collar prior to expansion to ensure the surfaces were clean, allow for a path of escape of welding-generated gases, and to provide the maximum desirable root gap for the material being welded. This allows for the ability to repair welds that have failed in service [44]. Tubes were expanded to the length of the collar minus 1/8” using tube rolling technique. A cap was welded onto the collar of the sample to create a pressure seal. Finally, samples were pressurized to check for leaks. The finished sample and schematic of sample are shown in Figure 3-9.

Figure 3-9 : Finished Sample and Sample Drawing. Fitting on the right is for sealing the connection to the VACE Vessel

Modeling was performed using COMSOL Multiphysics®[45]. COMSOL is a finite element analysis, solver, and Multiphysics simulation software. COMSOL was used to map the von Mises stress in a sample during VACE operation. The criterion for yield failure is that the von Mises stress exceeds the material's yield strength.

The model dimensions matched the dimensions of the actual sample other than capping the tube end in order to have a pressure differential in the model, something not needed in the physical samples. The tube and collar were joined together as one domain. The weld was assumed to be 1/32 inch deep with a 0.049-inch bead on top. A 1 μm gap was made over the un-welded length between the tube and the collar. Since the top of this gap was exposed to the exterior pressure of 2 MPa, the pressure was extended down into the gap and applied to all of those surfaces. Results for Von Mises stress mapping are shown in Figure 3-10. As expected, there are stress concentrations at the connection point between tube and collar[43].

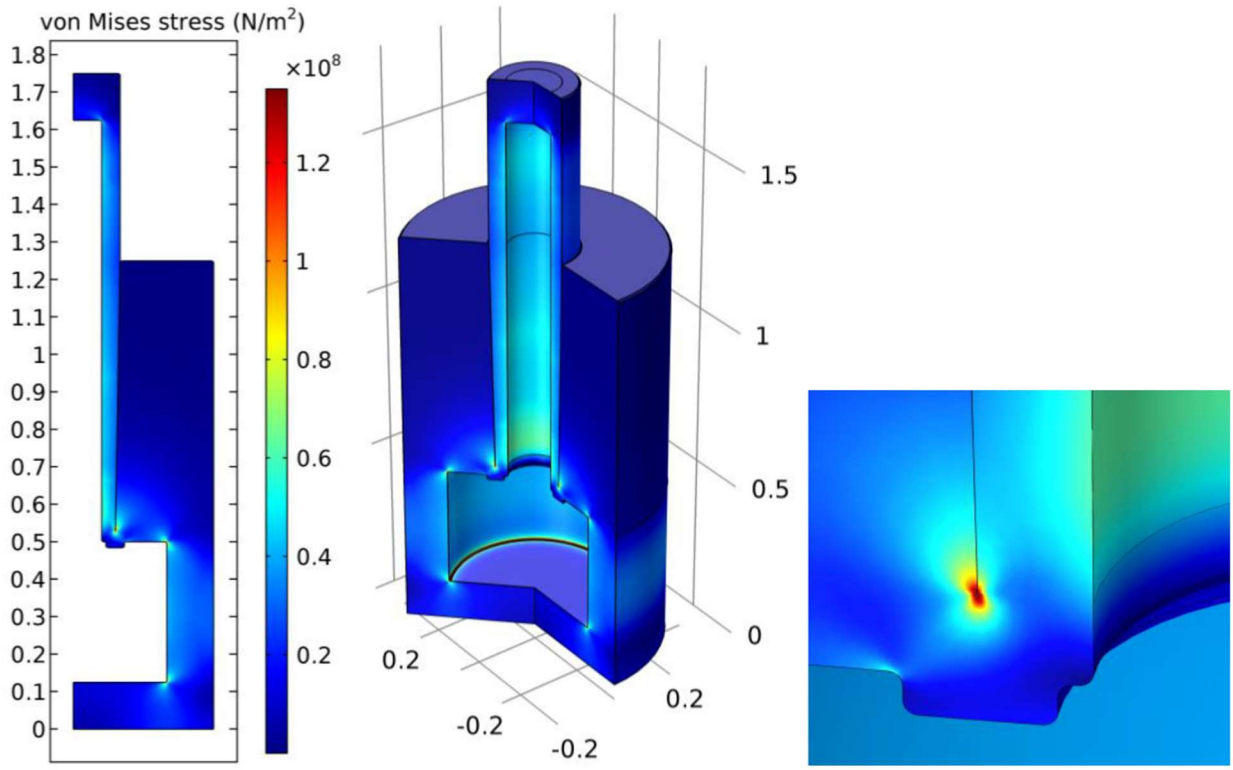

Figure 3-10: Von Mises stress Mapping on VACE Samples[43]

To determine how long the samples needed to be tested to correspond to a 30-year in-service life time, we used the Larson-Miller relationship [46], which comes from the observation that the creep rate (strain rate) is proportional to the product of the stress (raised to a power that depends on the creep mechanism) and the exponential of the creep mechanism's activation energy (normalized by the universal gas constant and the absolute temperature):

$$\frac{\partial \varepsilon}{\partial t} \propto \sigma^n e^{\frac{-Q}{RT}} \tag{1}$$

Integrating this proportionality with respect to time, while keeping the stress and the creep mechanism constant, produces the Larson-Miller Parameter (LMP):

$$LMP = T(C + \log_{10} t) \tag{2}$$

The LMP is a constant for a given stress level, and thus its value at 700 °C and 30 years can be used to calculate the corresponding duration for 900 °C. The Larson-Miller Constant, C, is typically assumed to be 20, however it can range from 9 to 30 depending on material and operating conditions[47]. Assuming a constant of 20 leads to an experimental time of around 12 hours, and assuming a constant of 9 leads to an experimental time of around 40 days. From this we determined to test the samples for 6 weeks (42 days) or until failure, whichever came first.

This calculation also assumes that the creep mechanism is the same at 900 °C as it is at 700 °C. The assumption is validated by referring to the deformation-mechanism map for SS316 in Frost and Ashby's book [48] shown in Figure 3-11. The map indicates that the creep mechanism likely remains as diffusional flow creep throughout our temperature region. Therefore, our use of the Larson-Miller relationship to calculate the creep acceleration is expected to be valid.

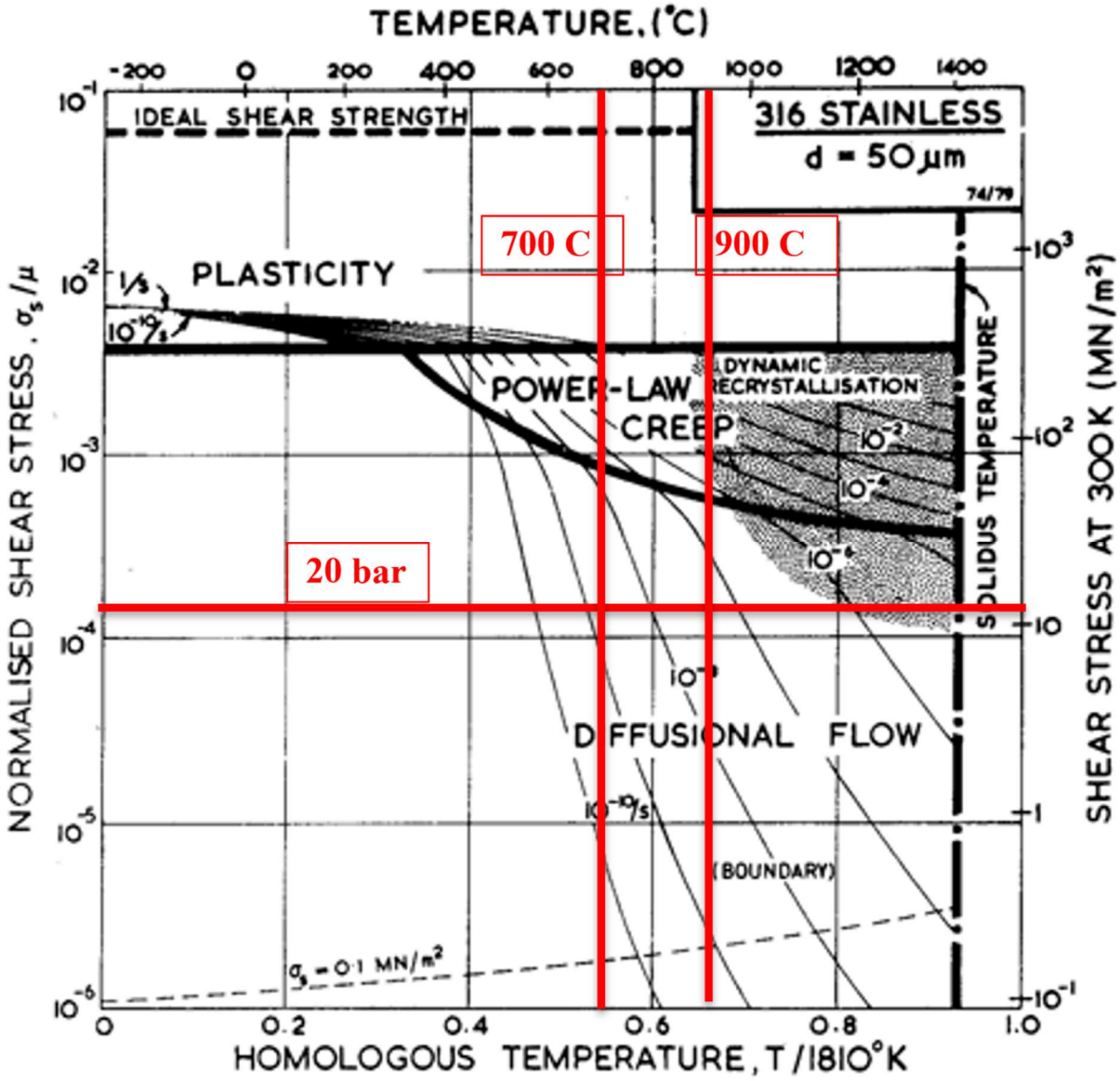

Figure 3-11: Deformation-mechanism map for SS316. Normalized maximum shear stress at an operating pressure of 20 bar at operating temperatures overlaid in red

3.3 Methodology

Three samples were tested in VACE at a time. Analyzing the samples required destroying them and so samples were manufactured in batches of six, three to be tested and three to be used as controls.

Samples to be tested were inserted into the bottom of the vessel and attached to the bottom of the vessel with Conax fittings for a pressure tight seal. This allows there to be a pressure differential across the sample with the inside of the tube being exposed to atmosphere and the outside of the collar being exposed to the high-pressure vessel interior.

A roughing pump was used to pull a vacuum in the vessel to remove unwanted moisture and air. The heater was then activated. Heating the vessel under vacuum ensured that most residual moisture in the insulation would be baked out. The vessel was then cycled through pressurizing and venting argon gas to further ensure displacement of any unwanted air and moisture. This process was critical for minimizing corrosion to the samples. The vessel was then pressurized and heated to VACE operating conditions of 20 bar and 900+ °C. (Due to unknown reasons VACE would fluctuate between 900 °C and 950 °C throughout the day). Once the vessel reached steady state, VACE was left to run for 6 weeks or until sample failure, whichever happened first. Sample failure would be recognized by a sudden decrease in pressure. Argon gas would occasionally be added to the vessel due to small leaks in the system.

After the samples were removed from the vessel, they were visually inspected, followed by a pin drop go/no-go test to determine inner diameter, next they were cut and polished in order to inspect the joint under microscope.

3.4 Results

VACE was operated twice at representative experimental conditions to demonstrate the testing method. During the first operation, an insufficient amount of time was given to bake out the moisture trapped in the insulation. This caused a significant amount of corrosion on the outside of the tubes. Also, since the inside of the tubes were exposed to atmosphere, they also experienced significant corrosion. The first VACE test lasted for 6 weeks before the samples were removed without failure.

For the second round of testing, the bake out time was significantly increased. Also, rather than expose the tubes to air, it was determined that they should be vacuumed and valved off to prevent corrosion. Unfortunately, this test began shortly before the COVID-19 pandemic and due to restrictions placed on on-campus research the test was prematurely terminated after 2 weeks. Once research was allowed to resume it was discovered that the heater had sustained damage that would require lengthy repairs. However, after 2 weeks of testing the results looked promising with very little corrosion.

Figure 3-12 shows the control samples, the samples that were tested for 6 weeks, and the samples that were tested for 2 weeks. Figure 3-13 shows the samples after having been cut. Figure 3-14 shows where the tube meets the collar at 5x magnification. Figure 3-15 shows the section of the tubes that were expanded into the collar at 10x magnification. Figure 3-16 shows the transition from not expanded to expanded. Table 3-3 shows the before and after tube dimensions.

Figure 3-12: Full Samples: Control (Left) 6-week (center) 2-week (right)

Figure 3-13: Cut Samples: Control (Left) 6-week (center) 2-week (right)

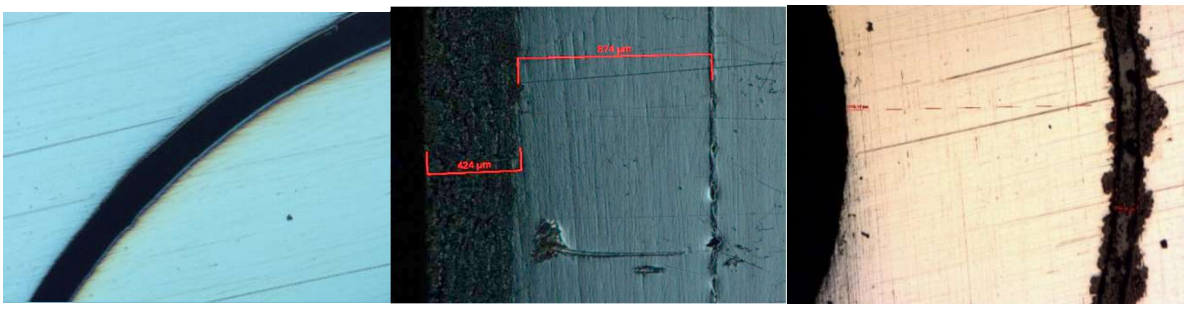

Figure 3-14: 5x Magnified, samples where tube was not expanded. Control (Left) 6-week (center) 2-week (right)

Figure 3-15: 10x Magnified, samples where tube was expanded Control (Left) 6-week (center) 2-week (right)

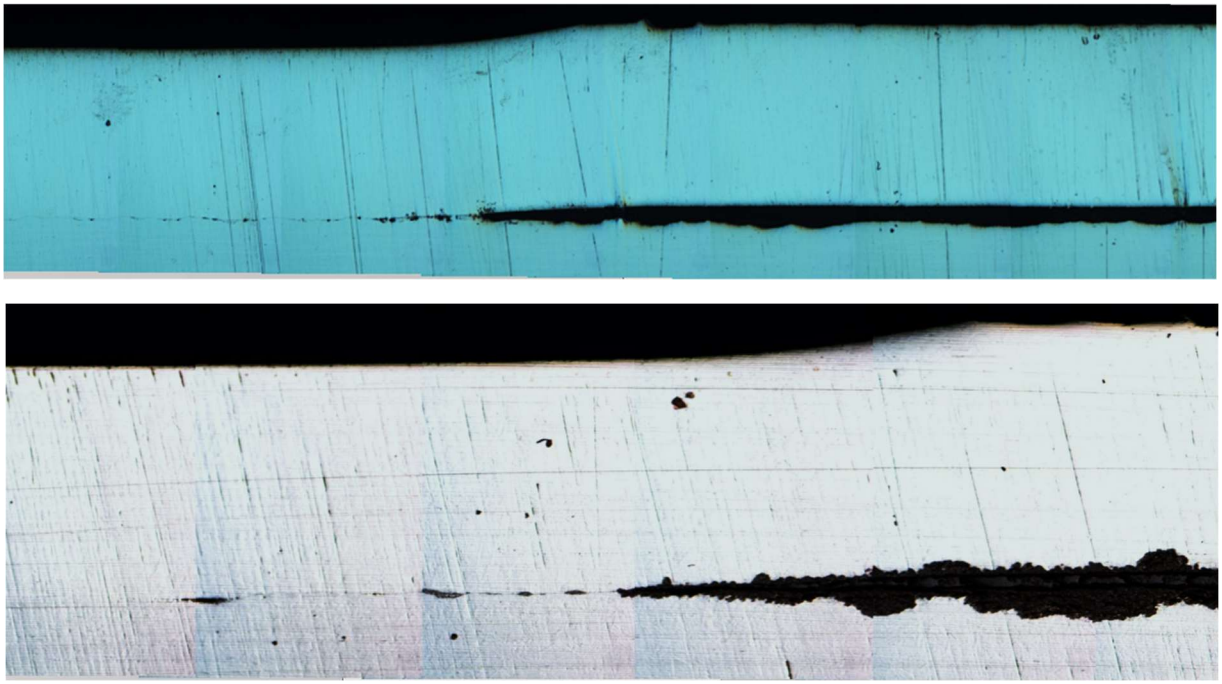

Figure 3-16: Length of tubing that was expanded. The top of the picture is the inside of the tube. The expanded tube is on the left and the unexpanded tube is on the right. Control (Top) 2-week (bottom)

Table 3-3: Sample dimensions, averaged

	Control	6 - week test	% change	2 - week test	% change
Tube Outer Diameter	0.2523	0.2433	3.57%	0.2518	0.20%
Tube Inner Diameter	0.1610	0.1483	7.87%	0.1590	1.24%
Expanded Tube Inner Diameter	0.1773	Not Measured	Not Measured	0.1750	1.27%
Collar Diameter	0.7500	0.7330	2.22%	0.7367	1.78%

3.5 Conclusions

Future work is necessary in order to determine if CTAH tube-to-tubesheet joints can sustain more than the 1% creep deformation limitation set by ASME B&PV codes. Pending repairs to the VACE heater, VACE will be able to continue to test this hypothesis. However, the fact that even with significant corrosion the samples did not fail makes a strong case that tubes loaded in compression can sustain much higher stress and tolerate thermal creep for much longer periods of time without failure.

It is also strongly recommended that sample geometry be adjusted. Using a larger, thinner walled tube would likely take less time to accumulate substantial creep deformation and would allow for the option to insert a small heater into the collar to have very localized heating of the sample. More localized heating would likely mean that less power would be necessary to reach operating conditions and more internal insulation could be used, allowing higher pressures to be reached.

4 RACC System Modeling

4.1 Motivation/Introduction

As mentioned in previous chapters, one of the primary reasons for the development of the RACC is to provide greater flexibility to previously inflexible power sources such as nuclear and solar thermal. Flexible operation provides stability to the grid and has the financial benefit of taking advantage of large electricity price fluctuations. Validation of the ability to load follow is necessary to justify the continuation of development of the RACC. Moreover, the RACC has an unconventional control method compared to typical combined cycle power plants, requiring investigation into the dynamics to develop the necessary control logic. Finally, it is also important to quantify the economic advantage to load following, if any compared to other power sources.

In this chapter, a review of the results from previous steady state models will be presented. A brief discussion on the choice of modeling software for this study will be presented, followed by a description of the dynamic model along with potential controller logic. Results from the proposed controller logic will be presented. Finally, future work will be suggested.

4.1.1 Previous Modeling Results

The UC Berkeley Nuclear Engineering Thermal Hydraulics lab has performed steady state performance analysis for the RACC using THERMOFLEX, a heat balance modeling and engineering design commercial software. This analysis was done in part of a larger effort to develop the preconceptual design the Mark 1 Power Plant, which is a power plant that utilizes a small modular nuclear reactor (SMR) called the Pebble-Bed Fluoride-Salt-Cooled High Temperature Reactor (PB-FHR). The Mk1 PB-FHR uses nuclear energy to produce 236-MWth to heat molten Fluoride salt to 700 °C. The coupled RACC power conversion system would use a modified gas turbine comparable to the GE 7FB in performance. Therefore, using THERMOFLEX, the values for efficiency, PR, and mass flow were derived for modeling of the modified GT. This study predicted the overall optimized RACC using the modified GE 7FB has a baseload operation net electric efficiency of 42.5% with an output of 100 MWe, and peaking performance efficiency of 66.4% with an output of 241.8MWe. This study also determined the Specific Capital Investment for the baseload 100MWe is $4,500-$5,100/kW which is reduced to $1,850-$2150/kW when accounting for the 142MWe of added output from co-firing. It is significantly reduced since all the required infrastructure is already accounted for. These values were reported separately for the Mk1 because the economics should be compared to a weighted average capital cost combination of standalone nuclear and NGCC. The results of this study as well as the Mk1 design became the benchmark for future dynamic models.

The Mk1 PB-FHR was designed such that up to 12 units could be built at the same site and require the same number of staff. Thus, the fixed operation and maintenance (O&M) costs can vary depending on the number of units built at a specific site. The fixed O&M costs are predicted to range from $29.65 - $70.88[18]. Variable O&M costs for the Mk1 consist of nuclear fuel and natural gas. Natural gas costs around $3.47/MWh with a 1.2-4x multiplier when operating in load following regime[49]. Since the Mk1 is able to significantly reduce the number of warm and cold starts with thermal energy storage and with low baseload operating costs, a

peaking cost multiplier of two was chosen for this study. There remains some uncertainty regarding the cost of nuclear fuel for the Mk1 since it does not use the typical fuel rods used in other nuclear power plants. This study uses the high end estimate of $16.91/MWh[18].

4.1.2 Choice of Modeling Software

Many dynamic modeling software programs exist, each with their own strengths and weaknesses. While not able to evaluate and compare all these programs, for this project the following three programs were chosen for evaluation, Apros, Dymola, and Simulink.

It was determined that Simulink and Dymola would not be used for the RACC dynamic model. Simulink was the least expensive option since all UCB students have access to it for free, it also uses a user-friendly interface. However, it lacks some desired functionality and does not include an extensive library of thermopower components. Dymola is a commercially available software built using Modelica. While Dymola offers a considerable amount of customization, it was discovered that many of the available component libraries did not contain everything needed for this simulation, requiring the user to build custom components, or mix components from multiple libraries. These are advanced techniques that were deemed unnecessary due to the availability of more user-friendly software.

Apros was chosen as the software of choice to develop the RACC dynamic model. Apros is a commercially available thermal hydraulic dynamic simulation software with wide use in industry for integrated thermal power plant process and automation design and engineering. It features a user-friendly interface, and comprehensive tutorials for first time users. It also features a large library of power plant components while also providing the flexibility to create custom components. It also features a large library of fluid and structural material properties with the ability to add user defined materials. It also has the capability of finely tuning the speed of simulation to be faster or slower than real time. Finally, it is capable of interfacing with other software via Open Platform Communication (OPC) communication[50].

Apros utilizes a high fidelity thermal hydraulic solver, solving the dynamic conservation equations for mass, momentum, energy, and mass fractions. These conservation equations are solved simultaneously for the entire model network. These equations are discretized, and non-linear terms are linearized before solving the pressures, flow velocities, void fractions, and enthalpies. Apros is a physics-based modeling software and is therefore able to capture capacitance, compressibility, and inertia effects which can affect transients in real systems. This is critical to accurately measuring the temperature transients within the HRSG which has large thermal masses in the multiple heat exchangers.

The fundamental building blocks of an Apros model are combinations of fluid volume nodes, heat structure nodes, and branches that connect nodes. An example of a heat exchanger is shown in Figure 4-1. Process models which are made up of process components can be controlled via automation models. Automation models are comprised of measurements, controls & logic, and actuators. An example of how these components come together is shown in Figure 4-2. The middle shows a simple process diagram of a pipe with heat tracing as well as heat loss to the environment. On the right is the node and branch diagram generated from the model. The blue boxes represent the fluid, and the green and red boxes represent heat structure materials,

SS316 and insulation respectively. The red dot on the nodalization represents atmospheric conditions. On the left is the automation model. It consists of a thermocouple placed on the heat structure connected to the center pipe node. The temperature is read into a PID controller. The heat flux output (connected to the bottom of the controller) changes depending on the difference between the set point (connected to the left side of the controller) and the measured temperature.

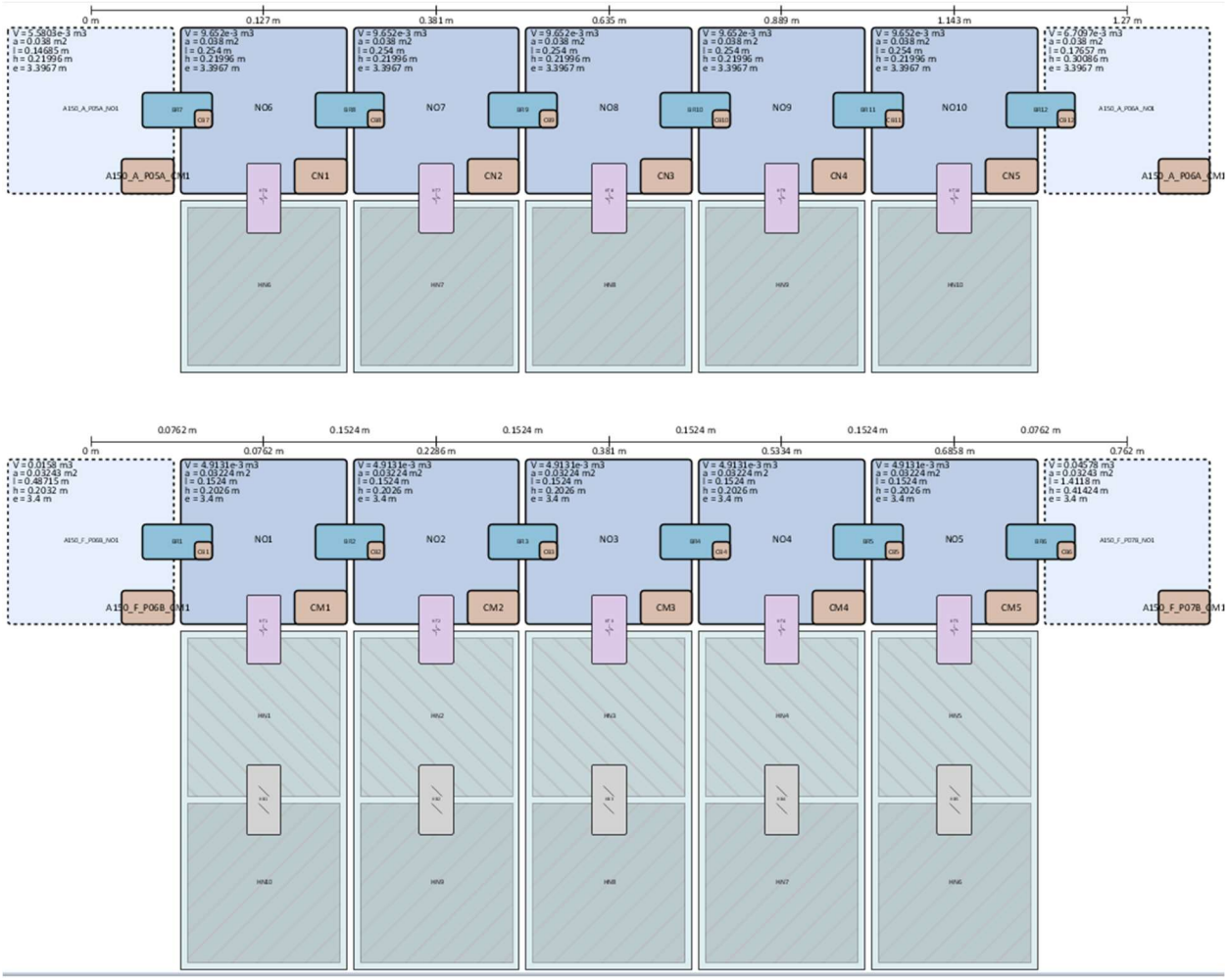

Figure 4-1: Example of a heat exchanger in Apros. It is modeled as parallel pipes connected to a shared heat structure.

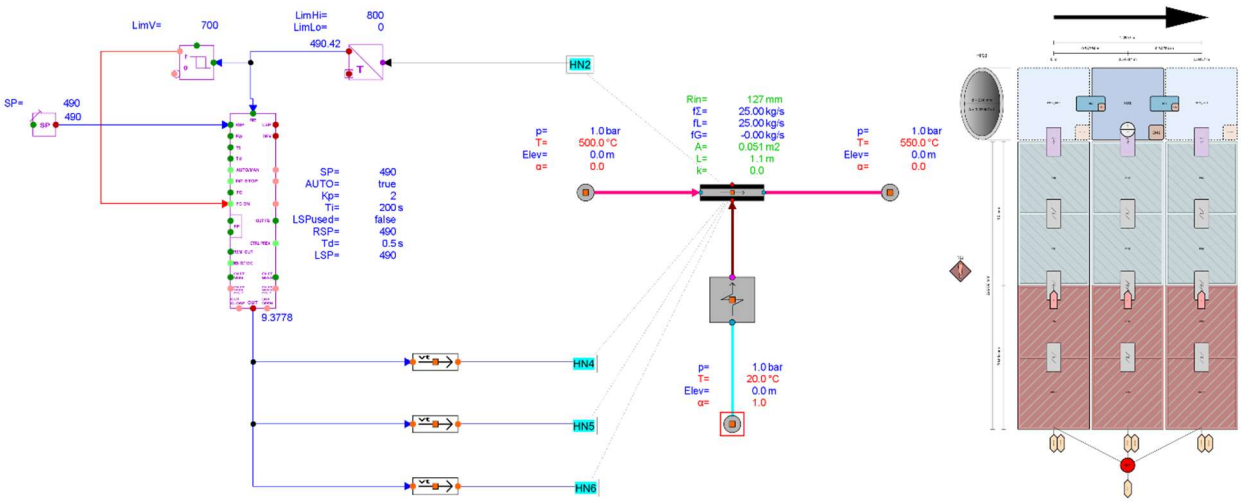

Figure 4-2: Model of heated pipe with heat loss to environment with automation on the left and nodalization on the right

4.2 Description of Models

The following section will describe the model for the various components of the RACC. The modeling philosophy for this model was to replicate as close as possible the component sizing performed in previous modeling efforts[19][18]. In order to develop a stable model, additional equipment was added. Basic sizing of these additional components was done; however, they have not been optimized for performance.

4.2.1 Molten Salt Heat Source and CTAH

The RACC can be coupled to any heat source capable of producing high temperature molten salt. Therefore, the heat source was modeled as a temperature and flowrate boundary condition. Using OPC UA (which will be discussed more in the following chapter), values for the temperature, pressure and flowrate of molten salt can be updated from pre-generated data or from models using other software. For the purposes of this study, the flowrate, temperature, and pressure were considered to be constant for the Mk1 PB-FHR operating at steady state. In practice, some variation in temperature and pressure is expected, however nuclear reactors are designed and operated to have very slow transients and therefore this assumption is valid for this study. Moreover, in future work, this model can be integrated with other software to accurate model transients in the primary salt loop.

Figure 4-3 shows one of the two CTAH heat exchangers. Properties for flibe were taken from the default flibe properties used in the System Analysis Module (SAM), a system analysis tool developed at Argonne National Laboratory under the support of U.S. Department of Energy (DOE) Nuclear Energy Advanced Modeling and Simulation (NEAM) program. Properties are shown inTable 4-1 [51][52].

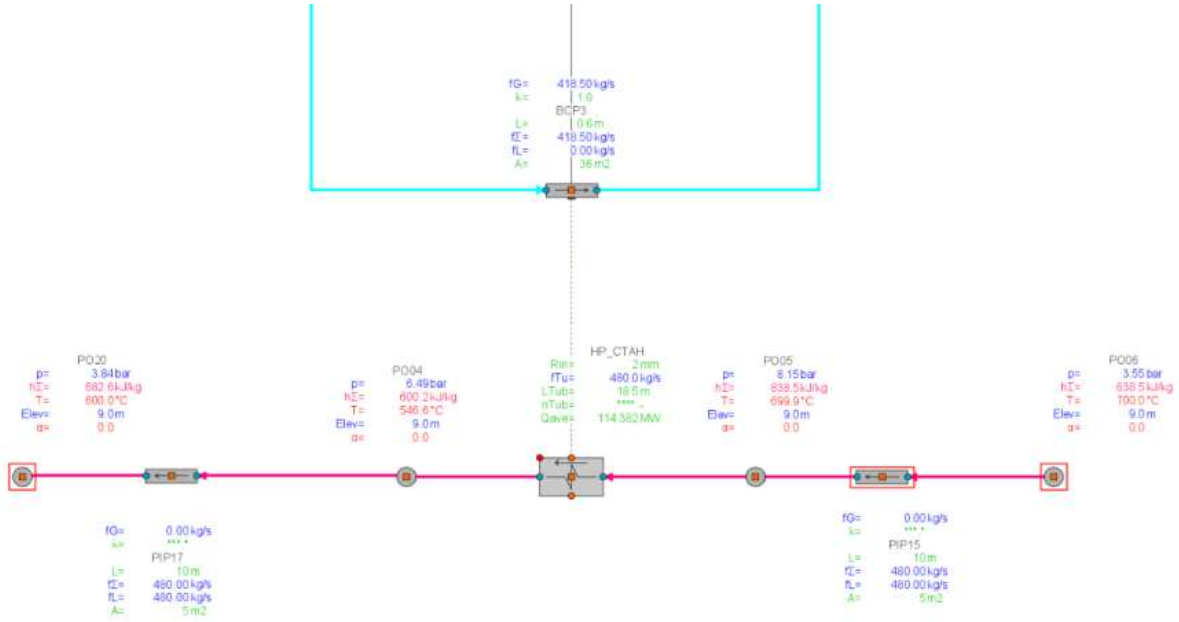

Figure 4-3: Molten Salt Heat Source. Fixed boundary conditions are outlined in red

Table 4-1: Liquid flibe properties

Flibe Property	SAM Default (T in C, SI units)
Density (kg/m^3)	227.79 – 0.488T
Conductivity (W/m·K)	0.7662 + 0.0005T
Specific Heat (J/kg·K)	2415.78
Viscosity (Pa·s)	$4.638 * 10^5 * T^{-2.79}$

4.2.2 Modified Gas Turbine

The modified gas turbine was modeled after the design proposed by Dr. Andreades [18]. Previous models did not size the necessary valves to divert air to the thermal energy storage system and have been added here. A valve was placed after the compressor to control the flow during transients when the valves to the combustion chamber and the thermal energy storage system are opening and closing. See Figure 4-4

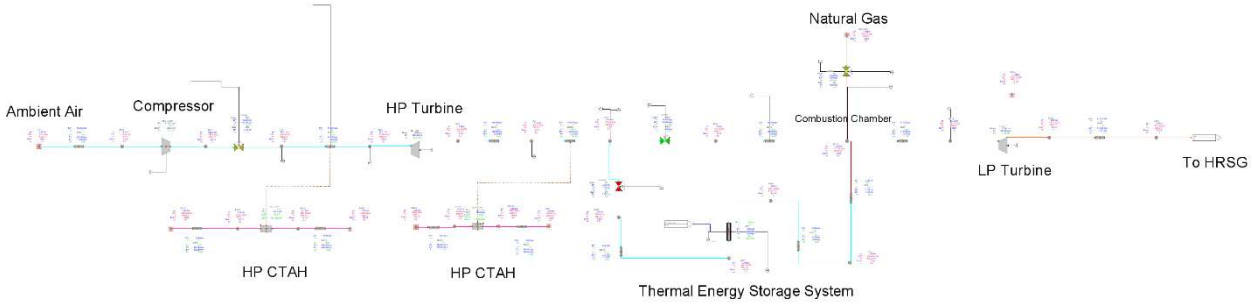

Figure 4-4: Modified Gas Turbine

4.2.3 Thermal Energy Storage System and Combustion Chamber

A closeup of the thermal energy storage system and natural gas co-firing system are shown in Figure 4-5. The thermal energy storage system was sized to match the properties and dimension of the FIRES system designed at MIT[19]. It is modeled as a bundle of firebrick tubes. When charging, the electricity being produced by the RACC is directed to resistively heat the firebrick volumetrically. Two valves are controlled to divert air directly to the combustion chamber or to the heat storage system, while maintaining a constant 418.5 kg/s flowrate. The RACC operates between base and peak load by adjusting the temperature. Options for adjusting the temperature include using only natural gas, using only heat storage, using both natural gas and heat storage, and using neither natural gas nor storage. A controller was designed to decide between these operating regimes. Also, due to the strain that sharp transitions between operating regimes can cause on dynamic simulation (and likely to the physical system) a method to gradually shift from one regime to another was created.

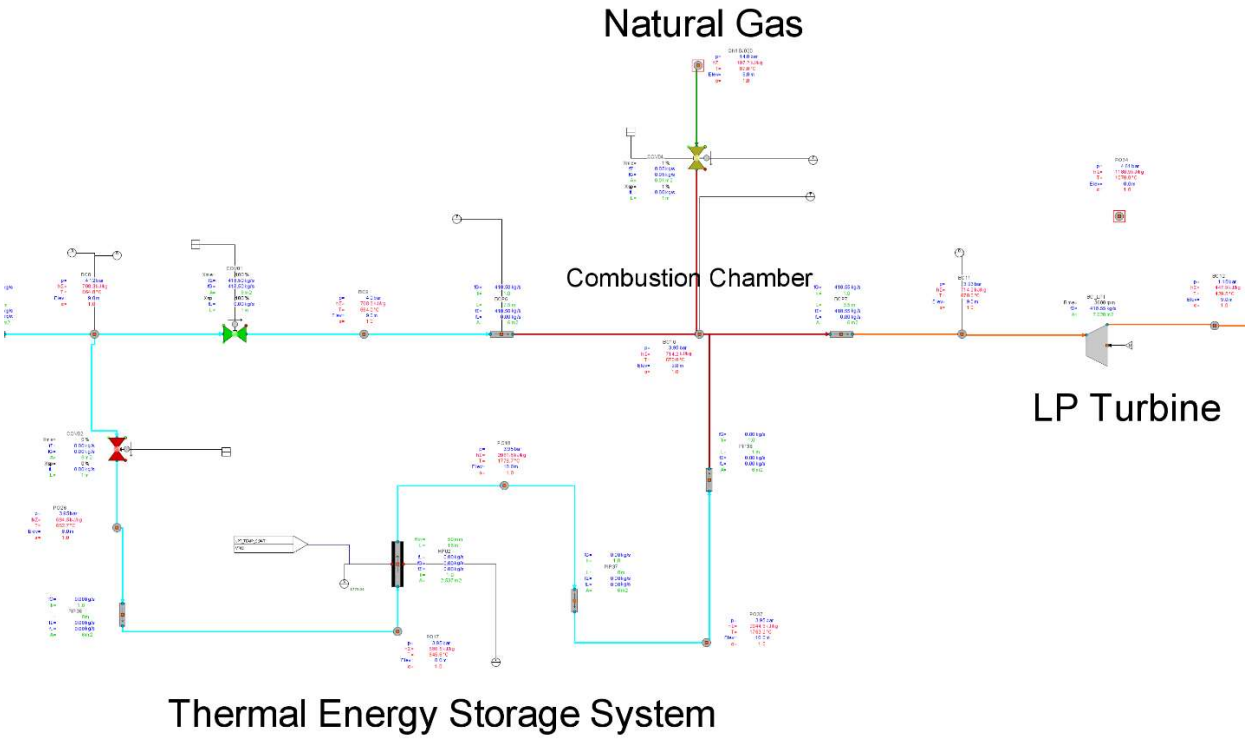

Figure 4-5: Thermal energy storage system and natural gas co-firing system

The primary input to this controller logic is the price of electricity. The price of electricity is compared to the current marginal cost of electricity. The marginal cost of electricity can vary significantly depending on the current efficiency of the system, if storage is being used, and if natural gas is being burned, therefore the marginal cost of electricity is constantly being updated by calculating the current cost of operation divided by current power production. Current cost of production is calculated by adding the fixed O&M costs, and the cost of the natural gas being consumed if any. Marginal cost calculation logic is shown in Figure 4-6. If the price of electricity

is greater than the current marginal cost, the combustion chamber temperature set point will be set to 1070 °C and if it is lower than the marginal cost, the temperature set point will be set to 670 °C, also, electricity will be diverted from the grid to the storage system. The temperature set point is passed through a filter to gradually increase or decrease the actual temperature set point used by the controllers, thus smoothing out the transients. This logic is shown in Figure 4-7.

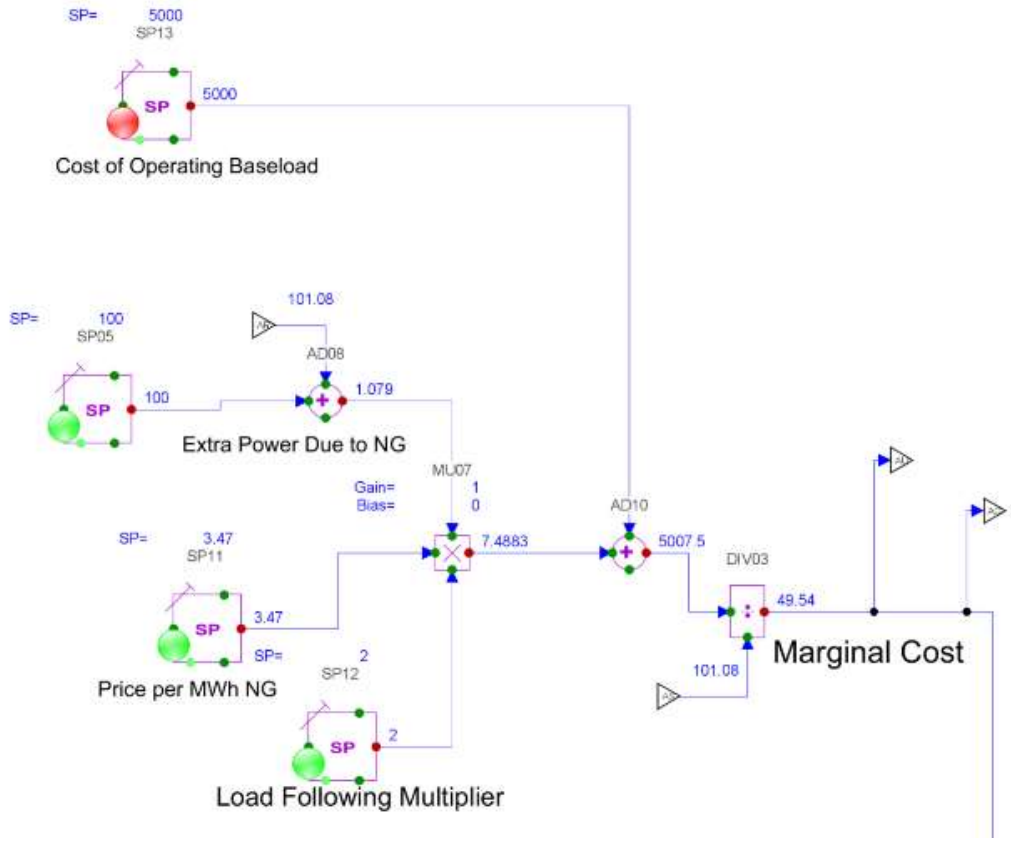

Figure 4-6: Marginal cost calculation

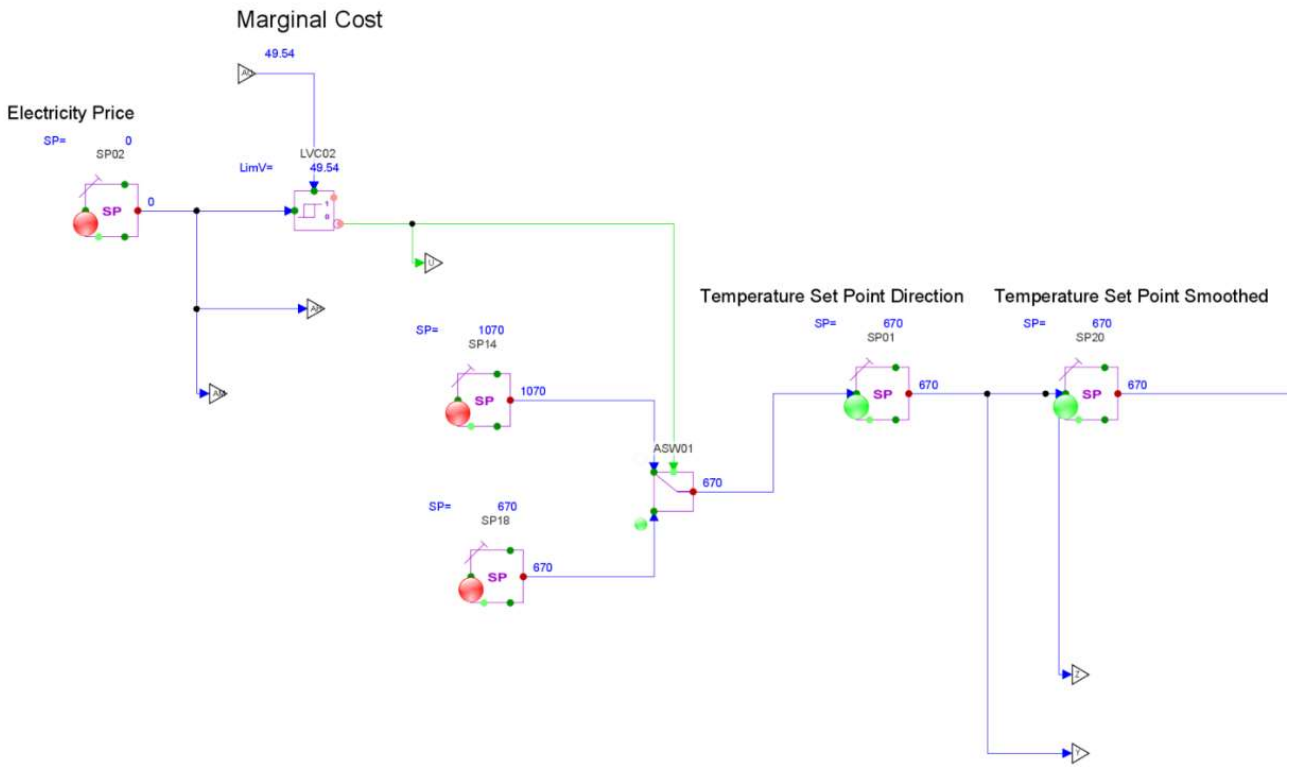

Figure 4-7: Logic to determine system temperature set point

Before placing the thermal energy storage system valve into active control, the filtered temperature set point, unfiltered temperature set point, and the current storage temperature must all be above a minimum value of 670. If not, heat from the storage system is either insufficient or not necessary. When the controller is turned from active control to inactive control, the set point will gradually decrease from the most recent active control signal to zero. A cascade controller was used where one controller determined the required flowrate and a second controller determined the valve position to reach the required flowrate. These controllers were used because it was discovered that it provided smoother control rather than directly controlling the temperature with valve position. The flow set point of the main line valve was simply 418.5 minus the set point set to the storage valve. Storage valve controller shown in Figure 4-8

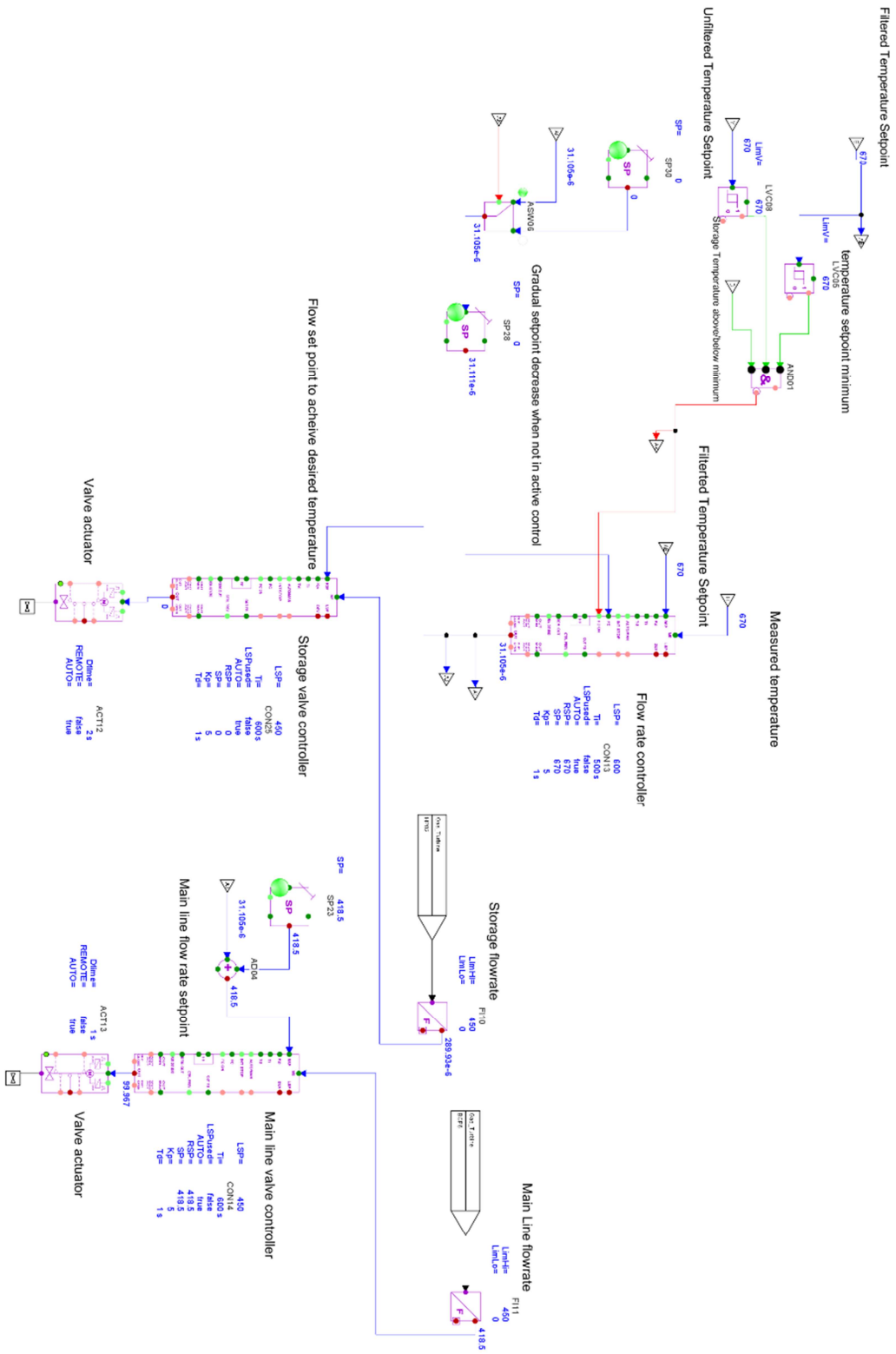

Figure 4-8: Storage valve controller logic

The natural gas valve control logic begins similarly to the storage valve control. The controller is inactive unless the following criteria are met:

1. The filtered set point temperature is above the current storage temperature.
2. The filtered set point temperature is above the unfiltered set point temperature.
3. The filtered set point temperature is above the combustion chamber temperature.

These criteria ensure that natural gas is only burned when needed. The natural gas valve is capable of much faster valve position adjustments since the flowrates are small compared to the air flow rates. Therefore, the speed at which the natural gas flowrate is changed is limited by material limitations and the price of electricity. To take advantage of this flexibility two controllers were developed. The first controller measures the current marginal cost of electricity and is given the current price of electricity as a set point. This controller is meant to follow the load demand as close as possible. The second controller directly measures the combustion chamber temperature and seeks to reach the filtered set point temperature. This second controller is only activated if the price controller varies too far from the filtered set point temperature or combustion chamber temperature limit. Also similar to the storage valve control, when the controller is switched from active to inactive, the valve position will gradually decrease from the last sent output to the closed position. Also, logic is put in place such that only one of the two controllers is active at a time and the output of the inactive controller follows the active controller to prevent discontinuities when switching between controllers. Controller logic is shown in Figure 4-9 and Figure 4-10.

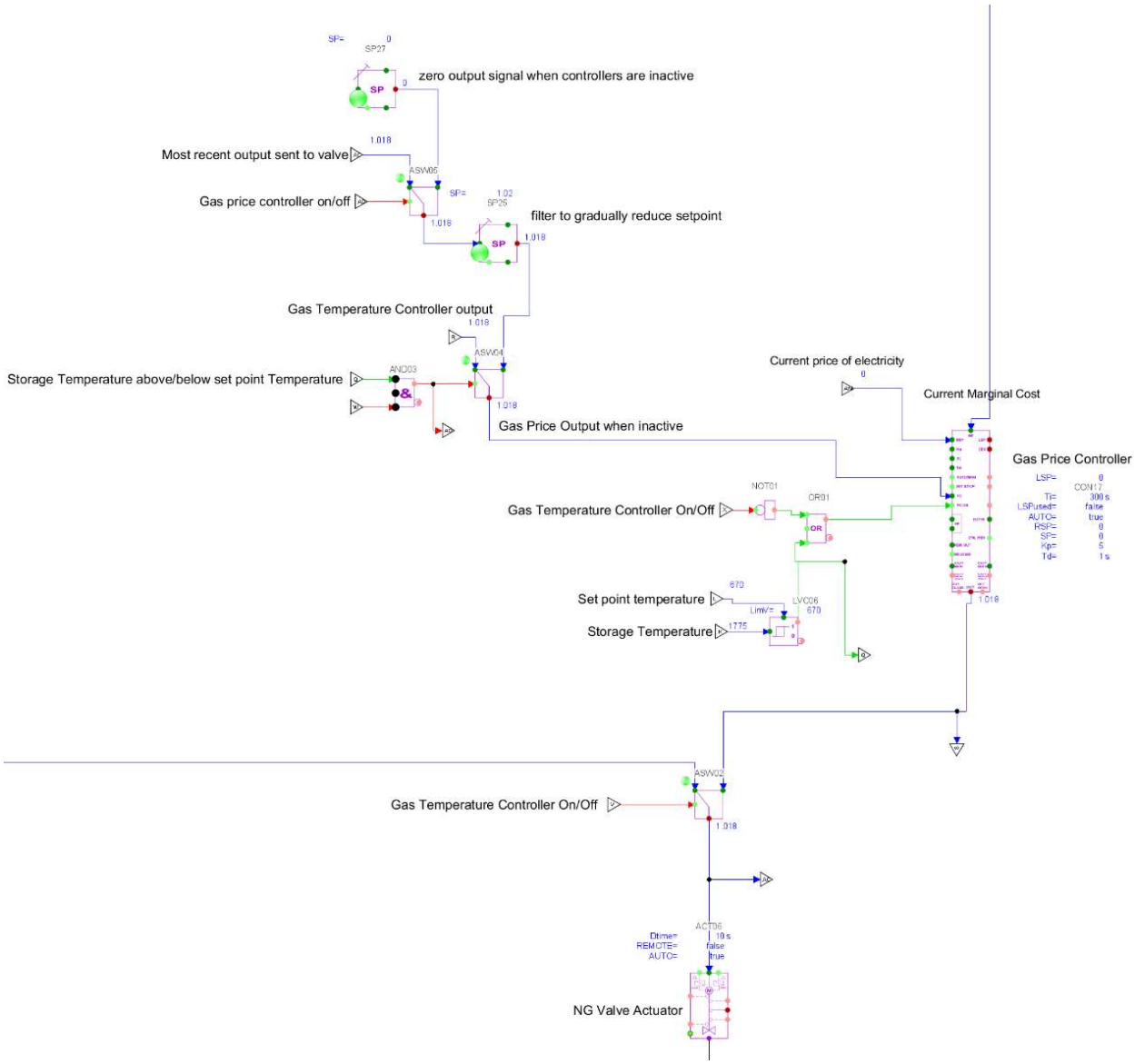

Figure 4-9: Natural gas valve controller logic for matching marginal cost of electricity to current price of electricity

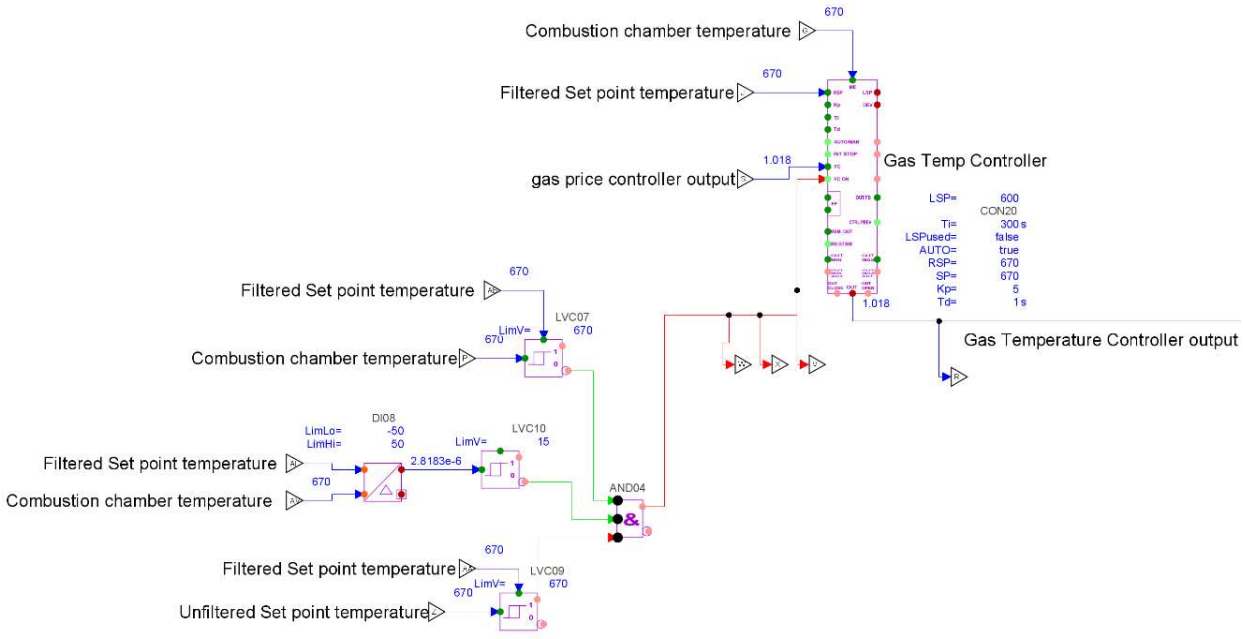

Figure 4-10: Natural gas valve control logic for temperature control

4.2.4 Heat Recovery Steam Generator

The HRSG equipment was sized to match the steady state models mentioned previously. The only additions were valves not present in the previous models. Basic sizing and design were performed for these valves but have not been optimized. The economizers, super heaters, and the once-through-boiler were modeled using heat exchangers. The evaporators were modeled with a tank module to represent the drum along with a series of heat exchangers for recirculation. See Figure 4-11 and Figure 4-12.

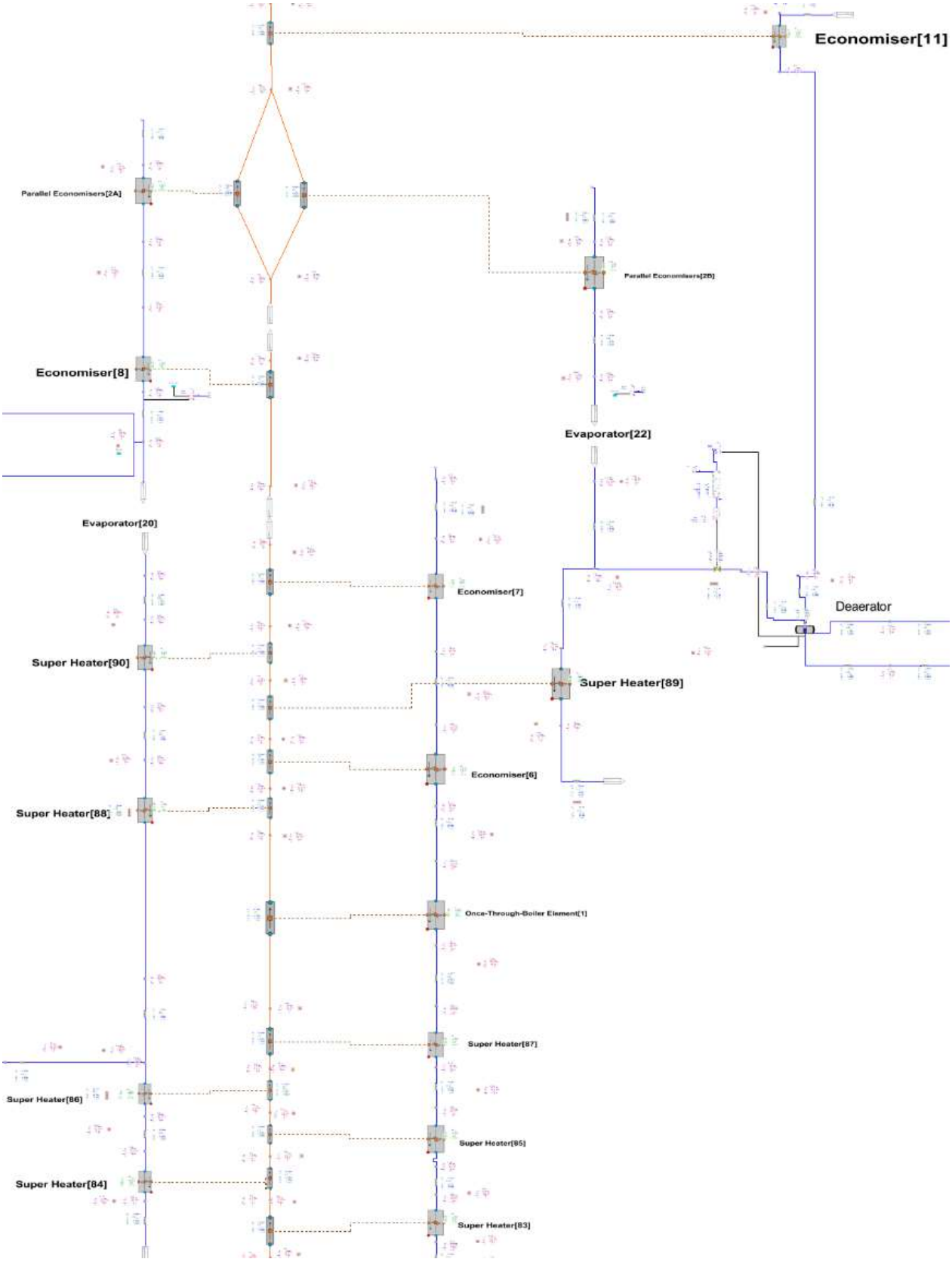

Figure 4-11: Heat Recovery Steam Generator Model

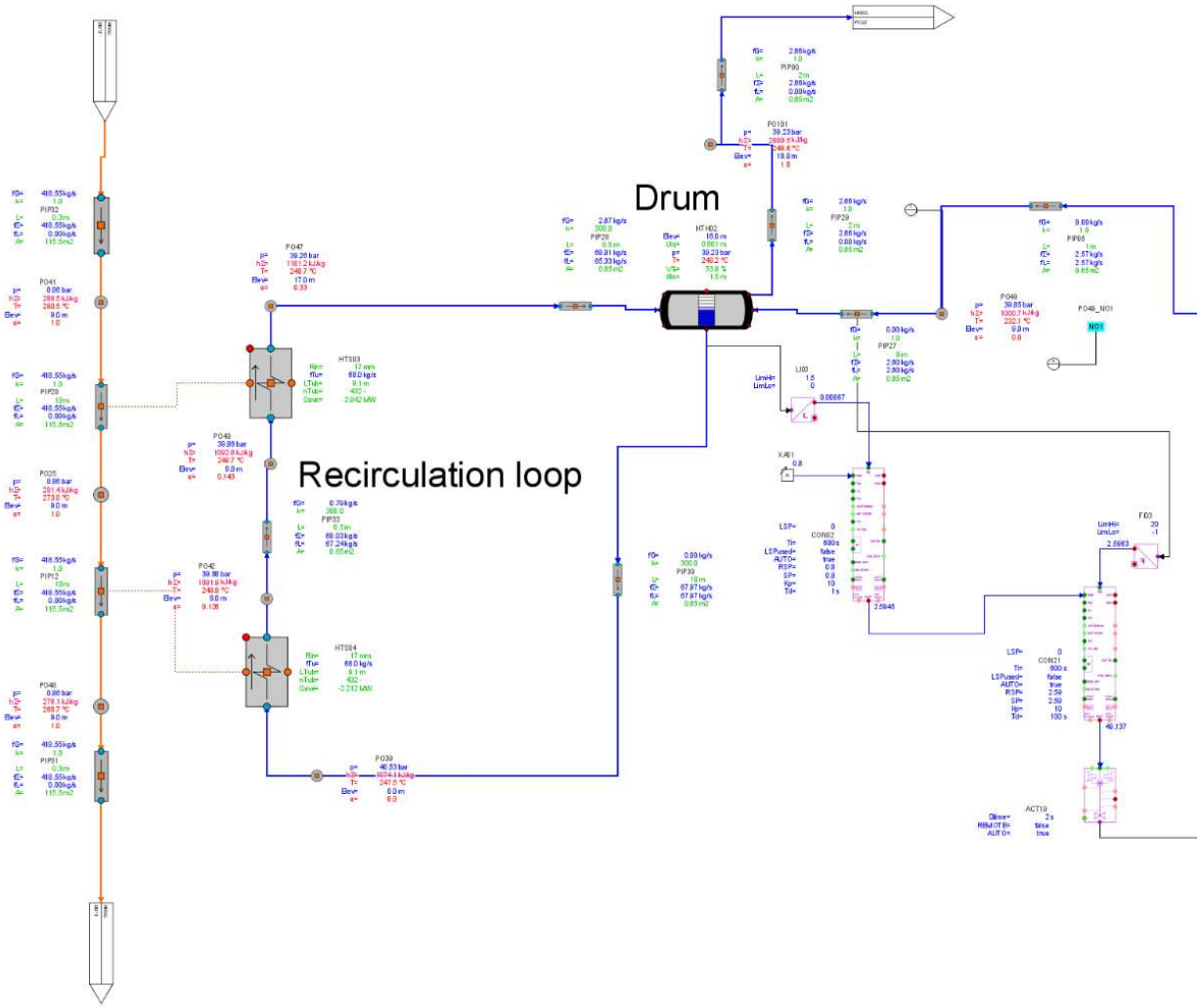

Figure 4-12: Evaporator

Commonly, control of HRSG systems is mostly passive. As long as the gas turbine exhaust does not fluctuate too quickly, the HRSG will gradually adjust to the higher flowrates. Evaporator drums, deaerators, and condensers will have some basic logic to maintain liquid level, however most of the control is done at the gas turbine[53].

Control of the Apros RACC HRSG model also included the previously mentioned controls. Evaporator drums, the deaerator, and the condenser liquid levels were controlled with control valves using cascade controllers, with the first controller measuring the level and determining flow rate and the second controller measuring flow rate and determining valve position. Pumps were controlled to maintain a constant pressure differential across control valves. The pressure of the deaerator was controlled simply with a control valve. Examples of these kinds of controllers are shown previously and are therefore these specific controllers are not shown here. Also, these controllers are typical to normal HRSGs[54].

The most significant departure from normal HRSG control was the inclusion of a valve in the intermediate pressure steam line to control the pressure of the intermediate pressure evaporator. Typically, evaporator pressures are not controlled and only one control valve is placed in the high-pressure steam line to control steam turbine power. This intermediate pressure steam line control valve was necessary to keep the upstream liquid water from boiling prematurely during transients, causing the flow to become unstable. This control valve maintained a delta T of 18 °C between the saturation temperature and measured temperature of the liquid entering the intermediate pressure evaporator. See Figure 4-13. While this unconventional technique was sufficient to maintain a stable simulation, it is possible that other methods exist that would be more effective in maintaining the stability of HRSG performance.

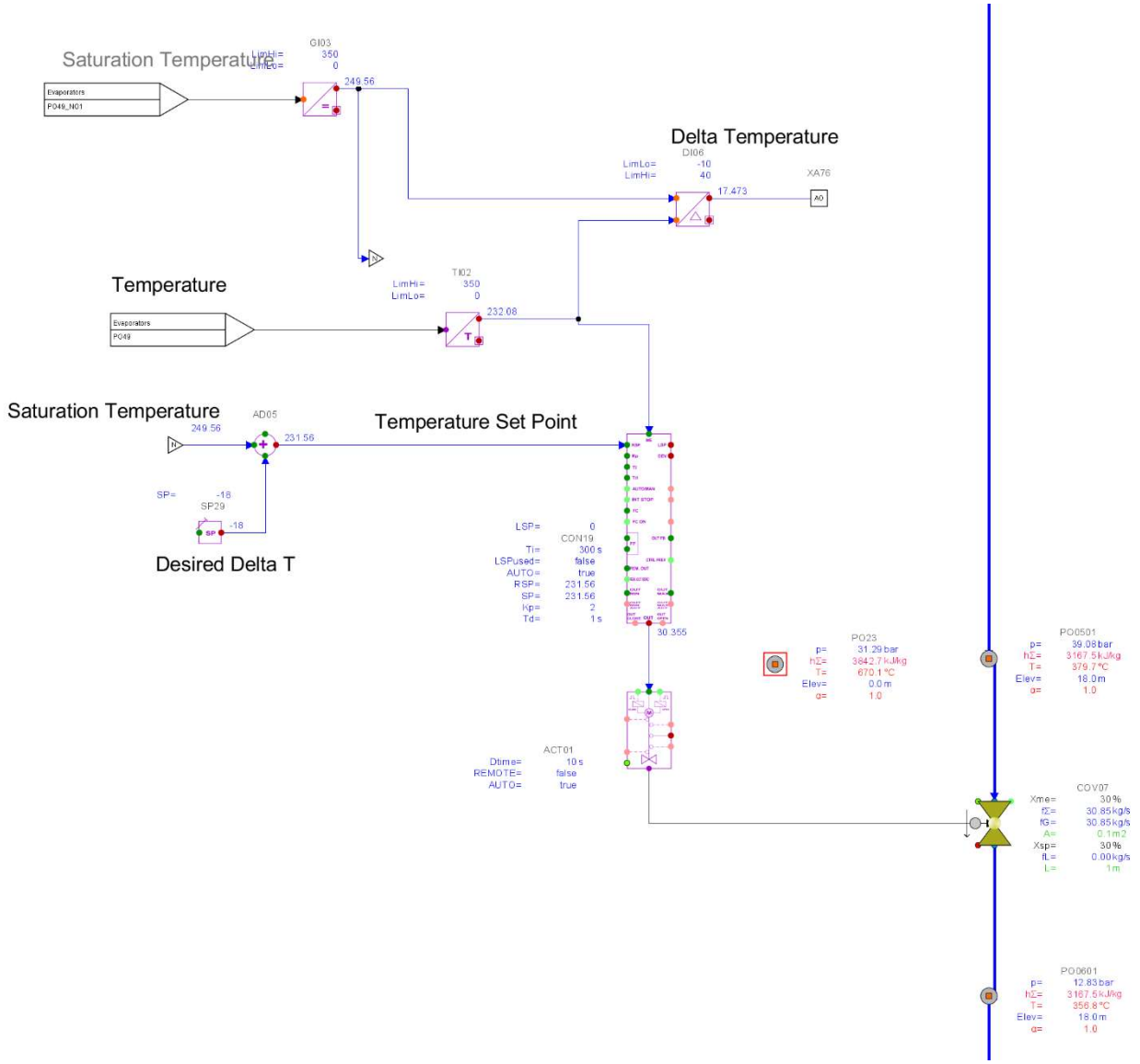

Figure 4-13: Intermediate Pressure Evaporator Upstream Boiling Prevention Controller

4.2.5 Steam Turbine Plant

As with previously mentioned equipment, the steam turbine and condenser were modeled to reflect previous steady state models, with the inclusion of control valves. A valve at the inlet of the high-pressure turbine is used to adjust the power output of the steam turbine plant. See Figure 4-14.

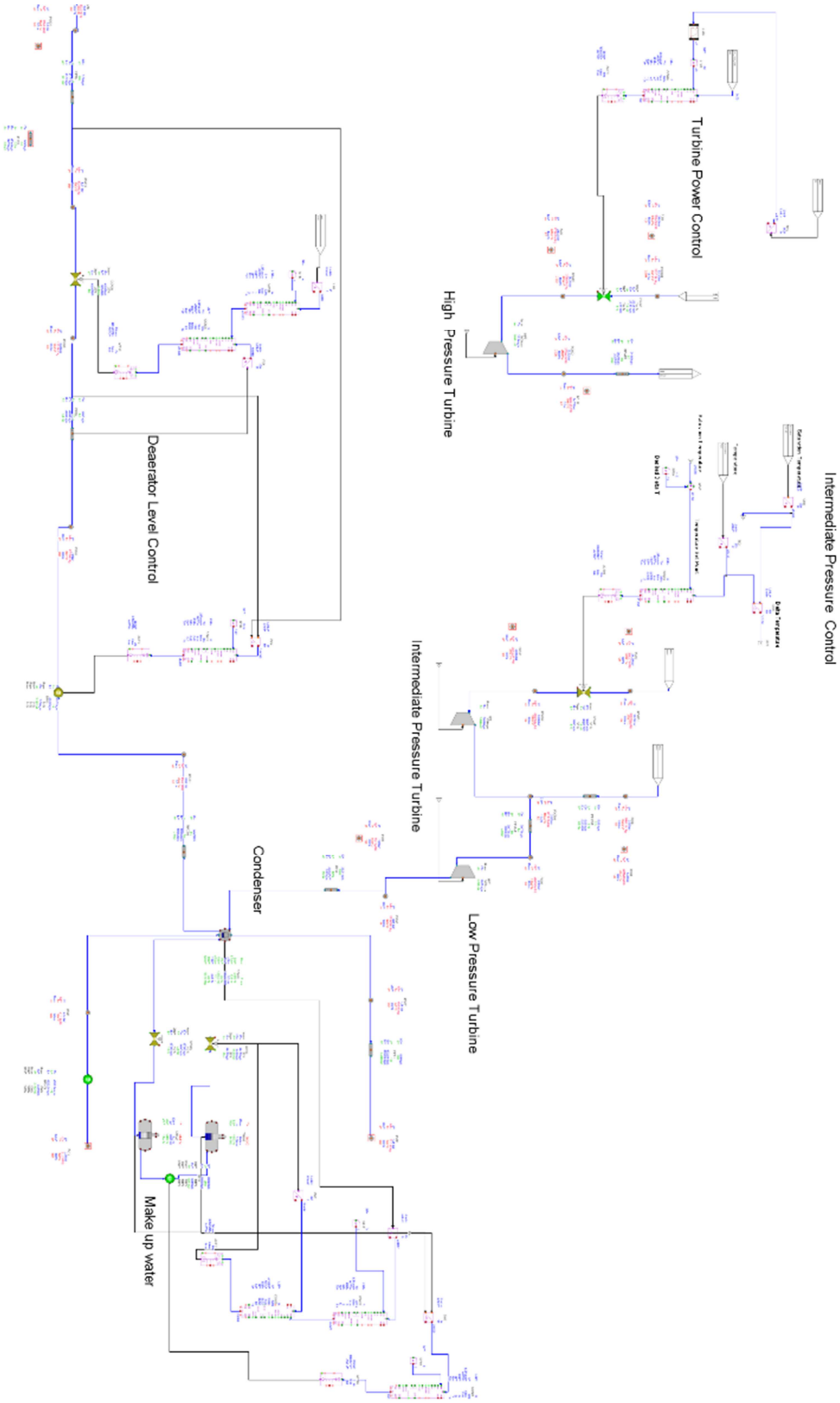

Figure 4-14: Steam Turbine and Condenser

It was discovered during simulation that the power level was more sensitive to a HRSG flow rate control valve in the liquid portion of the high-pressure steam line. The high-pressure line does not have an evaporator, rather it has a once through boiler. This is because the high-pressure line passes from liquid to supercritical water rather than traditional boiling. However, even in the absence of an evaporator drum, it is still vital to maintain a near constant liquid/vapor interface height. This ensures that the super heaters and economizers will contain the water phase they were designed to contain, and it also maintains simulation stability. This high-pressure steam line flow rate controller mimics the function of the evaporator drum level controllers by maintaining a constant flow rate into the high-pressure steam line and into the high-pressure turbine. As the system heats up or cools down, the high-pressure steam flow rate will increase or decrease, this flowrate controller maintains that flowrate at the entrance. This change in flowrate is the primary driver to steam turbine power dynamics, with the high-pressure turbine inlet valve being used to fine tune power levels and maintain steam quality at the inlet of the turbine. The high-pressure turbine valve controller measures the current power production of the steam plant and has a set point for steam plant power based on gas turbine exhaust gas temperature and linearly interpolating baseload and peak load steam plant power. Control logic shown in Figure 4-15 and Figure 4-16.

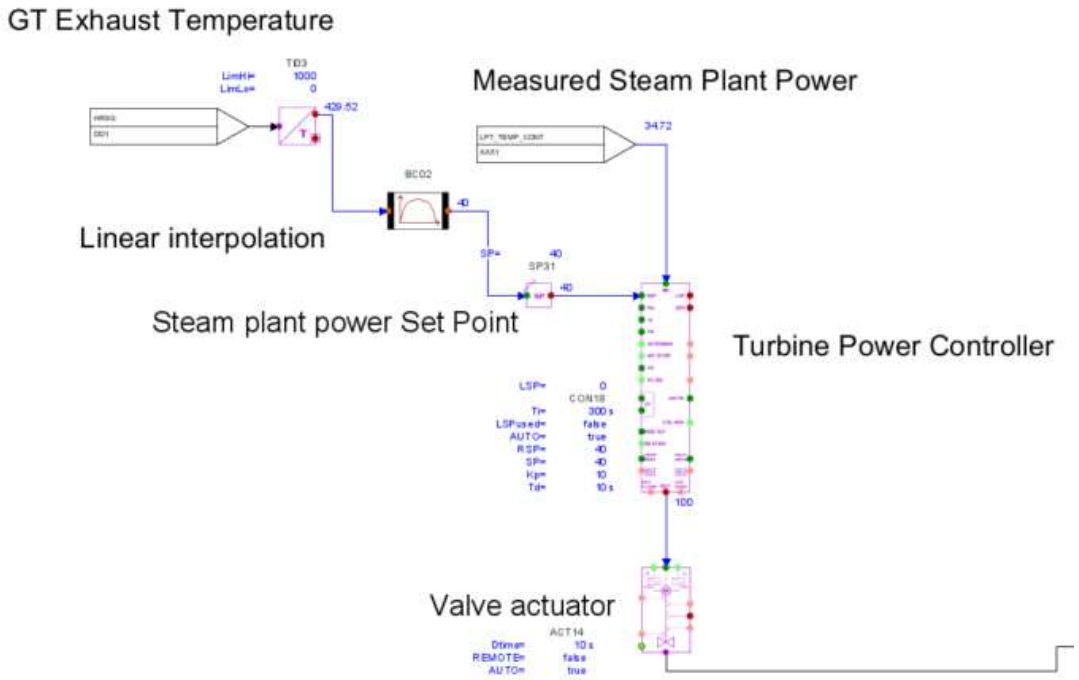

Figure 4-15: High-pressure Steam Turbine Controller

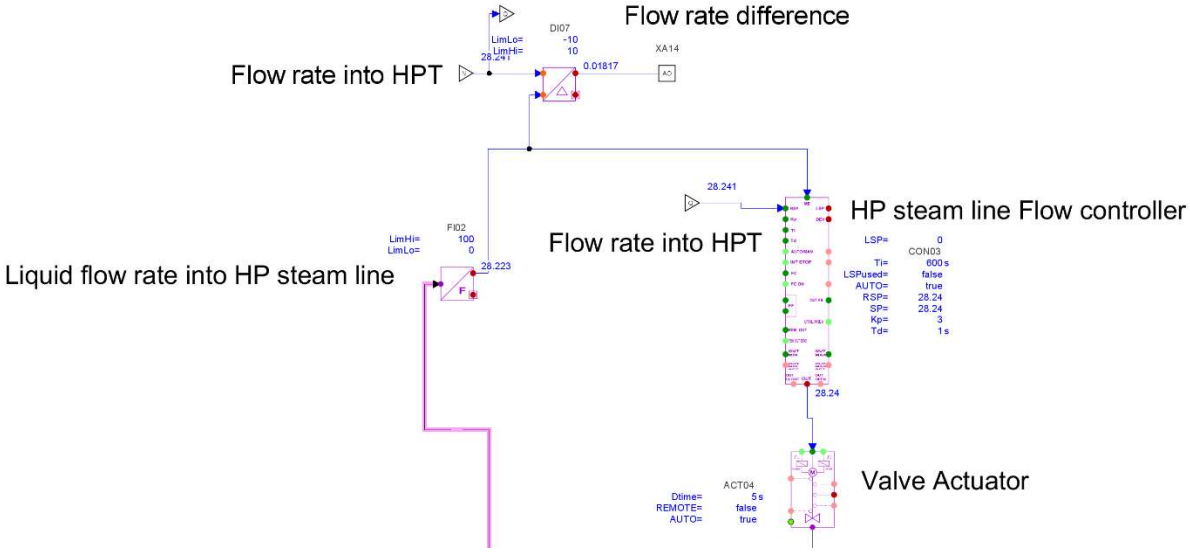

Figure 4-16: High-pressure Steam Line inlet flow controller

4.3 Modeling Results

To demonstrate the dynamics of the RACC model, the system was first ramped up from baseload operation with a full storage system to peak power. Then, once the heat storage was completely depleted, the system was ramped down back to baseload. Presented below is data from the simulation starting during the ramp up process.

The storage valve controller and natural gas valve controller were able to keep the temperature near the set point throughout the simulation with the exception of when the storage system temperature dropped below the temperature set point. See Figure 4-17 and Figure 4-18.

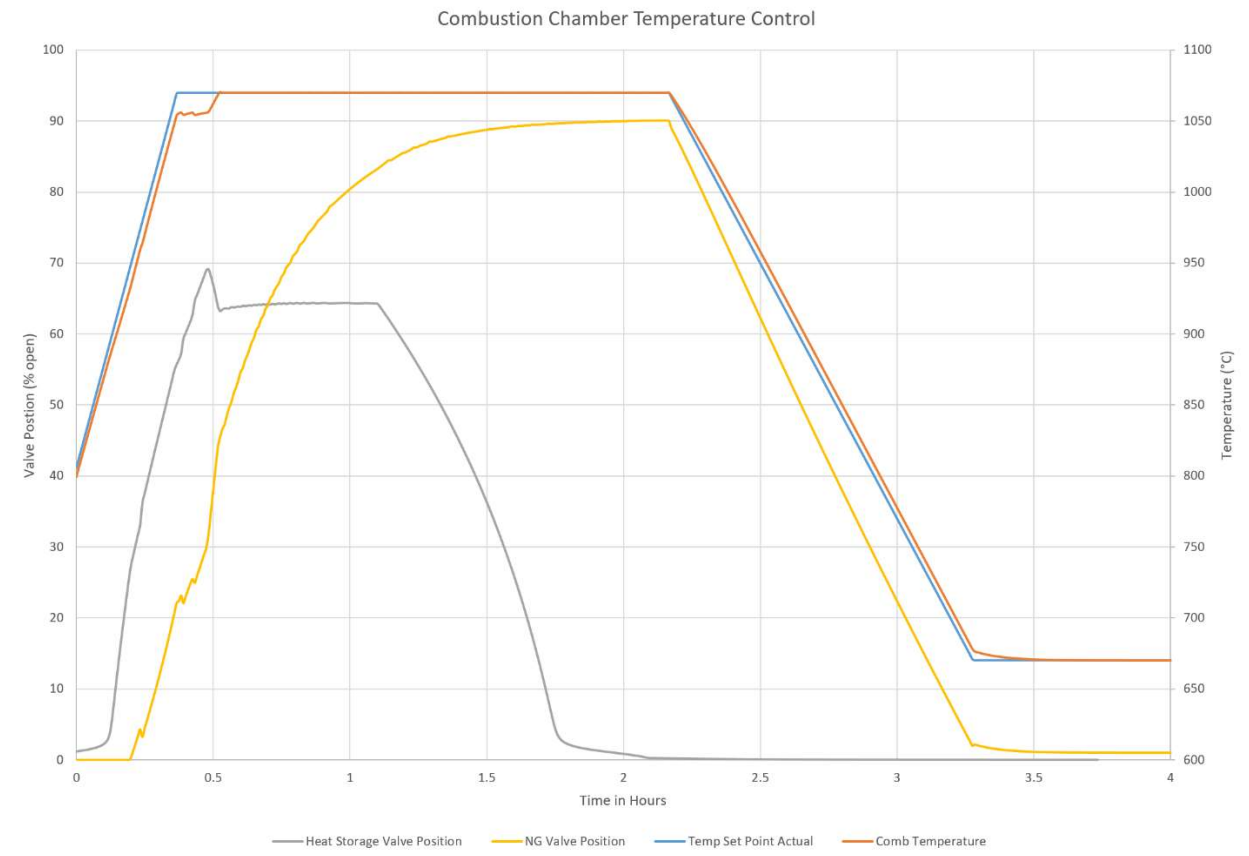

Figure 4-17: Combustion Chamber Temperature Control

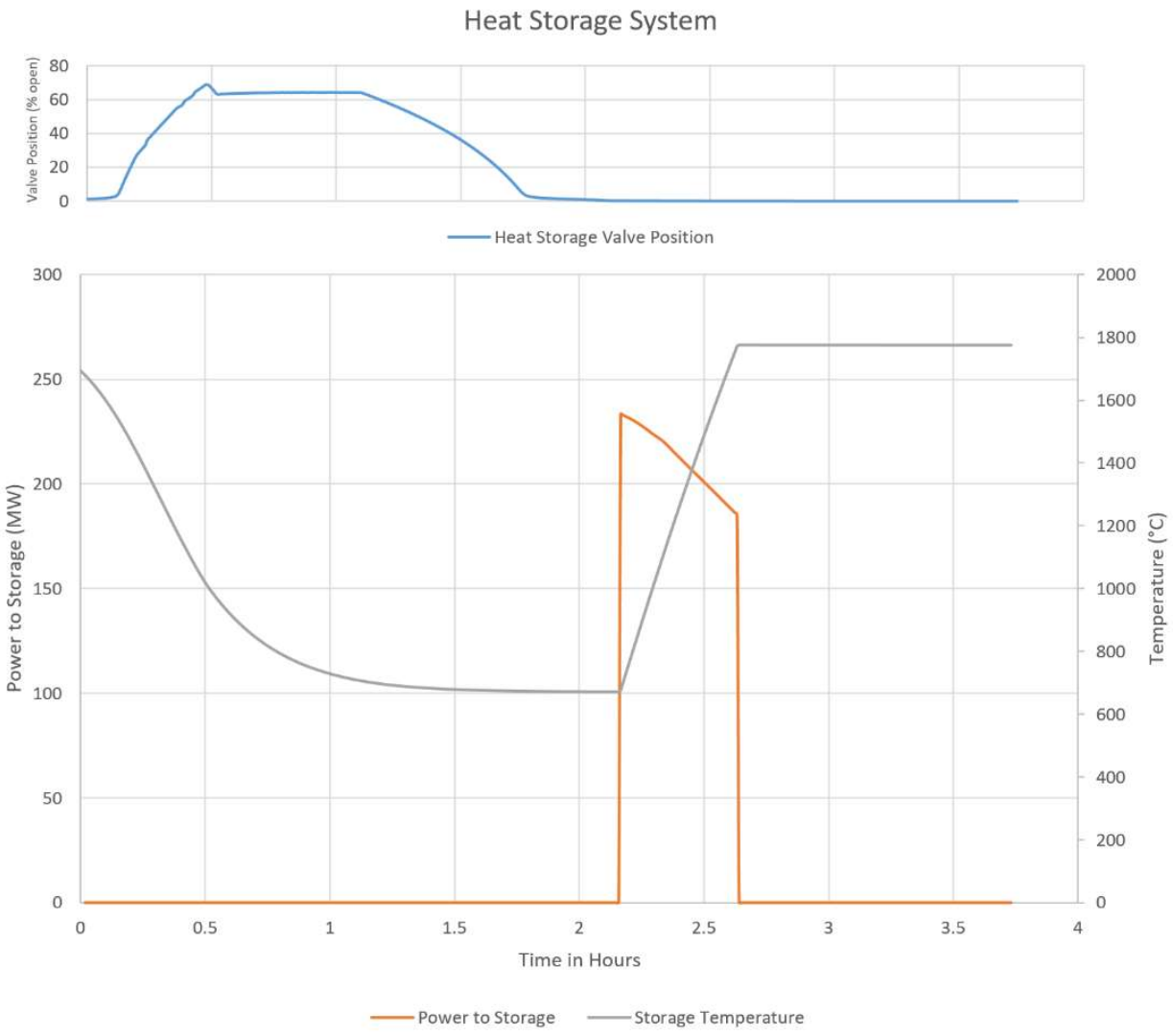

Figure 4-18: Heat Storage System Control

Power production values for baseload and peak load match well with previous modeling efforts. See Table 4-2. The speed at which power can be diverted from the grid to the storage system and back were assumed to be instantaneous in this study but requires further study for more realistic modeling. See Figure 4-19.

Table 4-2: Comparison of Apros and Thermoflex modeling results

	Thermoflex results	Apros Results
GT Baseload Power Production (MW)	66.3	66.5
ST Baseload Power Production (MW)	33.7	35.5
GT Peak load Power Production (MW)	124.1	119.6
ST Peak load Power Production (MW)	117.9	114.1
Total Baseload Power (MW)	100	102
Total Peak load Power (MW)	242	233.7

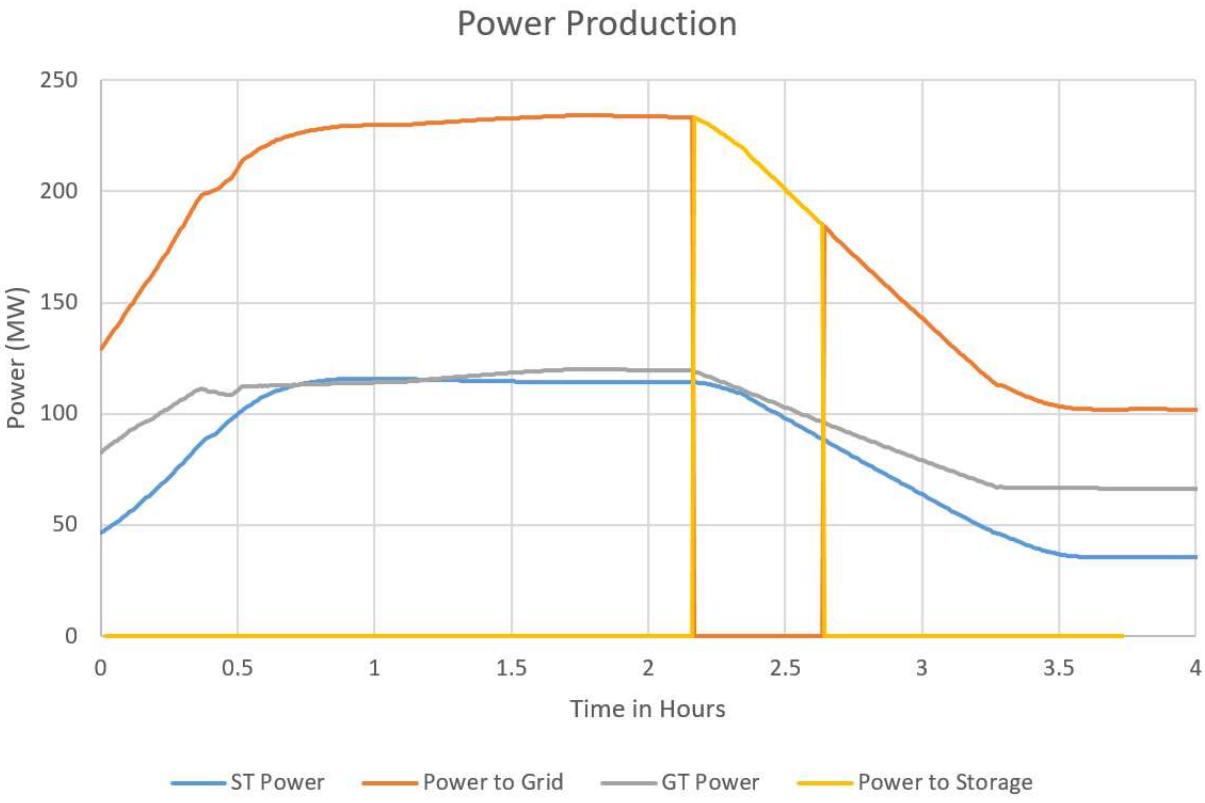

Figure 4-19: Power Production

Due to the low cost of natural gas, increasing the power actually lowered the marginal cost of electricity. This is also in part due to the boost in efficiency seen at higher temperatures. This has implications for operations since the only time it would make financial sense to operate in baseload is when the price is below $7/MWh. See Figure 4-20 and Table 4-3.

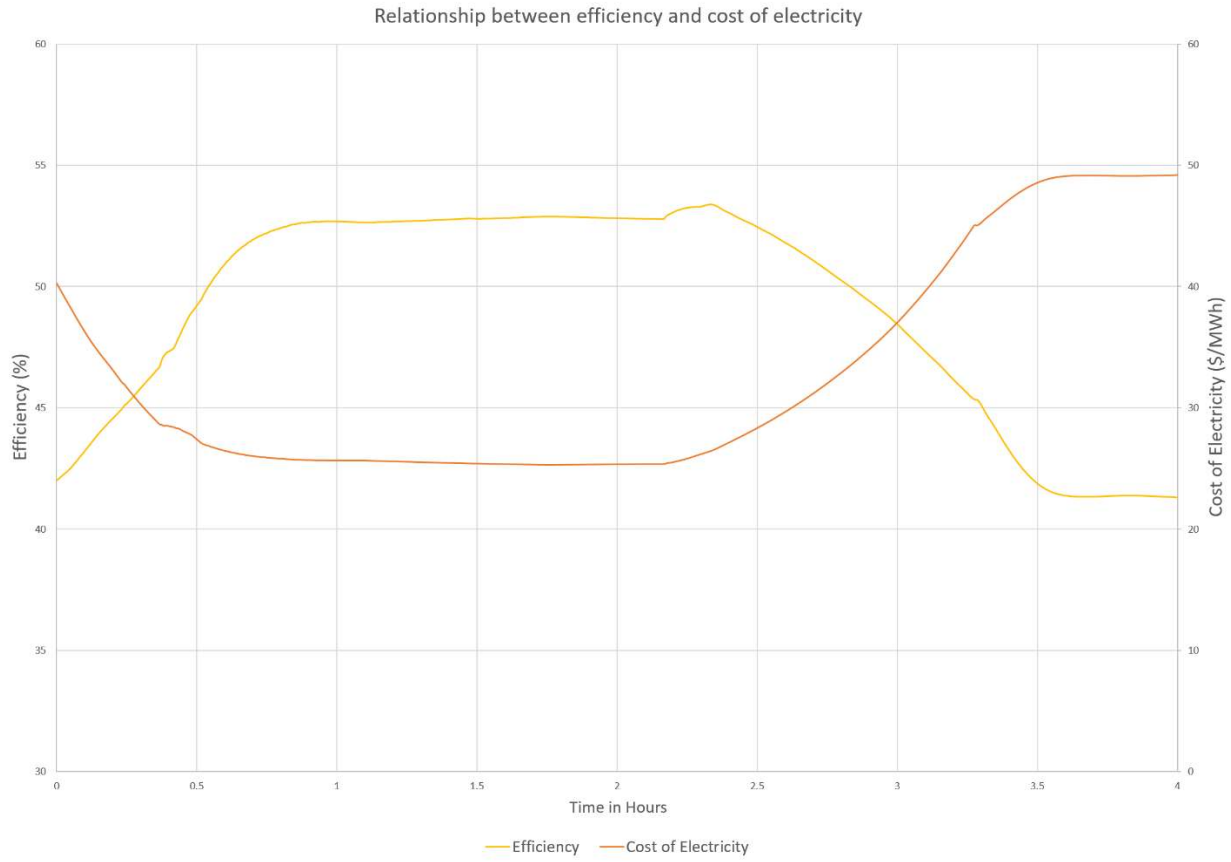

Figure 4-20: Relationship between efficiency and cost of electricity

Table 4-3: Profit/Loss estimation at different prices of electricity assuming the price of natural gas to be $3.47/MWh with a 2X multiplier for peaking

	Baseload – Cost of Electricity $50/MWh, 100MW capacity		Peak load – Cost of Electricity $25/MWh, 240MW capacity	
Price of electricity ($/MWh)	Profit/Loss ($/MWh)	Total Loss ($)	Profit/Loss ($/MWh)	Total Loss ($)
0	-50	-5000	-25	-6000
7	-43	-4300	-18	-4320
25	-25	-2500	0	0
50	0	0	25	6000

Figure 4-21, Figure 4-22, and Figure 4-23 show the phenomena described in the modeling section above. The boiling prevention controller was necessary to the temperature well below the saturation temperature for the points before the evaporator. The mass flow for the HRSG was controlled by the high-pressure steam line flow control and indirectly by the boiling prevention control, while also being influenced by the temperature dynamics of the gas turbine exhaust temperature. The mass flow rate was the primary factor in determining steam turbine power production. The valve at the inlet of the high-pressure turbine remained open during the entirety of this simulation.

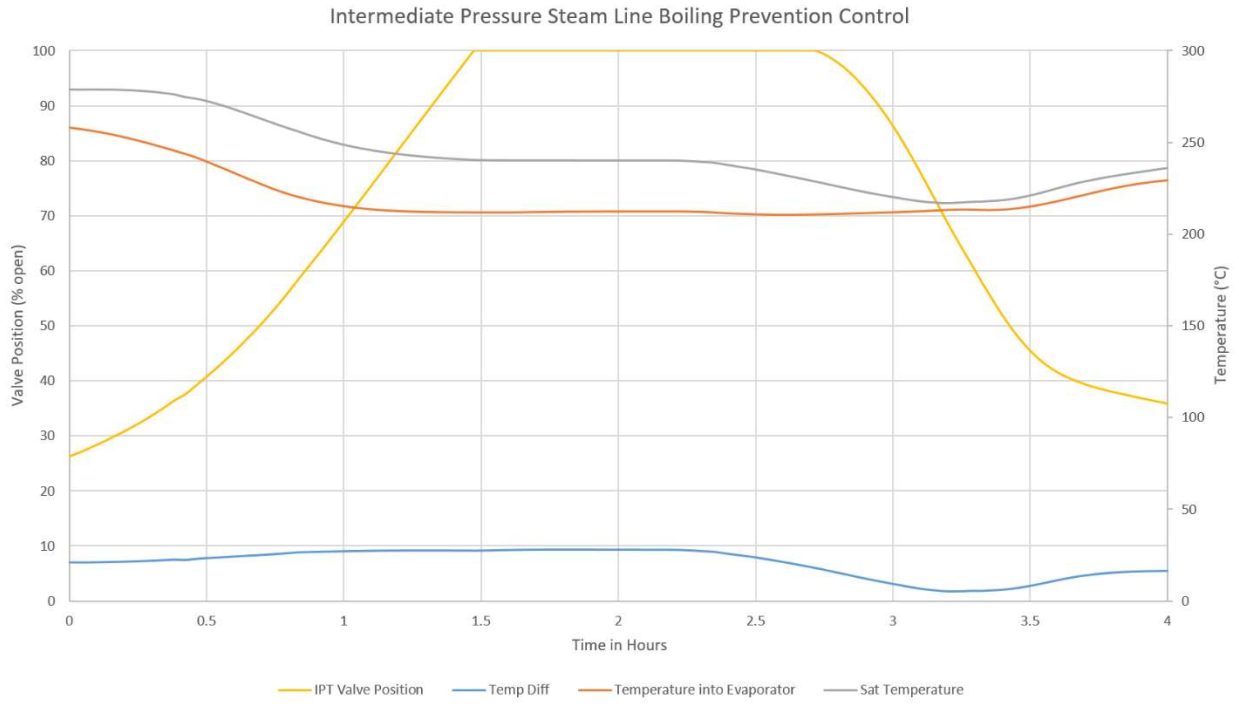

Figure 4-21: Intermediate Pressure Steam Line Boiling Prevention Control

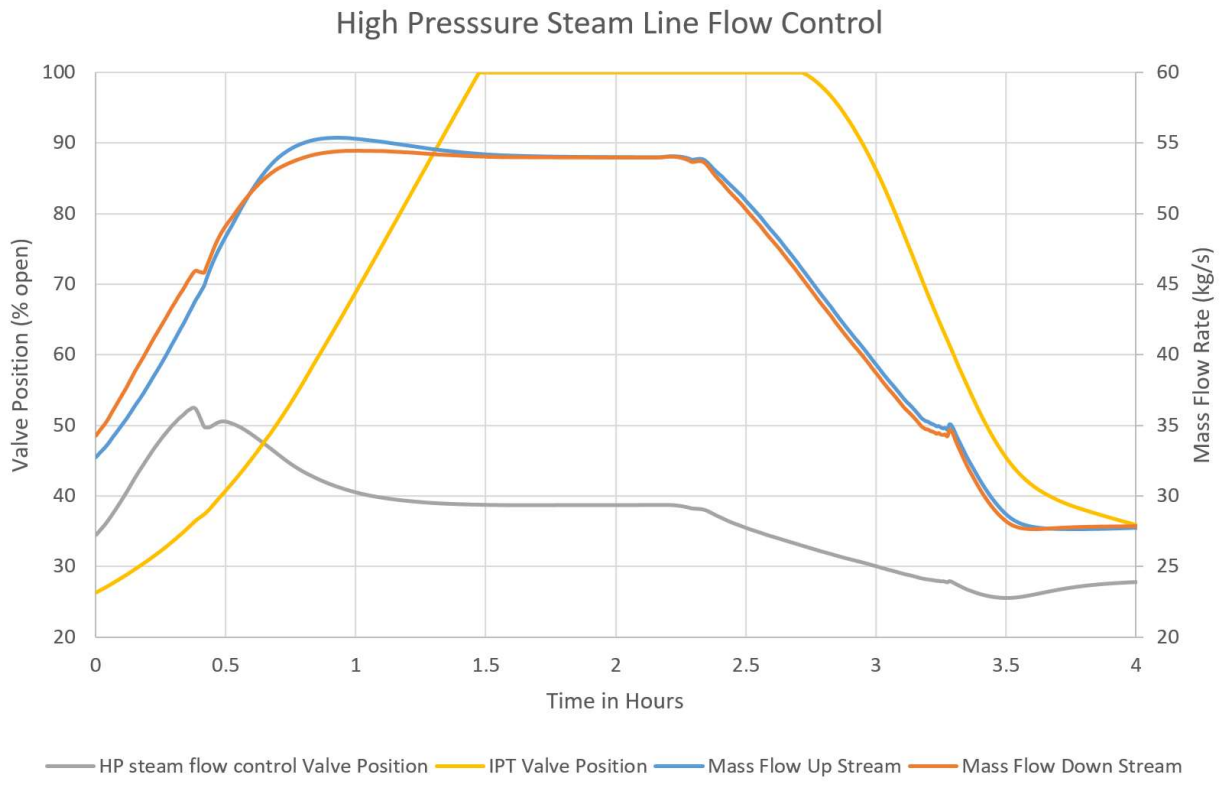

Figure 4-22: High-pressure Steam Line Flow Control

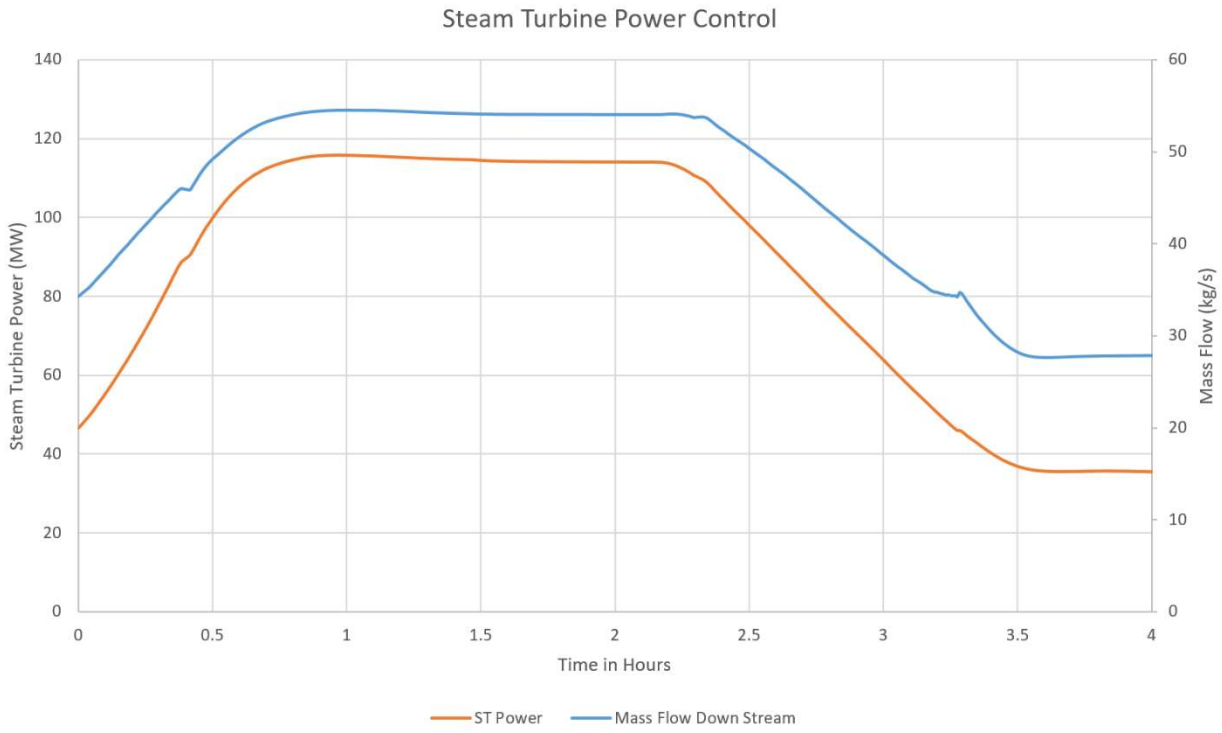

Figure 4-23: Steam Turbine Power relationship with Steam Flow Rate

4.4 Future Work

Data from the California Independent System Operator (CAISO) is readily available for electricity prices throughout California. For instance, as shown in Figure 4-24. Future work will include using this data to see how the RACC will perform given a realistic price profile rather than the simple ramp up and ramp down presented here.

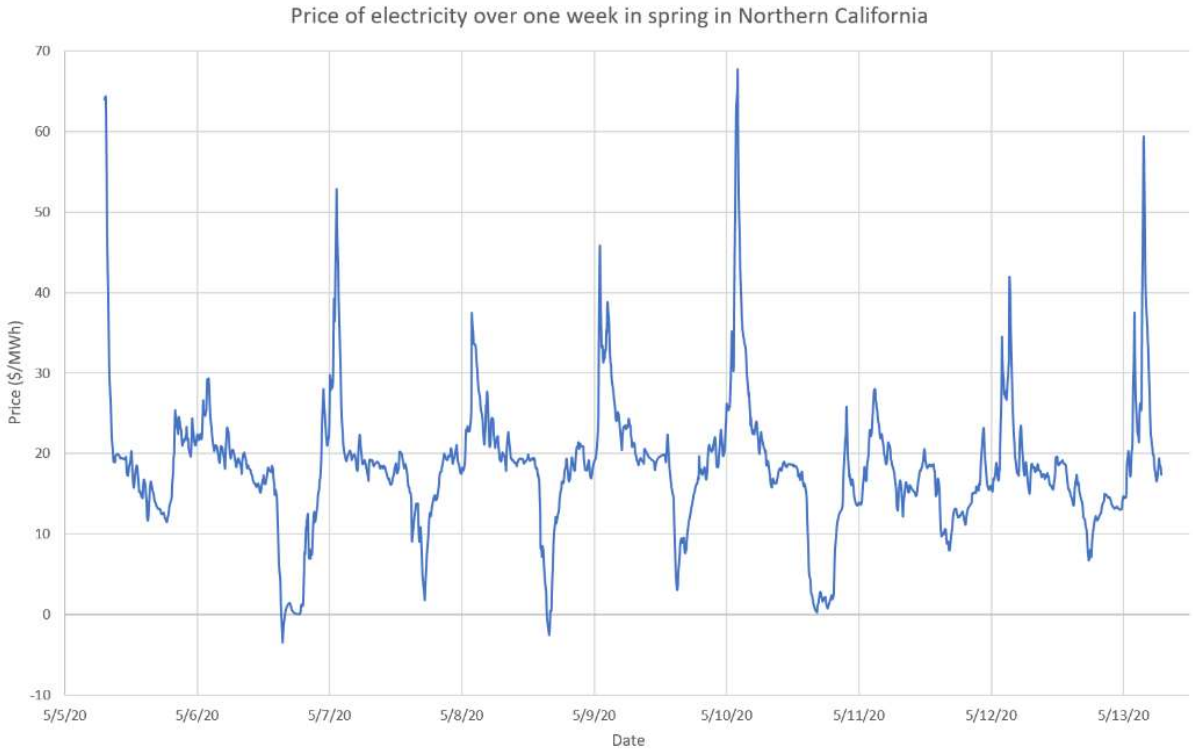

Figure 4-24: Electricity price profile for Northern California in Spring 2020

Further investigation into the limits of ramp rates needs to be done to optimize the load following capabilities of the RACC. The results shown here show ramp rates slower than predicted by previous studies. This implies that further design work into the optimal design and placement of valves throughout the system, as well as refinement of controller logic is necessary. PID controllers were used throughout this model, however, due to nonlinearity of many aspects of this system, more sophisticated controls are warranted. Development of the RACC will continue to be an iterative process. This dynamic model represents a significant step in that iterative process. It provides a platform on which different configurations and control techniques can now be tested on. The following chapter will also discuss further applications for this simulation.

While Apros has the capability of modeling electric system, the grid was not modeled in this simulation. The next iteration of this model would benefit from modeling the grid in order to test the transient effects of blackouts on the RACC and further refine the control logic to account for frequency response and load following.

5 Control and Operation of RACC Simulator

The RACC dynamic model described in the previous chapter was created as part of an advanced control room testbed - the Advanced Reactor Control and Operation (ARCO) Facility, developed by the UC Berkeley Nuclear Engineering Thermal Hydraulics Lab. Part of what makes ARCO unique is that it is used to control the Compact Integral Effects Test (CIET), an experimental thermal-hydraulic test loop which uses a simulant fluid to match the fluid properties and system dynamics of the primary loop of a PB-FHR. The RACC dynamic model can be implemented into ARCO using Open Platform Communications Unified Architecture (OPC UA).

This chapter will give a description of the CIET, ARCO, and the implementation of the RACC dynamic model using OPC UA. Finally, a description of potential future work will be presented.

5.1 The Compact Integral Effects Test

Validating thermal hydraulic codes is important for developing and licensing new reactor designs. Moreover, these codes and models must not only be validated for individual subsystems, but for entire integrated systems to accurately capture the phenomena produced from coupling subsystems together. Integral effect tests (IET) are able to generate the data necessary to validate thermal hydraulics codes for system level models[55].

The Compact Integral Effects Test uses a simulant fluid, Dowtherm A. At temperatures of 50-120 °C Dowtherm A simultaneously matches the Prandtl, Reynolds, and Grashof numbers of flibe molten salt at 50% geometric scale and requires only 2% of prototypical heating power[55]. CIET has been used to provide data as a scaled facility representing a PB-FHR for steady-state power operation, passive heat removal during shutdown, operational transients, and online inspection methods[56].

CIET consists of two coupled flow loops that replicate the two major flow paths in a prototypical PB-FHR: the natural circulation Direct Reactor Auxiliary Cooling System (DRACS) and the forced circulation primary loop. The CIET primary loop consists of a vertical heated section, the shell side of a vertical single-pass straight shell-and-tube heat exchanger representing the DRACS heat exchanger (DHX), a variable speed fan-driven air to oil heat exchanger used to simulate the coiled-tube air heater, and pump. The natural circulation loop representing the DRACS consists of the tube side of the vertical single-pass straight shell-and-tube heat exchanger and a Thermosyphon-Cooled Heat Exchanger (TCHX).

Control of heater power input, fan speed, and pump speed is done using a LabVIEW control system. Data acquisition of temperature and mass flow rates is performed using National Instruments data acquisition (DAQ) system. Pressure data is measured with manometers. LabVIEW is also used to display the acquired data. A schematic of CIET is shown in Figure 5-1.

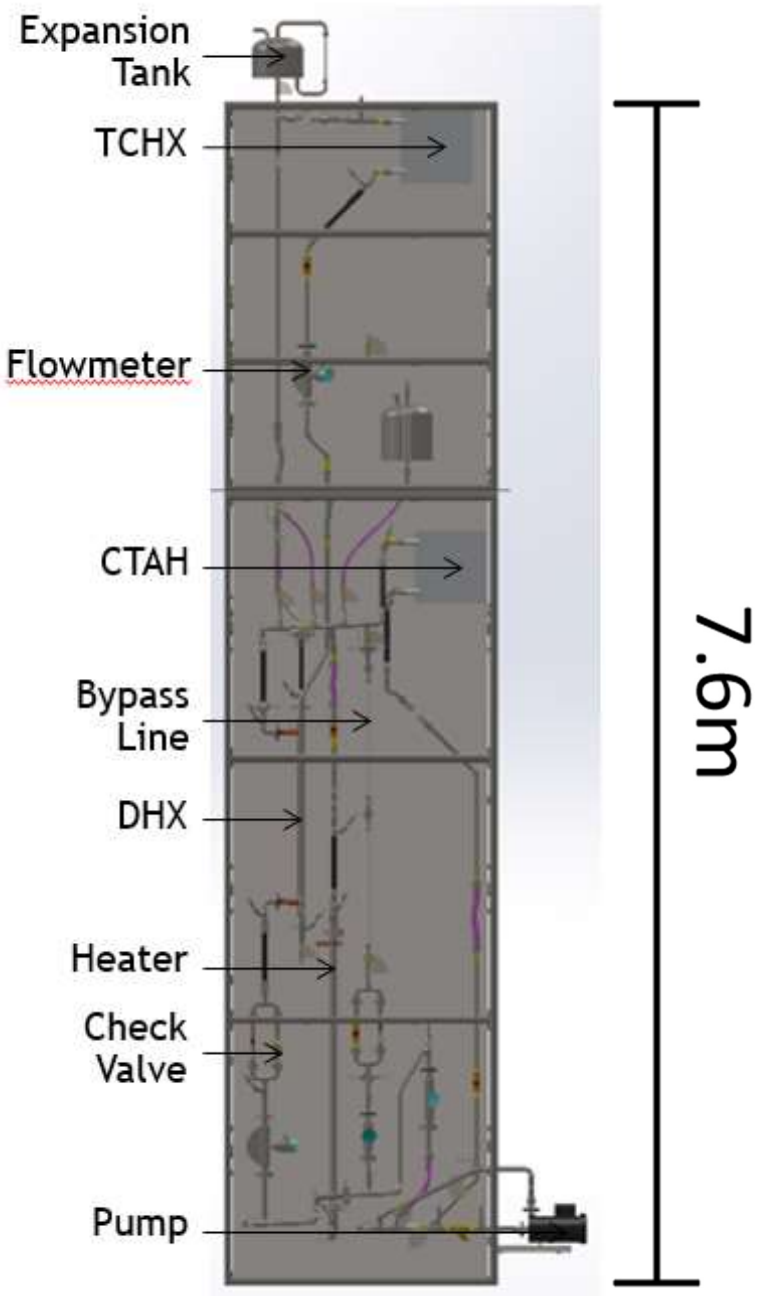

Figure 5-1: CIET Schematic

5.2 The Advanced Reactor Control and Operations Facility

The Advanced Reactor Control and Operations (ARCO) facility is a digital control room testbed designed to support the development and application of new digital technologies for advanced nuclear power plants[56]. Arco consists of three workstations and two displays as shown in Figure 5-2. This testbed allows for rapid iteration of human machine interface design,

operator communication protocol, and distributed control systems for advanced power systems. ARCO displays are designed using LabVIEW.

Figure 5-2: ARCO facility consisting of two overview displays, two operator stations (Balance of Plant under the overview panels and on the right and Reactor Operator on the left) and a supervisor station (on the desk behind the operator stations).

ARCO uses OPC UA, a networking protocol designed to allow the exchange of data between sources, independent of hardware platform or operation system[57]. OPC UA is commonly used in industry, including the nuclear industry[58]. OPC UA also has security options including encryption, authentication, and auditing. It allows real time data exchange, even for large, complex systems. OPC UA is based on client-server and server-server connections. The ARCO architecture is shown in Figure 5-3. OPC UA allows the various workstations, as well as the DAQ to communicate, allowing ARCO-CIET to operate as a control room and scaled reactor.

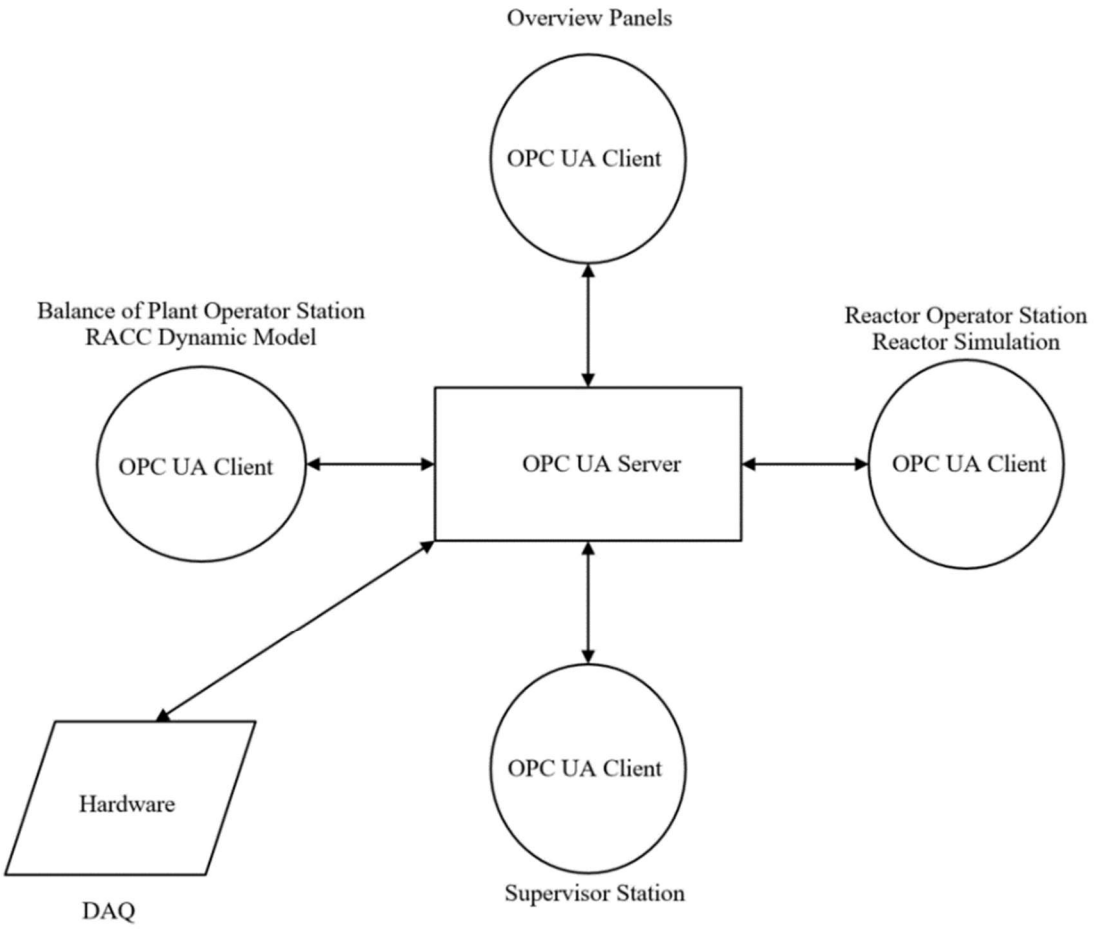

Figure 5-3: ARCO OPC UA Client-Server architecture. Overview panels, Balance of Plant Operator Station, Reactor Operator Station, and Supervisor Station are shown in Figure 5-2.

ARCO uses the RACC dynamic model to simulate a hypothetical power plant; and is also capable of controlling CIET. By coupling a power conversion system simulation to a physical experiment, researchers can operate ARCO as if it were a nuclear power plant. Operators are able to see and operate prototypical controls and observe prototypical results. This facilitates the ability to do a variety of research including operation optimization, cybersecurity, fault detection, health monitoring, and much more. While simulators and digital twins are common in industry, the ability to have a simulator during the design phase, and not after the plant is built allows the digital twin to influence development.

5.3 RACC Dynamic Model Implementation

Due to complications from the COVID-19 pandemic, access to ARCO has been limited. Moreover, the development of ARCO has been a highly collaborative effort and with the necessity to social distance, progress was hindered. However, the ability to connect the Apros RACC dynamic simulation to an external server, and to control that model with a separate client was demonstrated.

After configuring the necessary settings, Apros is capable of generating an OPC UA server. By manipulating a few XML files within its installation folder, this Apros server is able to communicate with external servers as a client. In order for Apros to then communicate with the server, a connection must be defined for each variable also within an XML file within the installation folder. This requires the address of the server reading the data, the address of the server writing the data, the address of the variable or 'tag' within each server, the data type (Boolean, float, double, etc.), and the name of the Apros component and variable.

The Apros RACC model has hundreds of variables that need to be either read from or written to the server, and in an actual power plant there are thousands of tags. Fortunately, it is possible to write code within Apros to automate certain functions using a modified version of Haskell called "Simantics Constraint Language" (SCL). Using SCL a CSV file of input and output tags was exported with the above-mentioned required information. A Python script was then used to generate the required XML file to establish the connections.

To confirm the above steps were completed correctly two free software were used. The first is PROSYS Simulation Server[59]. This software allows one to easily create an OPC UA server with customized tags. The second is UAexpert[60]. This software is an OPC UA Client. It allows you to browse for and connect to servers. It also allows you to browse tags within a server. Using these software, the ability to use one client to read data from and write data to Apros in real time through an external server was demonstrated successfully. Adjusting this for the ARCO server will require minimal additional work, since one simply changes the server address.

5.4 Future Work

With CIET and the RACC simulation coupled together through ARCO there are many research opportunities. The RACC model is made up of process components (pipes, valves, pumps, etc.) controllers, and actuators. While developing the RACC model described in chapter four, it was clear that the HRSG was quite sensitive to controller logic, requiring significant tuning to ensure the solver would not diverge during transients. While the current revision of the RACC model has stable control sufficient to observe system dynamics, it is likely that these results are not yet optimized. For instance, the ramp rates for the gas turbine can likely be increased without causing instabilities to the HRSG. Apros controllers are configured such that they can be operated with internal PID logic, or with manual input. This flexibility allows future researchers to use other software or techniques for controller logic to optimize control of the system.

Another feature of Apros is the ability to simulate valve failures, pump failures, pipe fouling, and many other malfunctions. These features enhance researchers' abilities to use ARCO to study fault detection, cybersecurity, and health monitoring.

6 Conclusion

The purpose of this dissertation has been to present the motivation for developing the RACC, discuss the state of the art of the various components of the RACC, and finally to present the efforts of the author to further the development of this technology. This chapter will provide a summary of how this dissertation fulfilled these purposes and will suggest future work.

The energy market is evolving. A variety of electricity producing technologies are reaching maturity, and each technology comes with strengths and weaknesses. Now, energy sources are evaluated based on capacity, dispatch ability, flexibility, reliability, environmental impact, price, and more. Energy sources such as wind and solar have been growing in popularity and implementation due to their low impact on the environment, however, their intermittent behavior has proven challenging for grid stability and will continue to be a challenge as the ratio of variable renewables increases.

Renewable energy intermittency can cause extreme electricity demand fluctuation, making it difficult for traditional energy sources to load follow. In California, it has caused an increasing amount of time periods when the price of electricity has been zero or negative due to overproduction. This trend is predicted to continue with California having zero or negative prices during 2,000+ hours in the year 2035[3]. This phenomenon is not financially sustainable for many traditional energy sources without political or technological intervention.

The RACC is an example of a technological innovation that is capable of being competitive in this new and changing energy market. The RACC iterates on the design of a typical NGCC power plant by replacing the natural gas heat source with any heat source capable of providing high temperature molten salt. The option to use natural gas remains an option for co-firing to boost power production. The RACC also includes a thermal energy storage system to further reduce dependency on natural gas. The TES system also allows the ability to redirect electricity from the grid during times of overproduction creating the opportunity to arbitrage electricity from low price to high price times, increasing profits. The RACC is capable of quick ramp rates, making it an ideal choice to complement intermittent energy sources.

The CTAH, modified gas turbine, FIRES, and HRSG system controls all represent novel aspects of RACC technology. In order to evaluate the state of the art of these different components, a technology readiness level was determined for each component using a rubric developed by NASA and the DOD and adapted by the DOE. The average TRL for the RACC is 4.6, implying that the RACC is in the early stages of transitioning from scientific research to engineering, and is the first step in determining whether the individual components will work together as a system[23].

No significant changes are envisioned for the HRSG hardware making it the most mature technology component of the RACC. The FIRES TES system utilizes a commonplace technology in the chemical industry known as a Cowper stove, suggesting that not much development is needed for this new application. Gas turbine design is an expensive process and therefore significant industrial participation is required to develop the modified gas turbine design beyond an initial conceptual design. Finally, the UC Berkeley Nuclear Engineering

Thermal Hydraulics lab is uniquely qualified to continue the development of the CTAH and system controls for the RACC.

The CTAH-VACE experiment was designed and performed to further the technology readiness of the CTAH. It provided experience in manufacturing a carbon steel pressure vessel and the use of internal insulation, a common technique used in FCCU's. The VACE experiment also provided experience in the manufacturing of tube-to-tube sheet joints, and safe operation of high temperature high-pressure equipment. Results from samples tested in VACE suggest that the CTAH salt to air heat exchangers are able to withstand a greater amount of creep deformation than currently allowed by ASME standards. In order to validate the results presented in this dissertation, further testing is required. It is also recommended that sample geometry be modified such that they are able to be driven to failure faster. While not a part of the scope of this research, the results of this study suggest that corrosion may be a far more significant factor to the lifetime of the CTAH.

After evaluating multiple dynamic simulation software, Apros Thermal 6.10 was chosen to develop a dynamic model of the RACC. This model was developed to demonstrate and evaluate the transient operation of the RACC. The design of the RACC was iterated on, specifically with the inclusion of control valves necessary for operation of the RACC. Controller logic was developed to achieve model stability as well as to automate the operation of the RACC based on the price of electricity. Key indicators of performance such as efficiency, cost of electricity, power production, etc. were measured to allow evaluation of RACC performance. Simulation results were presented and showed agreement between the dynamic model and previous steady state models performed. It is recommended that the design of the RACC continues to be iterated upon in order to optimize for maximum ramp rates while maintaining system stability. This will likely include a deeper investigation into valve sizing, design, and placement. For access to this model please contact the author or the UC Berkeley TH Lab.

This dynamic model was part of a greater effort to develop a power plant operator room simulator known as ARCO. The RACC model was incorporated into ARCO using OPC UA. This facility allows researchers the ability to study many different topics such as fault detection, human machine interface design, and control optimization to name a few. Apros allows for components to be controlled by external software, meaning development of more sophisticated controller logic is possible, and not limited to the PID controllers native to Apros. ARCO thus provides a test bed to optimize the operation of the RACC.

As mentioned in chapter two, the work of this dissertation was intended to increase the TRL of the RACC. Future work remains in order to further increase the TRL and develop the RACC for commercialization. Much of this development can only be performed by industrial partners due to high costs, such as the development of the modified gas turbine. In chapter two, a small-scale CTAH designed for prototypical conditions was presented. This represents the next step in the CTAH development and will further validate THEEM, provide more manufacturing experience, and provide more insight into creep and corrosion effects.

It is also proposed that development of the RACC Apros model continue. Refining this model will provide insight into the design of the RACC. Either within the Apros model itself, or through the ARCO facility, control logic should continue to be tuned and modified to demonstrate the maximum flexibility of the RACC. Other studies using ARCO to explore fault detection, health monitoring, and cyber security will also be beneficial to the economic success of the RACC.

References

[1] "What the duck curve tells us about managing a green grid," 2013. Accessed: Nov. 13, 2020. [Online]. Available: www.caiso.com.

[2] "The Duck Curve: A Review of California's Daily Load Predictions." https://blog.aurorasolar.com/the-duck-curve-a-review-of-californias-daily-load-predictions (accessed Sep. 25, 2020).

[3] M. Ruth, D. Cutler, F. Flores-Espino, and G. Stark, "The Economic Potential of Nuclear-Renewable Hybrid Energy Systems Producing Hydrogen," Apr. 2017. Accessed: Apr. 09, 2021. [Online]. Available: www.nrel.gov/publications.

[4] "OASIS." http://oasis.caiso.com/mrioasis/logon.do?reason=application.baseAction.noSession (accessed Apr. 09, 2021).

[5] H. K. Trabish, "Prognosis negative: How California is dealing with below-zero power market prices," *New Energy News*, Nov. 01, 2017. http://newenergynews.blogspot.com/2017/11/original-reporting-prognosis-negative.html (accessed Apr. 09, 2021).

[6] "Q3 2020 Report on Market Issues and Performance ," Feb. 2021.

[7] CAISO. PacifiCorp, "Third Party Settlement Overview," 2017. Accessed: Nov. 18, 2020. [Online]. Available: http://www.oasis.oati.com/PPW/PPWdocs/Third_Party_Settlements_Training_Master_Deck_Final.pdf.

[8] L. H. B. F. F. I. R. P. Deng, "What is the Cost of Negative Bidding by Wind? A Unit Commitment Analysis of Cost and Emissions ," *IEEE Trans. POWER Syst.*, vol. 30, no. 4, Jul. 2015, Accessed: Nov. 18, 2020. [Online]. Available: https://ieeexplore.ieee.org/stamp/stamp.jsp?arnumber=6917222.

[9] S. A. K. Amelang, "The causes and effects of negative power prices | Clean Energy Wire," *Clean Energy Wire*, Jan. 05, 2018. https://www.cleanenergywire.org/factsheets/why-power-prices-turn-negative (accessed Nov. 18, 2020).

[10] R. Dorsey-Palmateer, "Effects of wind power intermittency on generation and emissions," *Electr. J.*, vol. 32, no. 3, pp. 25–30, Apr. 2019, doi: 10.1016/j.tej.2019.02.007.

[11] "EIA forecasts natural gas to remain primary energy source for electricity generation - Today in Energy - U.S. Energy Information Administration (EIA)," Jan. 22, 2018. https://www.eia.gov/todayinenergy/detail.php?id=34612 (accessed Nov. 18, 2020).

[12] "Frequently Asked Questions (FAQs) - U.S. Energy Information Administration (EIA)." https://www.eia.gov/tools/faqs/faq.php?id=77&t=11 (accessed Nov. 18, 2020).

[13] C. Andreades, R. O. Scarlat, L. Dempsey, and P. Peterson, "Reheat-Air Brayton Combined Cycle Power Conversion Design and Performance Under Nominal Ambient Conditions," *J. Eng. Gas Turbines Power*, vol. 136, no. 6, p. 062001, Feb. 2014, doi:

10.1115/1.4026506.

[14] C. Forsberg, “Fluoride-Salt-Cooled High-Temperature Reactors (FHRs) Base-load Reactor Operation with Variable Output, Electricity Storage (as Heat) and Grid Management,” 2014. Accessed: Nov. 18, 2020. [Online]. Available: http://web.mit.edu/nse/people/research/forsberg.html.

[15] R. G. Reddy, “Molten salts: Thermal energy storage and heat transfer media,” *Journal of Phase Equilibria and Diffusion*, vol. 32, no. 4. Springer, pp. 269–270, Aug. 22, 2011, doi: 10.1007/s11669-011-9904-z.

[16] C. Andreades *et al.*, “Technical Description of the ‘Mark 1’ Pebble-Bed Fluoride-Salt-Cooled High-Temperature Reactor (PB-FHR) Power Plant,” 2014. Accessed: Nov. 06, 2018. [Online]. Available: http://fhr.nuc.berkeley.edu/wp-content/uploads/2014/10/14-002-PB-FHR_Design_Report_Final.pdf.

[17] A. Greenop, “Coiled Tube Gas Heater Effectiveness Modeling, Simulation, and Experiments for Nuclear Power Conversion Cycles,” 2018. Accessed: Apr. 22, 2019. [Online]. Available: https://escholarship.org/uc/item/9251z14k.

[18] C. Andreades, “Nuclear Air-Brayton Combined Cycle Power Conversion Design, Physical Performance Estimation and Economic Assessment,” 2015.

[19] D. C. Stack, D. Curtis, and C. Forsberg, “Performance of firebrick resistance-heated energy storage for industrial heat applications and round-trip electricity storage,” *Appl. Energy*, vol. 242, pp. 782–796, May 2019, doi: 10.1016/J.APENERGY.2019.03.100.

[20] S. C. Gülen, *Gas Turbine Combined Cycle Power Plants*. CRC Press, 2019.

[21] “Technology Readiness Level | NASA.” https://www.nasa.gov/directorates/heo/scan/engineering/technology/txt_accordion1.html (accessed Nov. 30, 2020).

[22] M. Héder, “From NASA to EU: the evolution of the TRL scale in Public Sector Innovation,” *Innov. J. Public Sect. Innov. J.*, vol. 22, no. 2, 2017, Accessed: Nov. 30, 2020. [Online]. Available: https://web.archive.org/web/20171011071816/https://www.innovation.cc/discussion-papers/22_2_3_heder_nasa-to-eu-trl-scale.pdf.

[23] “Technology Readiness Assessment Guide,” Washington, D.C., 2011. Accessed: Nov. 30, 2020. [Online]. Available: https://www2.lbl.gov/dir/assets/docs/TRL guide.pdf.

[24] *Advanced Technologies for Gas Turbines*. National Academies Press, 2020.

[25] R. K. Shah and D. P. Sekulic, *Fundamentals of Heat Exchanger Design*. Hoboken, NJ: John Wiley & Sons, Inc., 2003.

[26] P. Gilli, K. Fritz, J. Lippitsch, and G. Lurf, “Radial-flow heat exchanger,” Sep. 22, 1970.

[27] Thermflow Inc., “THERMOFLEX.” Southborough, MA 01745 1020, [Online]. Available: http://www.thermoflow.com.

[28] C. Andreades, A. Greenop, S. Gallagher, J. K. Choi, and P. Peterson, “Coiled Tube Air

Heater Test Loop Design," 2017, Accessed: Apr. 22, 2019. [Online]. Available: https://proceedings.asmedigitalcollection.asme.org.

[29] R. Sadeghbeigi, *Fluid Catalytic Cracking Handbook*, Third. Elsevier Inc., 2012.

[30] "Expansion Joints for Fluid Catalytic Cracking Units (FCCU)." Accessed: Dec. 03, 2020. [Online]. Available: www.eagleburgmann-ej.com.

[31] *STANDARDS OF THE TUBULAR EXCHANGER MANUFACTURERS ASSOCIATION*, Ninth Edition. Tarrytown, New York: Tubular Exchanger Manufacturers Association, Inc., 2007.

[32] "SAFETY DATA SHEET-NATURAL GAS," Edmonton, Alberta, Apr. 2019.

[33] S. C. Gülen, *Gas Turbines for Electric Power Generation*. Cambridge University Press, 2019.

[34] D. Z. S. Laing, "Using concrete and other solid storage media in thermal energy storage (TES) systems | Elsevier Enhanced Reader," in *Advances in Thermal Energy Storage Systems*, L. F. Cabeza, Ed. 2015.

[35] D. C. Stack, D. Curtis, and C. Forsberg, "Performance of firebrick resistance-heated energy storage for industrial heat applications and round-trip electricity storage," *Appl. Energy*, vol. 242, pp. 782–796, May 2019, doi: 10.1016/j.apenergy.2019.03.100.

[36] C. Forsberg, S. Brick, and G. Haratyk, "Coupling heat storage to nuclear reactors for variable electricity output with baseload reactor operation," *Electr. J.*, vol. 31, no. 3, pp. 23–31, Apr. 2018, doi: 10.1016/j.tej.2018.03.008.

[37] N. Mertens, F. Alobaid, R. Starkloff, B. Epple, and H. G. Kim, "Comparative investigation of drum-type and once-through heat recovery steam generator during start-up," *Appl. Energy*, vol. 144, pp. 250–260, Apr. 2015, doi: 10.1016/j.apenergy.2015.01.065.

[38] F. Alobaid, N. Mertens, R. Starkloff, T. Lanz, C. Heinze, and B. Epple, "Progress in dynamic simulation of thermal power plants," *Prog. Energy Combust. Sci.*, vol. 59, pp. 79–162, Mar. 2017, doi: 10.1016/j.pecs.2016.11.001.

[39] R. Starkloff, F. Alobaid, K. Karner, B. Epple, M. Schmitz, and F. Boehm, "Development and validation of a dynamic simulation model for a large coal-fired power plant," *Appl. Therm. Eng.*, vol. 91, pp. 496–506, Dec. 2015, doi: 10.1016/j.applthermaleng.2015.08.015.

[40] F. Alobaid, R. Starkloff, S. Pfeiffer, K. Karner, B. Epple, and H. G. Kim, "A comparative study of different dynamic process simulation codes for combined cycle power plants-Part A: Part loads and off-design operation," *Fuel*, vol. 153, pp. 692–706, Aug. 2015, doi: 10.1016/j.fuel.2015.02.010.

[41] F. Alobaid, N. Mertens, R. Starkloff, T. Lanz, C. Heinze, and B. Epple, "Progress in dynamic simulation of thermal power plants," *Progress in Energy and Combustion Science*, vol. 59. Elsevier Ltd, pp. 79–162, 2017, doi: 10.1016/j.pecs.2016.11.001.

[42] F. Alobaid, R. Postler, J. Ströhle, B. Epple, and H.-G. Kim, “Modeling and investigation start-up procedures of a combined cycle power plant,” *Appl. Energy*, vol. 85, no. 12, pp. 1173–1189, Dec. 2008, doi: 10.1016/j.apenergy.2008.03.003.

[43] P. et al. Peterson, “Coiled Tube Gas Heaters for Nuclear Gas-Brayton Power Conversion,” 2018.

[44] S. Yokell, “Expanded, and welded-and-expanded tube-to-tubesheet joints,” *J. Press. Vessel Technol. Trans. ASME*, vol. 114, no. 2, pp. 157–165, May 1992, doi: 10.1115/1.2929023.

[45] “COMSOL Multiphysics® v5.2a.” www.comsol.com COMSOL AB, Stockholm, Sweden.

[46] F. R. Larson and J. Miller, “A time-temperature relationship for rupture and creep stresses,” *Trans. ASME*, vol. 74, pp. 765–775, 1952.

[47] K. Maruyama, F. Abe, H. Sato, J. Shimojo, N. Sekido, and K. Yoshimi, “On the physical basis of a Larson-Miller constant of 20,” *Int. J. Press. Vessel. Pip.*, vol. 159, pp. 93–100, Jan. 2018, doi: 10.1016/j.ijpvp.2017.11.013.

[48] H. J. Frost and M. Ashby, *Deformation-Mechanism Maps: The Plasticity and Creep of Metals and Ceramics*. Oxfordshire, UK: Pergamon Press, 1982.

[49] N. Kumar, P. Besuner, S. Lefton, D. Agan, and D. Hilleman, “Power Plant Cycling Costs,” 2012. Accessed: Aug. 01, 2019. [Online]. Available: http://www.osti.gov/bridge.

[50] V. Fortum, “Apros 6 Thermal.” 2021, [Online]. Available: http://www.apros.fi.

[51] R. Hu, “SAM Theory Manual,” Argonne, Mar. 2017. Accessed: Apr. 26, 2021. [Online]. Available: www.anl.gov.

[52] K. K. Ahmed, R. O. Scarlat, and R. Hu, “Benchmark Simulation of Natural Circulation Cooling Systems With Salt Working Fluid Using SAM,” Sep. 2017, Accessed: Apr. 26, 2021. [Online]. Available: https://www.osti.gov/servlets/purl/1392061.

[53] R. Smith, “Phone discussion with Raub Smith, Chief Consulting Engineer - Performance at GE Energy.” 2020.

[54] J. Kuronen, “Power Plant Apros Modeling Training.” fortum, 2021.

[55] N. Zweibaum, J. E. Bickel, Z. Guo, J. C. Kendrick, and P. F. Peterson, “Design, Fabrication And Startup Testing In The Compact Integral Effects Test Facility In Support Of Flouride-Salt-Cooled, High-Temperature Reactor Technology,” Chicago, 2015.

[56] C. Poresky, “Model Network Methodology for Experimental Development of Industrial Monitoring Systems,” University of California, Berkeley, Berkeley, CA, 2019.

[57] “OPC Foundation.” https://opcfoundation.org/ (accessed Apr. 18, 2021).

[58] T. J. Burke, “OPC Unified Architecture Interoperability for Industrie 4.0 and the Internet of Things 4.0 Industrie IoT M2M,” Scottsdale AZ, 2010. Accessed: May 14, 2021. [Online]. Available: www.opcfoundation.org.

[59] “Prosys OPC.” https://www.prosysopc.com/ (accessed Apr. 19, 2021).

[60] “UaExpert ‘UA Reference Client’ - Unified Automation.” https://www.unified-automation.com/products/development-tools/uaexpert.html (accessed Apr. 19, 2021).